AN ABSTRACT OF THE DISSERTATION OF

Igor Vytyaz for the degree of Doctor of Philosophy in
Electrical and Computer Engineering presented on June 2, 2008.

Title: Automated Analysis, Design, and Optimization
of Low Noise Oscillators

Abstract approved:

Kartikeya Mayaram Un-Ku Moon

Low noise oscillators are universally needed in digital systems for clock generation and synchronization, and in radio-frequency communication front-ends for frequency up- and down-conversion. Noise in oscillators results in timing jitter, and limits the clock frequency of digital systems. In radio-frequency communication systems, phase noise in oscillators lowers the signal-to-noise ratio of transmitters and receivers, and degrades the overall bit-error-rate. Therefore, accurate simulation and optimization of oscillator noise performance is of utmost importance.

The focus of this dissertation is on automated analysis, design and optimization of low noise oscillators. Several advances in oscillator analysis that facilitate automated oscillator design and optimization are presented. These include a new

sensitivity analysis for oscillators, a design-oriented circuit analysis technique, and an oscillator design optimization approach. The sensitivity analysis calculates sensitivities of an oscillator's periodic steady-state and perturbation projection vector to design, process, or environmental parameters. In the design-oriented approach to circuit analysis the circuit response is computed together with the values of circuit parameters that result in a desired circuit performance. These analyses form the foundation for an efficient oscillator optimization technique that is general and applicable to all oscillator types.

Automated Analysis, Design, and Optimization of Low Noise Oscillators

by

Igor Vytyaz

A DISSERTATION

submitted to

Oregon State University

in partial fulfillment of
the requirements for the
degree of

Doctor of Philosophy

Presented June 2, 2008
Commencement June 2009

Doctor of Philosophy dissertation of Igor Vytyaz presented on June 2, 2008.

APPROVED:

Co-Major Professor, representing Electrical and Computer Engineering

Co-Major Professor, representing Electrical and Computer Engineering

Director of the School of Electrical Engineering and Computer Science

Dean of the Graduate School

I understand that my dissertation will become part of the permanent collection of Oregon State University libraries. My signature below authorizes release of my dissertation to any reader upon request.

Igor Vytyaz, Author

ACKNOWLEDGEMENTS

During my studies here at Oregon State University, my professors, friends, and family have given me invaluable assistance. I would like to take this opportunity to express my sincere appreciation to all these people.

In the first place, I would like to express my utmost gratitude to my advisors, Kartikeya Mayaram, and Un-Ku Moon for giving me an opportunity, both financial and intellectual, to start and accomplish this work. Without their support and insights, none of this work would have been possible.

Working with David C. Lee on challenging projects at Berkeley Design Automation proved to be a wonderful experience. I would like to thank him for helpful discussions and for his encouragement through these years. I am grateful to Pavan Kumar Hanumolu for inspiring conversations about my research.

My parents, Oleg and Larisa, and my brother Oleksii kept bringing me their love and support, when I was far away from home. They have helped me to finish what I started. Special thanks to my patient and loving wife Ira, who has been a great source of strength through out this work.

Many thanks to my many friends, but especially to Oleksii Fedorenko and Volodymyr Kratyuk for their friendship and support during my years of study. I am thankful to my lab mates in Kelley Engineering Center 4130 for their friendship, and my soccer team mates for great games.

Finally, I would like to acknowledge the financial support from SRC.

I may have forgotten someone. I apologize for my oversight in advance.

TABLE OF CONTENTS

TABLE OF CONTENTS (Continued)

LIST OF FIGURES

Figure Page

LIST OF FIGURES (Continued)

LIST OF TABLES

Chapter 1 – Introduction

Low noise oscillators are universally needed in digital systems for clock generation and synchronization, and in radio-frequency communication front-ends for frequency up- and down-conversion. Noise in oscillators causes timing jitter, and limits the clock frequency of digital systems. In radio-frequency communication systems, phase noise in oscillators lowers the signal-to-noise ratio of transmitters and receivers, and degrades the overall bit-error-rate. Therefore, accurate simulation and optimization of oscillator noise performance is of utmost importance.

The large-signal operation of oscillators causes noise translation to different frequencies due to circuit nonlinearities. This makes the modeling and simulation of noise in oscillators a difficult problem. Simplified noise models for hand calculations use approximations that degrade accuracy. Circuit simulators with RF capabilities can account for all noise frequency translation mechanisms and can predict oscillator noise performance with high accuracy.

Today, methods for analyzing the large-signal performance of oscillators are well established [1], [2], as are methods for predicting the noise performance [3], [4]. Important, yet less developed are methods for the sensitivity analysis of oscillator performance to design, process, or environmental parameters. A sensitivity analysis of an oscillator's periodic steady-state (PSS) solution, and its perturbation projection vector (PPV) can provide useful guidance on how to improve the design of a circuit, predict the impact of local and global process variations, and pave the way for automated circuit design optimization.

In a typical design flow, a designer determines the topology and the values of circuit parameters that result in a desired circuit performance. However, conventional analyses available in circuit simulators solve the inverse problem. For a given circuit topology and parameters, these analyses determine the performance of a circuit without accounting for the design specifications. The conventional analyses have to be used in an iterative manner to improve a design in order to achieve the desired specifications. Therefore, a new design-oriented approach to circuit analysis is needed to find the values of circuit parameters such that the performance of a circuit meets a set of desired objectives. This analysis is also the basis for constrained circuit optimization.

The contribution of this dissertation is on advancing automated analysis, design and optimization of low noise oscillators.

Specifically, sensitivity analysis for oscillators is presented, whereby, sensitivities of the PSS solution and the PPV to design, process, or environmental parameters can be computed. In forced circuits, a change in a circuit parameter only affects the shape of the PSS solution waveform. The PSS solution period does not change as it is defined by the periodic input. Oscillators have no external time reference, and therefore, a change in a circuit parameter could affect the oscillation frequency. As a result, sensitivity analysis techniques for forced circuits can not be used to analyze oscillators. The PSS sensitivity analysis presented in this dissertation accounts for changes in the oscillation frequency due to a change in a parameter [5], [6], and overcomes the problem inherent in previous techniques. The PPV sensitivity analysis is novel and does not have a corresponding equivalent analysis in forced circuits.

Also, the design-oriented circuit analysis technique is proposed. This is an elegant and efficient approach for solving problems with equality constraints, whereby nominal design specifications, or intermediate design goals can be met. The new analysis also has applications in accurately predicting the impact of parameter variations. The largest acceptable parameter variations for which the circuit performance remains within some boundaries, specified by equality constraints, can be determined.

Finally, a new gradient-based technique for automated design and optimization of low-noise oscillators is presented. It relies on a circuit simulator to accurately predict noise performance, and employs the proposed sensitivity analysis for oscillators to obtain directions for rapid design improvement. The new optimization technique is general and applicable to all types of oscillators, independent of circuit topology.

1.1 Dissertation Outline

The dissertation is organized as follows. Chapter 2 presents an analysis for calculating sensitivities of an oscillator's periodic steady-state and perturbation projection vector to design, process, or environmental parameters. Chapter 3 presents new design-oriented circuit analysis that is augmented with design constraints. Chapter 4 presents a technique for automated design and optimization of low noise oscillators. The dissertation is concluded in Chapter 5.

Chapter 2 – Sensitivity Analysis for Oscillators

Low noise oscillators are universally needed in digital systems for clock generation and synchronization, and in radio-frequency communication front-ends for frequency up- and down-conversion. Noise in oscillators causes timing jitter, and limits the clock frequency of digital systems. In radio-frequency communication systems, phase noise in oscillators lowers the signal-to-noise ratio of transmitters and receivers, and degrades the overall bit-error-rate. Therefore, accurate simulation and optimization of oscillator noise performance is of utmost importance.

Today, methods for analyzing the large-signal performance of oscillators are well established [1], [2], as are methods for predicting the noise performance [3], [4]. Important, yet less developed are methods for the sensitivity analysis of oscillator performance to design, process, or environmental parameters. A sensitivity analysis of an oscillator's periodic steady-state (PSS) solution, and its perturbation projection vector (PPV) can provide useful guidance on how to improve the design of a circuit, predict the impact of local and global process variations, and pave the way for automated circuit design optimization.

Standard small-signal analyses (AC, noise, sensitivity) are based on the assumption that small input perturbations lead to small output changes. These analyses are applicable to most forced circuits, but not to autonomous circuits. In oscillators, small input perturbations may result in arbitrarily large output changes. For this reason, small-signal noise [3] and AC [9] analyses have been developed specifically for oscillators. Similarly, PSS sensitivity analyses for forced circuits [11], [12], [13] are not applicable to autonomous circuits. Therefore, an alternative sensitivity analysis formulation is required for oscillators [5], [6].

In this chapter, sensitivity analysis for oscillators is presented, whereby, sensitivities of the PSS solution and the PPV to design, process, or environmental parameters can be computed. In forced circuits, a change in a circuit parameter only affects the shape of the PSS solution waveform. The PSS solution period does not change as it is defined by the periodic input. Oscillators have no external time reference, and therefore, a change in a circuit parameter could affect the oscillation frequency. As a result, sensitivity analysis techniques for forced circuits can not be used to analyze oscillators. The PSS sensitivity analysis presented in this chapter accounts for changes in the oscillation frequency due to a change in a parameter [5], [6], and overcomes the problem inherent in previous techniques. The PPV sensitivity analysis is novel and does not have a corresponding equivalent analysis in forced circuits.

The PSS of an oscillator and its PPV are reviewed in Section 2.1. In Section 4.2.2, continuous-time descriptions of an oscillator's PSS and PPV sensitivities are presented and their properties are discussed. In Section 3.3 a discrete-time oscillator sensitivity representation suitable for computer simulation [14] is presented. Based on this representation the time-domain finite difference, shooting, and monodromy matrix methods for oscillator sensitivity analysis are presented. Sensitivities of the PSS and the PPV of a ring oscillator are analyzed in Section 3.4.

It is shown how the oscillator sensitivity analysis can be used as an aid in applications such as oscillator design optimization, macromodeling, and predicting the impact of process variations.

2.1 Fundamental Oscillator Characteristics

In this section, the periodic steady-state and the perturbation projection vector of oscillators are defined. A continuous-time mathematical description of these fundamental oscillator characteristics is presented.

2.1.1 Periodic Steady State (PSS)

Any nonlinear oscillator circuit can be modeled as a set of m differential-algebraic equations (DAEs) in $x(t)$ given by

$$\frac{d}{dt}q\big(x(t)\big) + f\big(x(t)\big) + b = 0 \tag{2.1}$$

where

$$
\begin{aligned}
t \in \mathbb{R} \quad &: \text{ time, independent variable,} \\
x : \mathbb{R} \to \mathbb{R}^m &: \text{ oscillator state variables,} \\
q : \mathbb{R}^m \to \mathbb{R}^m &: \text{ contribution of reactive components,} \\
f : \mathbb{R}^m \to \mathbb{R}^m &: \text{ contribution of resistive components,} \\
b \in \mathbb{R}^m &: \text{ independent sources.}
\end{aligned}
$$

The T-periodic solution $x(t)$ of the DAEs in (2.1) is called the PSS solution if it satisfies $x(t) = x(t+T)$. This periodicity constraint can be expressed as

$$x(0) = x(T) \tag{2.2}$$

Notice that if $x(t)$ is a PSS solution, then $x(t + \Delta t)$, $\forall \Delta t$ is also a valid PSS solution. A unique isolated solution can be selected by imposing a phase condition

$$\varphi\big(x(0)\big) = 0, \quad \varphi : \mathbb{R}^m \to \mathbb{R} \tag{2.3}$$

One possible phase condition is to let a component of $x(0)$ be a fixed value.

The oscillator PSS is uniquely defined by (2.1), (2.2), and (2.3), resulting in the continuous-time equations for the oscillator in the steady-state

$$\begin{cases} \frac{d}{dt} q\big(x(t)\big) + f\big(x(t)\big) + b = 0 \\ x(0) = x(T) \\ \varphi\big(x(0)\big) = 0 \end{cases} \tag{2.4}$$

This is a periodic boundary value problem (BVP) in $x(t)$ and T, a special case of a two-point BVP [15]. The PSS solution $x_s(t)$ can be found by solving (2.4) in the time domain by the finite difference, or shooting methods, as well as in the frequency domain by the harmonic balance method [1], [2].

2.1.2 Perturbation Projection Vector (PPV)

The oscillator perturbed by a small time-dependent noise $b_n(t) : \mathbb{R} \to \mathbb{R}^p$ modulated by a state-dependent function $B(x) : \mathbb{R}^m \to \mathbb{R}^{m \times p}$ can be modeled by a set of m DAEs

$$\frac{d}{dt} q\big(x(t)\big) + f\big(x(t)\big) + b + B\big(x(t)\big) b_n(t) = 0 \tag{2.5}$$

The noisy solution x_n of (2.5) can be expressed in terms of the noiseless PSS solution x_s of (2.1) as [3]

$$x_n(t) = x_s\big(t + \alpha(t)\big) + a(t) \tag{2.6}$$

where

$$\begin{aligned} a : \mathbb{R} \to \mathbb{R}^m &: \text{orbital deviation that remains small} \\ \alpha : \mathbb{R} \to \mathbb{R} \quad &: \text{phase deviation that can grow unbounded} \end{aligned}$$

The phase deviation $\alpha(t)$ is the solution of the following nonlinear DAE

$$\frac{d}{dt}\alpha(t) = v_1^T\big(t + \alpha(t)\big)B\Big(x_s\big(t + \alpha(t)\big)\Big)b_n(t) \tag{2.7}$$

where $v_1 : \mathbb{R} \to \mathbb{R}^m$ is a T-periodic vector, known as the perturbation projection vector. The time-dependent PPV quantitatively describes how additive noise is converted by the oscillator into phase deviation.

Consider a system of m linear DAEs in $x(t)$

$$\frac{d}{dt}\big(C(t)x(t)\big) + G(t)x(t) = 0 \tag{2.8}$$

with T-periodic coefficients

$$C(t) \equiv C\big(x_s(t)\big) = \left.\frac{dq(x)}{dx}\right|_{x_s(t)}, \; C : \mathbb{R} \to \mathbb{R}^{m\times m} \tag{2.9}$$

and

$$G(t) \equiv G\big(x_s(t)\big) = \left.\frac{df(x)}{dx}\right|_{x_s(t)}, \; G : \mathbb{R} \to \mathbb{R}^{m\times m} \tag{2.10}$$

known as the capacitance and conductance matrices, respectively. The system in (2.8) is obtained by differentiation of (2.1) with respect to x at the PSS solution.

The corresponding adjoint system of m linear DAEs in $y(t)$ is given by

$$C^T(t)\frac{d}{dt}y(t) - G^T(t)y(t) = 0 \tag{2.11}$$

The adjoint system is satisfied by any linear combination of its eigenmodes $v_k(t)e^{-\mu_k t}$, $k = 1, \ldots, r$, where $r = \text{rank}(C)$, μ_k are the characteristic exponents, and $\lambda_k = e^{\mu_k T}$ are characteristic multipliers of the original linear system in (2.8). Assuming that the oscillator circuit has one asymptotic orbitally stable PSS solution, the PPV $v_1(t)$ is the only periodic and nonzero eigenmode. It corresponds to the oscillatory characteristic multiplier $\lambda_1 = 1$. The rest of the eigenmodes are either zero, or decay quickly as time decreases, as $|\lambda_k| < 1$, $k = 2, \ldots, r$, and $\lambda_{r+1} = \ldots = \lambda_m = 0$.

Any scaled version of the PPV satisfies the adjoint system. A properly scaled PPV is selected by requiring that

$$-v_1^T(t)C(t)\dot{x}_s(t) = 1, \quad \forall t \tag{2.12}$$

The oscillator PPV is defined by the system of linear DAEs in y which ensures that the solution $v_1(t)$ satisfies the adjoint system, is periodic, and is properly scaled

$$\begin{cases} C^T \frac{d}{dt}y - G^T y = 0 \\ y(0) = y(T) \\ -y^T C\dot{x}_s = 1, \quad t = 0 \end{cases} \tag{2.13}$$

The PPV is found by solving (2.13) directly [8], or by reducing it to an initial value problem (IVP) [7].

The IVP approach is based on integration of the adjoint system in (2.11), starting from an initial condition $v_1(0)$ that is properly scaled and results in a T-periodic solution $v_1(t)$. The initial condition $v_1(0)$ for the IVP is the right eigenvector of the monodromy matrix $M \in \mathbb{R}^{m\times m}$ [7], corresponding to the oscillatory eigenvalue[1] $\lambda_1 = 1$. The monodromy matrix is the state-transition matrix $\Omega(t,0)$ of the adjoint system evaluated at time T

$$M = \Omega(T,0) \tag{2.14}$$

Any solution of the adjoint system with initial condition $y(0)$ can be expressed in terms of the state-transition matrix as

$$y(t) = \Omega(t,0)y(0) \tag{2.15}$$

The state-transition matrix Ω can be found as a solution of the adjoint system with the identity matrix $I \in \mathbb{R}^{m\times m}$ as the initial condition

$$C^T(t)\frac{d}{dt}Y(t,0) - G^T(t)Y(t,0) = 0, \quad Y(0,0) = I \tag{2.16}$$

Therefore, the IVP, or the monodromy matrix based formulation for the PPV,

[1]The nonzero eigenvalues of the monodromy matrix $M = \Omega(T,0)$ are reciprocals of the characteristic multipliers of (2.8), λ_k^{-1}, $k = 1,\ldots,r$. For simplicity, for the rest of this section, and in Section 4.2.4 we will use λ_1 instead of λ_1^{-1} to denote the oscillatory eigenvalue of M.

is given by

$$\begin{cases} My(0) = \lambda_1 y(0) \\ -y^T(0)C(0)\dot{x}_s(0) = 1 \\ C^T \frac{d}{dt}y - G^T y = 0 \end{cases} \tag{2.17}$$

The PPV $v_1(t)$ is found from (2.17) by finding the oscillatory eigenvector of M, properly scaling it, and using it as the initial condition for integration of the adjoint DAEs.

2.2 Oscillator Sensitivity Analysis

An oscillator's PSS and PPV can change in response to a change in the design, process, or environmental parameters of an oscillator. In this section, the sensitivities of these fundamental oscillator characteristics to the parameter are defined. A continuous-time mathematical description for oscillator PSS and PPV sensitivities is derived. This is accomplished by differentiating the continuous-time oscillator equations presented in Section 2.1 with respect to the parameter.

Let $\gamma_p \in \mathbb{R}$ be an oscillator design parameter, such as MOSFET geometry parameters W_M, L_M, values of passive components R, L, C, process parameters, or environmental parameters, such as temperature, power supply voltage, etc. The oscillator component contributions q, f, their derivatives C, G, independent sources b, oscillation period T, PSS and PPV waveforms x_s, v_1 are now functions of γ_p. For example, the PSS solution and PPV are now defined as

$$T(\gamma_p) : \mathbb{R} \to \mathbb{R}$$

$$x_s(t, \gamma_p) : \mathbb{R} \times \mathbb{R} \to \mathbb{R}^m$$

$$v_1(t, \gamma_p) : \mathbb{R} \times \mathbb{R} \to \mathbb{R}^m$$

The sensitivity of the oscillation period with respect to γ_p, evaluated at a specific value of $\gamma_p = \gamma_p^*$, is the rate at which the period changes with respect to a small change $\Delta\gamma_p$ in γ_p and is given by

$$\left.\frac{dT(\gamma_p)}{d\gamma_p}\right|_{\gamma_p^*} = \lim_{\Delta\gamma_p \to 0} \frac{T(\gamma_p^* + \Delta\gamma_p) - T(\gamma_p^*)}{\Delta\gamma_p} \tag{2.18}$$

Consider a T-periodic waveform $s(t, \gamma_p)$, which can be the PSS waveform x_s, or the PPV waveform v_1. The sensitivity of this waveform with respect to γ_p is given by

$$\left.\frac{ds(t, \gamma_p)}{d\gamma_p}\right|_{\gamma_p^*} = \lim_{\Delta\gamma_p \to 0} \frac{\Delta_t s}{\Delta\gamma_p}, \quad \forall t \tag{2.19}$$

with

$$\Delta_t s = s\big(t, \gamma_p^* + \Delta\gamma_p\big) - s(t, \gamma_p^*) \tag{2.20}$$

As shown in Figure 2.1, a small change $\Delta\gamma_p$ may alter the oscillation frequency, and result in a large, non-periodic difference $\Delta_t s$. It follows that in general the

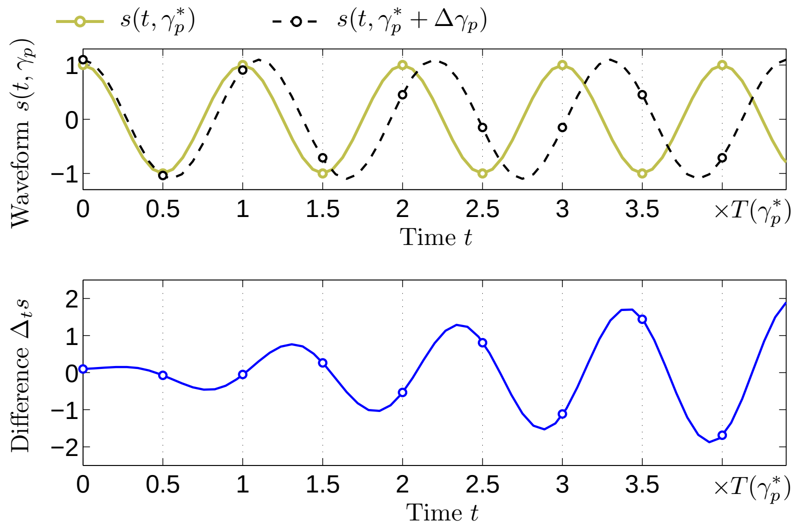

Figure 2.1: PSS waveforms and their difference in absolute time. The difference $\Delta_t s$ is large for small $\Delta\gamma_p$ and not periodic.

limit in (2.19) does not exist.

Let us define a normalized time as

$$\tau \equiv t/T(\gamma_p), \quad \tau \in \mathbb{R} \tag{2.21}$$

This allows us to define a difference waveform

$$\Delta_\tau s = s\big(\tau T(\gamma_p^* + \Delta\gamma_p), \gamma_p^* + \Delta\gamma_p\big) - s\big(\tau T(\gamma_p^*), \gamma_p^*\big) \tag{2.22}$$

that is small for small $\Delta\gamma_p$, and periodic in τ with a period of 1. Two periodic waveforms s and the corresponding difference $\Delta_\tau s$ are illustrated in Figure 2.2. The sensitivity of s with respect to γ_p in the normalized time

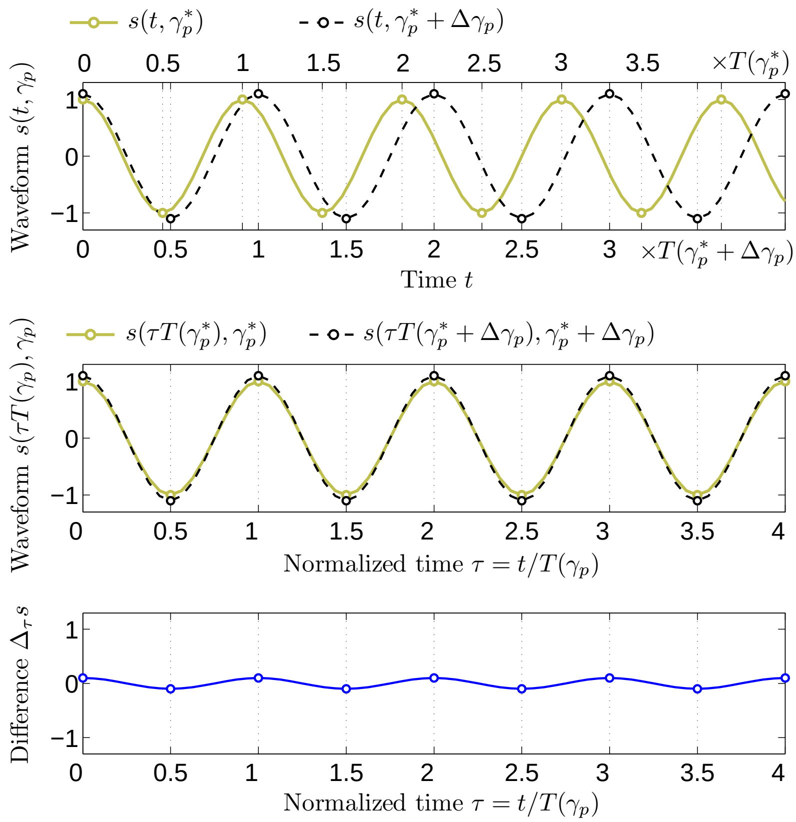

Figure 2.2: PSS waveforms and their difference in normalized time. The difference $\Delta_\tau s$ is small for small $\Delta\gamma_p$ and periodic.

$$\left.\frac{ds\big(\tau T(\gamma_p),\gamma_p\big)}{d\gamma_p}\right|_{\gamma_p^*} = \lim_{\Delta\gamma_p\to 0}\frac{\Delta_\tau s}{\Delta\gamma_p}, \quad \forall\tau \tag{2.23}$$

is periodic in τ with a period of 1, and exists for any τ. For a given normalized time τ this sensitivity relates a pair of points at different absolute time instances $\tau T(\gamma_p^*)$ and $\tau T(\gamma_p^*+\Delta\gamma_p)$. These time instances correspond to a fixed fraction τ of a varying oscillation period $T(\gamma_p)$.

Let us redefine the absolute time t, and the d/dt operator as

$$t \equiv \tau T(\gamma_p) \tag{2.24}$$

and

$$\frac{d}{dt} \equiv \frac{1}{T(\gamma_p)} \frac{d}{d\tau} \tag{2.25}$$

and use the normalized time τ as the independent variable in the oscillator sensitivity analysis.

With the new definition of time t, the sensitivity of a T-periodic waveform $s(t, \gamma_p^*)$ should be interpreted as

$$\begin{aligned}\left.\frac{ds(t,\gamma_p)}{d\gamma_p}\right|_{\gamma_p^*} &\equiv \left.\frac{ds\big(\tau T(\gamma_p),\gamma_p\big)}{d\gamma_p}\right|_{\tau\,=\,\frac{t}{T(\gamma_p^*)},\ \gamma_p^*} \\ &= \lim_{\Delta\gamma_p\to 0} \frac{s\left(\tau T(\gamma_p^*+\Delta\gamma_p),\gamma_p^*+\Delta\gamma_p\right) - s\big(\tau T(\gamma_p^*),\gamma_p^*\big)}{\Delta\gamma_p} \\ &= \lim_{\Delta\gamma_p\to 0} \frac{s\left(t\dfrac{T(\gamma_p^*+\Delta\gamma_p)}{T(\gamma_p^*)},\gamma_p^*+\Delta\gamma_p\right) - s\big(t,\gamma_p^*\big)}{\Delta\gamma_p}\end{aligned} \tag{2.26}$$

which is a T-periodic function of the absolute time t.

Thus, the oscillator PSS and PPV sensitivity analyses find the oscillation period sensitivity $dT/d\gamma_p$ as in (2.18), and periodic sensitivities of PSS and PPV waveforms $dx_s/d\gamma_p$ and $dv_1/d\gamma_p$ as in (2.23) or (2.26).

2.2.1 Periodic Steady-State Sensitivity Analysis

The oscillator steady-state equations in (2.4) with parameter γ_p are given by a periodic BVP in x and T

$$\begin{cases} \frac{d}{dt}q\big(x(t,\gamma_p),\gamma_p\big) + f\big(x(t,\gamma_p),\gamma_p\big) + b(\gamma_p) = 0 \\ x(0,\gamma_p) = x\big(T(\gamma_p),\gamma_p\big) \\ \varphi\big(x(0,\gamma_p)\big) = 0 \end{cases} \tag{2.27}$$

The PSS sensitivity is obtained by a differentiation of the PSS equations in (2.27) with respect to the parameter γ_p at the steady-state solution where $x = x_s$. Recall that not only x, and T but also q, f, b, t, and d/dt are functions of γ_p.

The contribution of the resistive circuit components to (2.27) at the steady-state x_s

$$f\big(x_s(t,\gamma_p),\gamma_p\big) = f\Big(x_s\big(\tau T(\gamma_p),\gamma_p\big),\gamma_p\Big) \tag{2.28}$$

depends on γ_p directly, as well as indirectly through the PSS waveform x_s and period T that are affected by γ_p. Therefore, the total derivative of f with respect to γ_p is composed of three terms

$$\begin{aligned}
&\frac{d}{d\gamma_p}\left[f\Big(x\big(\tau T(\gamma_p),\gamma_p\big),\gamma_p\Big)\right] \\
&= \frac{\partial f}{\partial \gamma_p} + \frac{\partial f}{\partial x}\cdot\frac{dx}{d\gamma_p} + \underbrace{\frac{\partial f}{\partial x}\cdot\frac{dx}{dT}\cdot\frac{dT}{d\gamma_p}}_{3} \\
&= \underbrace{\frac{\partial f}{\partial \gamma_p}}_{1} + \underbrace{G\cdot\frac{dx}{d\gamma_p}}_{2} + \underbrace{0}_{3}
\end{aligned} \tag{2.29}$$

which have the following interpretations:

1. Direct effect of parameter γ_p on f. Resistive circuit components that directly depend on γ_p, such as a resistor with resistance being the parameter $\gamma_p \equiv R$, contribute to this term.

2. Chain effect of parameter γ_p on f caused by a change in the PSS waveform x_s. Resistive circuit components, such as a resistor, or a MOSFET, contribute to this term.

3. Chain effect of parameter γ_p on f caused by a change in the oscillation period T. This term is zero because a change in the period alone causes the PSS waveform x_s to stretch or shrink in the absolute time t, without affecting the value of x in the normalized time

$$\frac{dx_s(\tau T,\gamma_p)}{dT} = 0 \tag{2.30}$$

Consequently, f is not affected in the normalized time.

The contribution of the reactive circuit components to (2.27) at the steady-state is

$$\frac{d}{dt}q\big(x_s(t,\gamma_p),\gamma_p\big) = \frac{1}{T(\gamma_p)}\frac{d}{d\tau}q\Big(x_s\big(\tau T(\gamma_p),\gamma_p\big),\gamma_p\Big) \tag{2.31}$$

and its total derivative with respect to γ_p is composed of three terms as well

$$\begin{aligned}
&\frac{d}{d\gamma_p}\left[\frac{1}{T(\gamma_p)}\frac{d}{d\tau}q\Big(x\big(\tau T(\gamma_p),\gamma_p\big),\gamma_p\Big)\right] \\
&= \frac{d}{d\tau}\left(\frac{\partial}{\partial\gamma_p}\frac{q}{T} + \frac{\partial}{\partial x}\frac{q}{T}\cdot\frac{dx}{d\gamma_p} + \frac{\partial}{\partial x}\frac{q}{T}\cdot\frac{dx}{dT}\cdot\frac{dT}{d\gamma_p}\right) \\
&= \frac{d}{d\tau}\left(\frac{\frac{\partial q}{\partial\gamma_p}T - \frac{dT}{d\gamma_p}q}{T^2} + \frac{1}{T}\frac{\partial q}{\partial x}\cdot\frac{dx}{d\gamma_p}\right) \\
&= \frac{1}{T}\frac{d}{d\tau}\frac{\partial q}{\partial\gamma_p} - \frac{1}{T^2}\frac{d}{d\tau}q\cdot\frac{dT}{d\gamma_p} + \frac{1}{T}\frac{d}{d\tau}\left(\frac{\partial q}{\partial x}\cdot\frac{dx}{d\gamma_p}\right) \\
&= \underbrace{\frac{d}{dt}\frac{\partial q}{\partial\gamma_p}}_{1} + \underbrace{\frac{d}{dt}\left(C\cdot\frac{dx}{d\gamma_p}\right)}_{2} - \underbrace{\frac{1}{T}\frac{dq}{dt}\cdot\frac{dT}{d\gamma_p}}_{3}
\end{aligned} \tag{2.32}$$

where (2.30) was used. The interpretation of the first two terms in (2.32) is similar to the corresponding terms in (2.29), and term 3 represents the chain effect of parameter γ_p on dq/dt caused by a change in the oscillation period T. A change in the period causes the waveform x_s and, consequently, q to stretch or shrink in the absolute time t. As a result, the slope dq/dt is decreased or increased accordingly.

Therefore, the oscillator PSS sensitivity equations are given by a system of linear DAEs that represent a periodic BVP in $dx/d\gamma_p$ and $dT/d\gamma_p$

$$\begin{cases} \frac{d}{dt}\big(C\frac{dx}{d\gamma_p}\big) + G\frac{dx}{d\gamma_p} - \frac{1}{T}\frac{dq}{dt}\frac{dT}{d\gamma_p} = -R_{\text{PSS}}(t) \\ \frac{dx(0,\gamma_p)}{d\gamma_p} - \frac{dx(T,\gamma_p)}{d\gamma_p} = 0 \\ \frac{\partial}{\partial x}\varphi(x)\big|_{x(0,\gamma_p)}\frac{d}{d\gamma_p}x(0,\gamma_p) = 0 \end{cases} \tag{2.33}$$

where

$$R_{\text{PSS}}(t) = \frac{\partial}{\partial \gamma_p}\Big[\frac{dq}{dt} + f + b\Big] \tag{2.34}$$

is a periodic forcing term that depends on the choice of γ_p.

Computation of PSS sensitivity requires a PSS analysis to be first performed to obtain the PSS waveforms x_s, and the oscillation period T, along with dq/dt in (2.33). Assuming that the underlying PSS analysis in based on the Newton-Raphson method, the periodic matrix coefficients C, and G in (2.33) are also available. The partial derivatives in (2.34), i.e., $\partial q/\partial\gamma_p$, $\partial f/\partial\gamma_p$, $\partial b/\partial\gamma_p$, are obtained from device models at the steady-state x_s.

Once assembled, the continuous-time PSS sensitivity equations in (2.33) can be solved in the time domain by the finite-difference, or shooting methods, as well as in the frequency domain by the harmonic balance method for $dx_s/d\gamma_p$, and $dT/d\gamma_p$.

In optimization problems, the gradient of an objective function ∇F_{obj} with respect to a P-vector of design parameters $[\gamma_1, \ldots, \gamma_P]^T$ is often needed. In this case, (2.33) must be solved P times with different forcing terms R_{PSS} to compute PSS sensitivities with respect to all optimization parameters γ_p, $p = 1, \ldots, P$. The periodic coefficients G, C, dq/dt, and T in (2.33) are properties of the periodic steady-state, and do not depend on the choice of a parameter.

The PSS sensitivity DAEs in (2.33) are linear, and therefore, easier and faster to solve than the nonlinear DAEs for the PSS in (2.4). Therefore, the proposed PSS sensitivity analysis is more efficient compared to finding a numerical approximation of PSS sensitivity, which requires an additional nonlinear PSS analysis with a perturbed value of the parameter. With multiple parameters, this is a significant benefit of the proposed PSS sensitivity analysis.

2.2.2 Phase Condition in Sensitivity Analysis

Figure 2.3(a) shows a simple steady-state orbit $x_s(\tau T, \gamma_p^*)$, and its perturbed version $x_s(\tau T, \gamma_p^* + \Delta\gamma_p)$ corresponding to a parameter variation $\Delta\gamma_p$.

Due to the freedom in choosing the initial time reference, the problem of finding the difference $\Delta_\tau x_s = [\Delta_\tau x_1, \Delta_\tau x_2]^T$ that maps the original orbit into the perturbed one does not have a unique solution for oscillators.

As discussed in Section 4.1.1, the initial point of the PSS solution is selected by imposing a phase condition in (2.4). Let the initial point of the original orbit be

$$x_s(\tau_0 T, \gamma_p^*) = [0.33, -0.94]^T \tag{2.35}$$

One way to select the initial point on the perturbed orbit is to apply the same phase condition as in the original PSS solution. The initial point in (2.35) satisfies

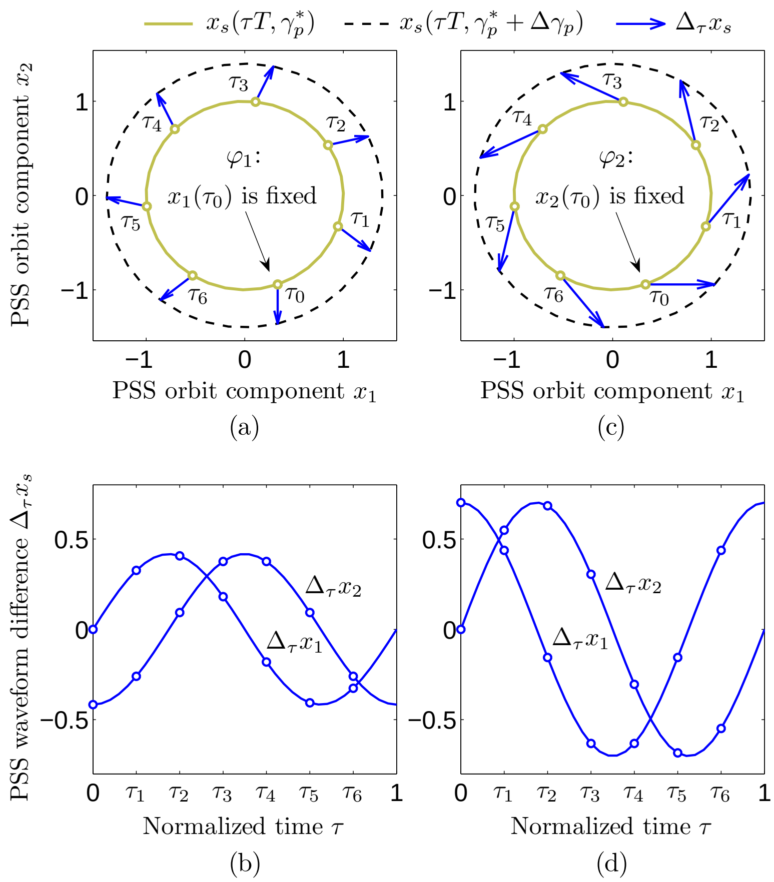

Figure 2.3: (a) The original and perturbed PSS orbits with a phase condition that fixes x_1, and (b) the corresponding PSS difference waveform components. The arrows correspond to the difference in PSS waveform samples and depict how the individual PSS orbit samples are affected by a change in the parameter. An example for fixed x_2 is shown in (c) and (d).

many phase conditions, and in particular

$$\varphi_1 : \; x_1(\tau_0 T, \gamma_p) = 0.33$$

and

$$\varphi_2 : \; x_2(\tau_0 T, \gamma_p) = -0.94$$

The two versions of the PSS difference $\Delta_\tau x_s$ corresponding to φ_1 and φ_2 are shown, respectively, in Figures 2.3(a) and (c) as arrows, and in Figures 2.3(b) and (d) as waveforms. Note that although the two sets of arrows have different magnitudes and directions, they describe the same change in the PSS orbit. Consequently, in the time domain, the two versions of $\Delta_\tau x_s$ describe the same change in the PSS waveform, although they have different amplitudes and phases, and generally may be of different shapes. It is difficult to favor one mapping over another, because all of them are equally good in describing the change in the steady-state due to $\Delta\gamma_p$.

It follows that depending on the phase condition equation, a single steady-state may have multiple valid PSS sensitivity waveforms $dx_s/d\gamma_p \approx \Delta_\tau x_s/\Delta\gamma_p$. However, independent of the phase condition, PSS waveform sensitivities have the same information. They describe the same change of the PSS orbit caused by a change in γ_p. It is important to understand that while the waveform sensitivities $dx_s/d\gamma_p$ may be different, the corresponding final results, such as sensitivity of power dissipation, duty cycle, harmonic content of the PSS and PPV power spectrum, etc., as well as $dT/d\gamma_p$, are scalars and do not depend on the phase condition equation. Any phase condition suitable for PSS analysis can be used in the sensitivity analysis.

In [9] it is shown that there is more than one solution in oscillator AC analysis, with a unique solution isolated by adding phase condition equations. In [10] it is pointed out that many phase conditions result in non-smooth AC solutions, and a smooth minimum norm AC solution is proposed.

A minimum norm PSS sensitivity can be obtained in a similar manner, by applying a least-square solver to the first two equations in (2.33). However, due to the time-invariant nature of the parameter variation $\Delta\gamma_p$, all phase conditions produce smooth, valid PSS sensitivities $dx_s/d\gamma_p$. Thus there is no need for a least-square solver in the oscillator sensitivity analysis. The use of the phase condition equation is a general and systematic way to isolate a unique sensitivity solution in a continuum of all valid sensitivities $dx_s/d\gamma_p$.

2.2.3 Perturbation Projection Vector Sensitivity Analysis

The oscillator equations for the PPV in (2.13) and (2.17) with parameter γ_p are given by linear DAEs in y

$$\begin{cases} C^T(t,\gamma_p)\frac{d}{dt}y(t,\gamma_p) - G^T(t,\gamma_p)y(t,\gamma_p) = 0 \\ y(0,\gamma_p) = y(T,\gamma_p) \\ -y^T(0,\gamma_p)C(0,\gamma_p)\dot{x}_s(0,\gamma_p) = 1 \end{cases} \tag{2.36}$$

and

$$\begin{cases} M(\gamma_p)y(0,\gamma_p) = \lambda_1 y(0,\gamma_p) \\ -y^T(0,\gamma_p)C(0,\gamma_p)\dot{x}_s(0,\gamma_p) = 1 \\ C^T(t,\gamma_p)\frac{d}{dt}y(t,\gamma_p) - G^T(t,\gamma_p)y(t,\gamma_p) = 0 \end{cases} \tag{2.37}$$

A PPV sensitivity analysis is based on differentiation of the PPV description in (2.36), or (2.37) with respect to the parameter γ_p at $y = v_1$. Differentiation of (2.36) is given by

$$\begin{cases} C^T \frac{d}{dt}\frac{dy}{d\gamma_p} - G^T \frac{dy}{d\gamma_p} = -R_{\mathrm{PPV}}(t) \\ \frac{dy(0,\gamma_p)}{d\gamma_p} - \frac{dy(T,\gamma_p)}{d\gamma_p} = 0 \\ [C\dot{x}_s]^T \frac{dy}{d\gamma_p} = -{v_1}^T \frac{d}{d\gamma_p}\left[C\dot{x}_s\right], \quad t = 0 \end{cases} \tag{2.38}$$

with

$$R_{\mathrm{PPV}}(t) = \frac{dC^T}{d\gamma_p}\frac{dv_1}{dt} - \frac{1}{T}\frac{dT}{d\gamma_p}C^T\frac{dv_1}{dt} - \frac{dG^T}{d\gamma_p}v_1 \tag{2.39}$$

and

$$\frac{d}{d\gamma_p}\left[C\dot{x}_s\right] = \frac{dC}{d\gamma_p}\dot{x}_s + C\frac{d\dot{x}_s}{d\gamma_p} - \frac{1}{T}\frac{dT}{d\gamma_p}C\dot{x}_s, \quad t = 0 \tag{2.40}$$

Not only y but also C, G, x_s, T, t, and d/dt have to be treated as functions of γ_p in order to obtain (2.38). The PPV sensitivity $dv_1/d\gamma_p$ is the solution of the linear system of DAEs (2.38) that represents a periodic BVP in $dy/d\gamma_p$.

The total derivative of the capacitance matrix with respect to parameter γ_p is expressed similar to (2.29) with the use of (2.30)

$$\frac{d}{d\gamma_p}C\Big(x_s\big(\tau T(\gamma_p), \gamma_p\big), \gamma_p\Big) = \frac{\partial C}{\partial \gamma_p} + \frac{\partial C}{\partial x_s}\cdot\frac{dx_s}{d\gamma_p} \tag{2.41}$$

with

$$\frac{\partial C}{\partial x_s}\cdot\frac{dx_s}{d\gamma_p} \equiv \sum_{j=1}^{m}\left(\frac{\partial C}{\partial x_j}\cdot\frac{dx_j}{d\gamma_p}\right) \tag{2.42}$$

where x_j is the j-th entry of x_s. The expression for the total derivative of the conductance matrix with respect to γ_p is similar to (2.41). These derivatives are obtained from device models at the steady-state x_s.

The PPV sensitivity $dv_1/d\gamma_p$ can be found by solving (2.38) directly, or by reducing it to an IVP. The IVP for PPV sensitivity is obtained by a differentiation of the IVP for PPV in (2.37) with respect to γ_p at $y = v_1$

$$\begin{cases} \frac{dM}{d\gamma_p} v_1 + M \frac{dy}{d\gamma_p} = \frac{d\lambda_1}{d\gamma_p} v_1 + \lambda_1 \frac{dy}{d\gamma_p}, \quad t = 0 \\ \left[\dot{x}_s C\right]^T \frac{dy}{d\gamma_p} = -y^T \frac{d}{d\gamma_p} \left[C \dot{x}_s\right], \quad t = 0 \\ C^T \frac{d}{dt} \frac{dy}{d\gamma_p} - G^T \frac{dy}{d\gamma_p} = -R_{\mathrm{PPV}}(t) \end{cases} \tag{2.43}$$

Ideally, $\lambda_1 = 1$ is insensitive to γ_p as an oscillator always has 1 as the oscillatory eigenvalue of the monodromy matrix M. Let us remove $d\lambda_1/d\gamma_p$ from (2.43) and rewrite its first m equations in the matrix form

$$\left[\ M - \lambda_1 I\ \right] \frac{dy}{d\gamma_p} = -\ \frac{dM}{d\gamma_p} v_1\ , \quad t = 0 \tag{2.44}$$

Since λ_1 is an eigenvalue of M, it follows that $\det\left[M - \lambda_1 I\right] = 0$ and the left-hand side matrix of (2.44) is singular. To make this matrix nonsingular, let us augment it by introducing an extra equation and an extra unknown in (2.44). The extra equation can be the scaling equation from (2.43). Keeping $d\lambda_1/d\gamma_p$ in (2.43) allows us to have the extra unknown. The resulting linear system of DAEs that represent the IVP, or the monodromy matrix formulation for the PPV sensitivity,

is given by

$$\left\{\begin{array}{l}\begin{bmatrix} M-\lambda_1 I & v_1 \\ [C\dot{x}_s]^T & 0 \end{bmatrix}\begin{bmatrix} \frac{dy(0,\gamma_p)}{d\gamma_p} \\ \frac{d\lambda_1}{d\gamma_p} \end{bmatrix} = -\begin{bmatrix} \frac{dM}{d\gamma_p}v_1 \\ v_1^T \frac{d}{d\gamma_p}[C\dot{x}_s] \end{bmatrix} \\ C^T \frac{d}{dt}\frac{dy}{d\gamma_p} - G^T \frac{dy}{d\gamma_p} = -R_{\mathrm{PPV}}(t) \end{array}\right. \tag{2.45}$$

The sensitivity of the monodromy matrix $dM/d\gamma_p$ in (2.45) is defined as the sensitivity of the state-transition matrix evaluated at time T

$$\frac{dM(\gamma_p)}{d\gamma_p} = \frac{\Omega(T,0,\gamma_p)}{d\gamma_p} \tag{2.46}$$

The sensitivity of the state-transition matrix is obtained from the adjoint system in (2.16) differentiated with respect to γ_p at $Y = \Omega$, with the zero matrix $dI/d\gamma_p = 0 \in \mathbb{R}^{m\times m}$ as the initial condition

$$C^T \frac{d}{dt}\frac{dY}{d\gamma_p} - G^T \frac{dY}{d\gamma_p} = -R_\Omega(t), \quad \frac{dY(0,0,\gamma_p)}{d\gamma_p} = 0 \tag{2.47}$$

where similar to (2.39)

$$R_\Omega(t) = \frac{dC^T}{d\gamma_p}\frac{d\Omega}{dt} - \frac{1}{T}\frac{dT}{d\gamma_p}C^T\frac{d\Omega}{dt} - \frac{dG^T}{d\gamma_p}\Omega \tag{2.48}$$

However, it is inefficient to compute the sensitivity of the monodromy matrix explicitly. Instead, its matrix-vector product with $v_1(0,\gamma_p)$ should be computed.

To do this, let us multiply all terms in (2.47) by $v_1(0, \gamma_p)$

$$C^T \frac{d}{dt}\big[\frac{d\Omega}{d\gamma_p} v_1(0, \gamma_p)\big] - G^T\big[\frac{d\Omega}{d\gamma_p} v_1(0, \gamma_p)\big] = -R_{\mathrm{PPV}}(t) \qquad (2.49)$$

where $R_{\mathrm{PPV}}(t) = R_\Omega(t) \cdot v_1(0, \gamma_p)$ was used in conjunction with (2.15). The unknown in (2.49) is the matrix-vector product

$$\frac{d\Omega(t, 0, \gamma_p)}{d\gamma_p} \cdot v_1(0, \gamma_p)$$

and the initial condition for integration is zero. Finding the the solution of (2.49) at time T concludes the assembly of the right-hand side of the linear system in (2.45).

Once the linear system in (2.45) is solved for the initial condition for PPV sensitivity $dv_1(0, \gamma_p)/d\gamma_p$, the IVP with DAEs in (2.45) can be solved for the PPV sensitivity waveform $dv_1(t, \gamma_p)/d\gamma_p$, where $R_{\mathrm{PPV}}(t)$ from (2.49) can be reused.

The PPV sensitivity analysis requires the PSS solution, the PPV, and a PSS sensitivity analysis. These provide elements of the PPV sensitivity equations such as C, and G at the steady-state x_s, as well as $dT/d\gamma_p$, $dx_s/d\gamma_p$, v_1, and M.

Similar to the PSS waveform sensitivity, the PPV sensitivity waveform depends on the phase condition equation. Also, PPV sensitivity waveforms corresponding to PSS solutions with different initial phases may not be simply phase-shifted copies of each other. This is because the PPV sensitivity analysis uses the PSS sensitivity waveform that possesses the same property.

2.3 Numerical Methods

In this section, numerical methods for computing the oscillator PSS and PPV sensitivities to parameter γ_p are presented.

Analysis of nonlinear oscillators using continuous-time equations is impractical. For a numerical time-domain analysis, time is discretized and the time-derivative operator is replaced by a finite-difference approximation. Let the continuous-time waveform $s(t)$ be sampled

$$s_i \equiv s(t_i) \tag{2.50}$$

with a constant timestep $h = T/n$ resulting in n uniformly spaced timepoints per oscillation period

$$t_i = ih,\ i \in \mathbb{N} \tag{2.51}$$

and the $d(\cdot)/dt$ operator be replaced by the backward Euler formula

$$\overrightarrow{\dot{s}_i} = \tfrac{1}{h}(s_i - s_{i-1}) \equiv \left.\tfrac{ds(t)}{dt}\right|_{t_i} \tag{2.52}$$

for numerical integration forward in time, or

$$\overleftarrow{\dot{s}_i} = \tfrac{1}{-h}(s_i - s_{i+1}) \equiv \left.\tfrac{ds(t)}{dt}\right|_{t_i} \tag{2.53}$$

for numerical integration backwards in time.

The oscillator DAEs for PSS and PPV sensitivity are converted into algebraic equations by applying the discretization rules in (2.50), (2.51), (2.52), or (2.53).

The best choice of numerical methods for the resulting discrete-time oscillator sensitivity analysis depends on the numerical methods used in the underlying PSS and PPV analyses. For example, if the nonlinear BVP for the PSS in (2.4) was reduced to a series of IVPs by applying the shooting method, the corresponding linear BVP for PSS sensitivity in (2.33) should be solved by reducing it to an IVP as well. It will be shown that using similar numerical methods allows the reuse of certain data structures and computation routines.

2.3.1 Discrete-Time PSS Sensitivity Equations

A simple discrete counterpart of the PSS sensitivity equations in (2.33) for $t \in (0, T]$ is given by a system of $nm+m+1$ linear algebraic equations at timepoints t_i, $i = 1, \ldots, n$

$$\begin{cases} \overset{-\cdot\rightarrow}{C_i \frac{dx_i}{d\gamma_p}} + G_i \frac{dx_i}{d\gamma_p} - \frac{1}{T}\dot{q}_i \cdot \frac{dT}{d\gamma_p} = -\frac{\partial}{\partial \gamma_p}\left[\, \overset{-\cdot\rightarrow}{q_i} + f_i + b\right] \\ \frac{dx_0}{d\gamma_p} = \frac{dx_n}{d\gamma_p} \\ \left.\frac{\partial \varphi(x)}{\partial x}\right|_{x_0} \cdot \frac{dx_0}{d\gamma_p} = 0 \end{cases} \tag{2.54}$$

where the unknowns are the sensitivity of the oscillation period $dT/d\gamma_p$, and $(n+1)m$ samples $dx_i/d\gamma_p$, $i = 0, \ldots, n$ of the PSS sensitivity waveform.

Computing the sensitivity of the oscillator PSS solution implies that a PSS analysis is successfully completed. The time discretization of the PSS analysis should be preserved for the PSS sensitivity analysis. In this case, sequences x_i, and q_i are known. Furthermore, if gradient-based methods, such as the Newton-

Raphson method, are used to find the PSS, matrices C_i, and G_i are known as well.

2.3.2 Discrete-Time PPV Sensitivity Equations

It is numerically unstable to integrate the adjoint system in (2.11) and its derivatives forward in time [7]. For the discrete-time PPV and PPV sensitivity analyses, numerical integration is performed backwards in time, and (2.53) is used to approximate the $d(\cdot)/dt$ operator.

The discrete-time equivalent of the periodic BVP formulation for PPV sensitivity in (2.38) along one period $t \in [0, T)$ is given by a system of $nm + m + 1$ linear algebraic equations for $i = 0, \ldots, n-1$

$$\begin{cases} C_i^T \overset{\leftarrow\cdot-}{\frac{dv_{1_i}}{d\gamma_p}} - G_i^T \frac{dv_{1_i}}{d\gamma_p} = -R_{\mathrm{PPV}i} \\ \frac{dv_{1_0}}{d\gamma_p} = \frac{dv_{1_n}}{d\gamma_p} \\ \frac{dv_{1_0}^T}{d\gamma_p} C_0 \overset{-\cdot\to}{x_0} + v_{1_0}^T \frac{d}{d\gamma_p} \left[C_0 \overset{-\cdot\to}{x_0} \right] = 0 \end{cases} \tag{2.55}$$

with

$$R_{\mathrm{PPV}i} = \frac{dC_i^T}{d\gamma_p} \overset{\leftarrow\cdot-}{dv_{1i}} - \frac{1}{T} \frac{dT}{d\gamma_p} C_i^T \overset{\leftarrow\cdot-}{dv_{1i}} - \frac{dG_i^T}{d\gamma_p} v_{1i} \tag{2.56}$$

and

$$\frac{d}{d\gamma_p} \left[C_0 \overset{-\cdot\to}{x_0} \right] = \frac{dC_0}{d\gamma_p} \overset{-\cdot\to}{x_0} + C_0 \frac{\overset{-\cdot\to}{dx_0}}{d\gamma_p} - \frac{1}{T} \frac{dT}{d\gamma_p} C_0 \overset{-\cdot\to}{x_0} \tag{2.57}$$

In (2.55) the unknowns are $(n+1)m$ samples $dv_{1_i}/d\gamma_p$, $i = 0, \ldots, n$ of PPV sensitivity waveforms. This system is overdetermined since there are more equations than unknowns.

Next, the discrete counterpart of the IVP formulation for the PPV sensitivity is presented. The linear system of equations from (2.45) that describe the initial condition for the PPV sensitivity waveform is given by

$$\begin{bmatrix} M - \lambda_1 I & v_{1_0} \\ \left[C_0 \, \overset{-\cdot\rightarrow}{x_0}\right]^T & 0 \end{bmatrix} \begin{bmatrix} \frac{dv_{1_0}}{d\gamma_p} \\ \frac{d\lambda_1}{d\gamma_p} \end{bmatrix} = - \begin{bmatrix} \frac{dM}{d\gamma_p} v_{1_0} \\ v_{1_0}^T \frac{d}{d\gamma_p}\left[C_0 \, \overset{-\cdot\rightarrow}{x_0}\right] \end{bmatrix} \tag{2.58}$$

The discrete-time versions of the DAEs from (2.45) and (2.49) along one period $t \in [-T, 0)$ are given by

$$C_i^T \, \overset{\leftarrow\cdot-}{\frac{dv_{1_i}}{d\gamma_p}} - G_i^T \frac{dv_{1_i}}{d\gamma_p} = -R_{\mathrm{PPV}i} \tag{2.59}$$

and

$$C_i^T \Big[\overset{\leftarrow\cdot-}{\frac{d\Omega_i}{d\gamma_p}} v_{1_0} \Big] - G_i^T \Big[\frac{d\Omega_i}{d\gamma_p} v_{1_0} \Big] = -R_{\mathrm{PPV}i} \tag{2.60}$$

for $i = -1, \ldots, -n$. The sensitivity of the monodromy matrix on the right-hand side of (2.58) is given by[2]

$$\frac{dM}{d\gamma_p} = \frac{d\Omega_{-n}}{d\gamma_p} \equiv \frac{d\Omega(-T, 0, \gamma_p)}{d\gamma_p} \tag{2.61}$$

[2]Note that since numerical integration is performed backwards, the monodromy matrix in (2.58), and (2.61) is redefined as $M = \Omega(-T, 0)$, and its nonzero eigenvalues are the characteristic multipliers of (2.8), λ_k, $k = 1, \ldots, r$.

2.3.3 Finite Difference Method for PSS Sensitivity Analysis

The finite difference method for PSS sensitivity analysis is efficient if the underlying PSS analysis is based on the finite-difference method as well.

In this method, the sensitivity of the oscillation period $dT/d\gamma_p$ and the sensitivities of the PSS waveform samples $dx_i/d\gamma_p$, $i = 1, \ldots, n$ are found simultaneously by solving the linear system in (2.62), derived from (2.54),

$$
\left[\begin{array}{cccc|c}
\frac{1}{h}C_1 + G_1 & & & -\frac{1}{h}C_n & -\frac{1}{T}\,\vec{\dot{q}}_1 \\
-\frac{1}{h}C_1 & \frac{1}{h}C_2 + G_2 & & & -\frac{1}{T}\,\vec{\dot{q}}_2 \\
& \ddots & \ddots & & \vdots \\
& & -\frac{1}{h}C_{n-1} & \frac{1}{h}C_n + G_n & -\frac{1}{T}\,\vec{\dot{q}}_n \\
\hline
0 & \cdots & 0 & \left.\frac{\partial \varphi(x)}{\partial x}\right|_{x_n} & 0
\end{array}\right]
\cdot
\begin{bmatrix}
\frac{dx_1}{d\gamma_p} \\
\frac{dx_2}{d\gamma_p} \\
\vdots \\
\frac{dx_n}{d\gamma_p} \\
\frac{dT}{d\gamma_p}
\end{bmatrix}
= -\begin{bmatrix}
\frac{1}{h}\left(\frac{\partial q_1}{\partial \gamma_p} - \frac{\partial q_n}{\partial \gamma_p}\right) + \frac{\partial f_1}{\partial \gamma_p} + \frac{db}{d\gamma_p} \\
\frac{1}{h}\left(\frac{\partial q_2}{\partial \gamma_p} - \frac{\partial q_1}{\partial \gamma_p}\right) + \frac{\partial f_2}{\partial \gamma_p} + \frac{db}{d\gamma_p} \\
\vdots \\
\frac{1}{h}\left(\frac{\partial q_n}{\partial \gamma_p} - \frac{\partial q_{n-1}}{\partial \gamma_p}\right) + \frac{\partial f_n}{\partial \gamma_p} + \frac{db}{d\gamma_p} \\
0
\end{bmatrix}
\tag{2.62}
$$

Note that the periodicity constraint $dx_0/d\gamma_p = dx_n/d\gamma_p$ is not explicitly present in (2.62). The periodicity constraint equation was used to eliminate $dx_0/d\gamma_p$ from the list of unknowns. The remaining $nm+1$ equations represent the finite difference formulation of the PSS sensitivity analysis.

The matrix in (2.62) is the same as the Jacobian of the Newton-Raphson based finite difference method for the PSS analysis at the solution point. The linear solver used for the Newton-Raphson iterations of the underlying PSS analysis should be used again to solve the linear system in (2.62). If the solver is iterative [17], the matrix-vector product computation routine can be reused. In case of a direct solver, the LU-factors of the matrix are available from the PSS analysis.

Note that it is necessary to compute the derivatives of device contributions with respect to the parameter γ_p on the right-hand side of (2.62). The device models have to be extended to provide these derivatives.

The computation cost of the finite difference method for PSS sensitivity analysis is comparable to the cost of one Newton-Raphson iteration of the underlying PSS analysis.

2.3.4 Finite Difference Method for PPV Sensitivity Analysis

The finite difference method for PPV sensitivity analysis is efficient if the underlying PPV analysis is based on finding the nullspace of the transposed unaugmented finite difference Jacobian matrix.

The first $nm + m$ equations in (2.55) can be written as a system of nm linear equations in matrix form

$$J_{fd}^T \cdot \begin{bmatrix} \frac{dv_{1_1}}{d\gamma_p} \\ \frac{dv_{1_2}}{d\gamma_p} \\ \vdots \\ \frac{dv_{1_n}}{d\gamma_p} \end{bmatrix} = \begin{bmatrix} R_{\mathrm{PPV}1} \\ R_{\mathrm{PPV}2} \\ \vdots \\ R_{\mathrm{PPV}n} \end{bmatrix} \tag{2.63}$$

Note that the periodicity constraint $dv_{1_0}/d\gamma_p = dv_{1n}/d\gamma_p$ is not explicitly present in (2.63). The periodicity constraint equation was used to eliminate $dv_{1_0}/d\gamma_p$ from the list of unknowns.

The matrix J_{fd}^T is singular. Similar to the underlying PPV computation technique [8], J_{fd}^T is augmented by a row vector $\left[[C_1 \; \dot{\vec{x}}_1]^T, \ldots, [C_n \; \dot{\vec{x}}_n]^T\right]$ and a column vector $[p_1, \ldots, p_n]^T$ chosen to make the matrix nonsingular. This is equivalent to introducing an extra equation and an extra unknown in (2.63). The extra equation is given by a sum of the differentiated scaling equations for all PPV samples along one period $i = 1, \ldots, n$. It is equivalent to the last equation in (2.55) as both equations serve the same purpose of properly scaling the PPV sensitivity waveform. The extra unknown is ideally zero, and in practice it is small, similar to the extra unknown in the underlying PPV analysis [8]. The resulting system of $nm + 1$ linear equations (2.64) represent the finite difference formulation for the

PPV sensitivity analysis,

$$
\left[\begin{array}{cccc:c}
\frac{1}{h}C_1^T + G_1^T & -\frac{1}{h}C_1^T & & & p_1 \\
 & \frac{1}{h}C_2^T + G_2^T & \ddots & & p_2 \\
 & & \ddots & -\frac{1}{h}C_{n-1}^T & \vdots \\
-\frac{1}{h}C_n^T & & & \frac{1}{h}C_n^T + G_n^T & p_n \\
\hdashline
\left[C_1 \overrightarrow{\dot{x}_1}\right]^T & \left[C_2 \overrightarrow{\dot{x}_2}\right]^T & \cdots & \left[C_n \overrightarrow{\dot{x}_n}\right]^T & 0
\end{array}\right] \cdot \left[\begin{array}{c}
\frac{dv_{1_1}}{d\gamma_p} \\
\frac{dv_{1_2}}{d\gamma_p} \\
\vdots \\
\frac{dv_{1_n}}{d\gamma_p} \\
0
\end{array}\right]
= \left[\begin{array}{c}
R_{\mathrm{PPV}1} \\
R_{\mathrm{PPV}2} \\
\vdots \\
R_{\mathrm{PPV}n} \\
-v_{1_0}^T \sum_{i=1}^{n} \left(\frac{dC_i}{d\gamma_p} \overrightarrow{\dot{x}_i} + C_i \frac{d\overrightarrow{\dot{x}_i}}{d\gamma_p} - \frac{1}{T}\frac{dT}{d\gamma_p} C_i \overrightarrow{\dot{x}_i} \right)
\end{array}\right] \tag{2.64}
$$

Solving the linear system in (2.64) results in the sensitivities of the PPV waveform samples $dv_{1_i}/d\gamma_p$, $i = 1, \ldots, n$.

The matrix-vector product computation routine for J_{fd}^T is available from the underlying PPV analysis. It can be easily extended to compute the matrix-vector product of the matrix of the linear system in (2.64).

The entries on the right-hand side of (2.64) require the sensitivities of matrices G and C with respect to the samples of x_s and γ_p, and can be computed from the device models.

2.3.5 Shooting Method for PSS Sensitivity Analysis

The shooting method for the PSS sensitivity analysis is efficient in conjunction with an underlying PSS analysis that is based on the shooting method as well.

The last $m+1$ equations in (2.54) represent a shooting formulation of the PSS sensitivity analysis

$$\begin{bmatrix} \frac{dx_n}{d\gamma_p} - \frac{dx_0}{d\gamma_p} \\ \left.\frac{\partial\varphi(x)}{\partial x}\right|_{x_0} \cdot \frac{dx_0}{d\gamma_p} \end{bmatrix} = \begin{bmatrix} 0 \\ 0 \end{bmatrix} \tag{2.65}$$

where $dx_0/d\gamma_p$ and $dT/d\gamma_p$ are the unknowns. Given $dT/d\gamma_p$, $dx_n/d\gamma_p$ is obtained by integrating the first nm equations in (2.54) starting from the initial condition $dx_0/d\gamma_p$. After the solution, $dx_0/d\gamma_p$ and $dT/d\gamma_p$, is found, the remaining PSS waveform sensitivity samples $dx_i/d\gamma_p$, $i = 1, \ldots, n$ are obtained from an additional integration of the first nm equations in (2.54).

Let us rewrite the shooting method formulation in (2.65) as

$$F'_{sh\gamma_p}\left(\frac{dx_0}{d\gamma_p}, \frac{dT}{d\gamma_p}\right) = 0 \tag{2.66}$$

where $F'_{sh\gamma_p}$ is the same as the derivative of the underlying shooting PSS analysis function F_{sh} with respect to γ_p. The shooting method applied to the linear BVP in (2.54) finds the solution at the first iteration. The solution is found by solving a linear system

$$J_{sh} \begin{bmatrix} \frac{dx_0}{d\gamma_p} \\ \frac{dT}{d\gamma_p} \end{bmatrix} = -F'_{sh\gamma_p}(0,0) \tag{2.67}$$

where

$$F'_{sh\gamma_p}(0,0) = \begin{bmatrix} \frac{dx_n}{d\gamma_p} \\ \\ 0 \end{bmatrix} \tag{2.68}$$

and

$$J_{sh} = \begin{bmatrix} \dfrac{\partial \frac{dx_n}{d\gamma_p}}{\partial \frac{dx_0}{d\gamma_p}} - I & \dfrac{\partial \frac{dx_n}{d\gamma_p}}{\partial \frac{dT}{d\gamma_p}} \\ \left.\frac{\partial \varphi(x)}{\partial x}\right|_{x_0} & 0 \end{bmatrix} = \begin{bmatrix} \frac{\partial x_n}{\partial x_0} - I & \frac{\partial x_n}{\partial T} \\ \left.\frac{\partial \varphi(x)}{\partial x}\right|_{x_0} & 0 \end{bmatrix} \tag{2.69}$$

is the Jacobian matrix of $F'_{sh\gamma_p}$, and I is the identity matrix. Note that J_{sh} is the same as the Jacobian matrix of the Newton-Raphson based shooting method for the underlying PSS analysis at the solution point.

Computing $dx_n/d\gamma_p$ for $F'_{sh\gamma_p}(0,0)$ requires integration of the first nm equations in (2.54). This is done iteratively for $i = 1, \ldots, n$

$$\begin{aligned} \left[\frac{1}{h}C_i + G_i\right]\frac{dx_i}{d\gamma_p} &= \frac{1}{T}\overrightarrow{\dot{q}_i}\cdot\frac{dT}{d\gamma_p} + \frac{1}{h}C_{i-1}\frac{\partial x_{i-1}}{\partial \gamma_p} \\ &\quad - \left[\frac{1}{h}\left(\frac{\partial q_i}{\partial \gamma_p} - \frac{\partial q_{i-1}}{\partial \gamma_p}\right) + \frac{\partial f_i}{\partial \gamma_p} + \frac{\partial b}{\partial \gamma_p}\right] \end{aligned} \tag{2.70}$$

starting from the initial condition $dx_0/d\gamma_p = 0$. Note that the first term on the right-hand side of (2.70) vanishes since $F'_{sh\gamma_p}$ is evaluated at $dT/d\gamma_p = 0$. At any iteration $i = 1, \ldots, n$, the matrix in (2.70) is the same as the Jacobian at the corresponding timepoint of the final transient analysis of the shooting method for the underlying PSS analysis.

The sensitivities of PSS waveform samples along one period are found from (2.70) iteratively with the initial condition $dx_0/d\gamma_p$, obtained by solving (2.67). This time, the first term on the right-hand side of (2.70) needs to be taken into account since $dT/d\gamma_p$ found from (2.67) is not necessarily zero.

Matrix-vector product computation routines or LU-factors for the matrices of linear systems in (2.67) and (2.70) are available from the underlying PSS analysis. The computation cost of the shooting method is similar to the computation cost of one Newton-Raphson iteration of the underlying PSS analysis.

2.3.6 Monodromy Matrix Method for PPV Sensitivity Analysis

The monodromy matrix method for the PPV sensitivity analysis is efficient if the underlying PPV analysis is based on the eigenvalue decomposition of the monodromy matrix.

First, equations in (2.60) are integrated backwards in time. This is done iteratively for $i = -1, ..., -n$

$$\left[\frac{1}{h}C_i^T + G_i^T\right]\frac{d\Omega_i}{d\gamma_p}v_{1_0} = \frac{1}{h}C_i^T\frac{d\Omega_{i+1}}{d\gamma_p}v_{1_0} + R_{\mathrm{PPV}i} \tag{2.71}$$

starting from the initial condition $d\Omega_0/d\gamma_p \cdot v_{1_0} = 0$. The solution at $i = -n$ is the sensitivity of the monodromy matrix multiplied by v_{1_0}

$$\frac{dM}{d\gamma_p}v_{1_0} = \frac{d\Omega_{-n}}{d\gamma_p}v_{1_0} \tag{2.72}$$

It is used to form the right hand side of (2.58).

The solution of the linear system in (2.58) is the initial condition for the PPV sensitivity waveform $v_{1_0}/d\gamma_p$, and the sensitivity of the oscillatory eigenvalue $d\lambda_1/d\gamma_p$. The eigenvalue sensitivity is ideally zero but the numerical solution is normally a small nonzero value.

Finally, the periodic sensitivity $dv_{1_i}/d\gamma_p$ of the PPV waveform along one period $i = -1, ..., -n$ is found by integrating equations in (2.59) backwards in time. This is done iteratively for $i = -1, ..., -n$

$$\left[\frac{1}{h}C_i^T + G_i^T\right]\frac{dv_{1_i}}{d\gamma_p} = \frac{1}{h}C_i^T\frac{dv_{1_{i+1}}}{d\gamma_p} + R_{\mathrm{PPV}i} \tag{2.73}$$

starting from the initial condition $v_{1_0}/d\gamma_p$ found from (2.58). Note that $R_{\mathrm{PPV}i}$ is available from (2.71) for all i.

The matrix-vector product computation routines or LU-factors for the matrices of the linear systems in (2.71) and (2.73) are available from the underlying PPV analysis employing the monodromy matrix method. Moreover, if the eigenvalue decomposition of the monodromy matrix M is done based on an Arnoldi iterative process, the matrix-vector product computation routine for matrix M is available. This routine can be easily extended to compute the matrix-vector product for the matrix in (2.58).

2.4 Examples and Results

We have implemented PSS and PPV sensitivity analyses in our Matlab-based circuit simulator, and in Berkeley Design Automation's RF FastSPICE. In this section the sensitivity of a ring oscillator to control voltage and device geometry is analyzed. It is shown that the PSS and PPV sensitivities can provide valuable information for applications such as oscillator design optimization, macromodeling, and predicting the impact of process variations.

The oscillator under consideration is a differential four-stage ring oscillator in Figure 2.4 that consists of four identical Maneatis delay cells [16]. The schematic

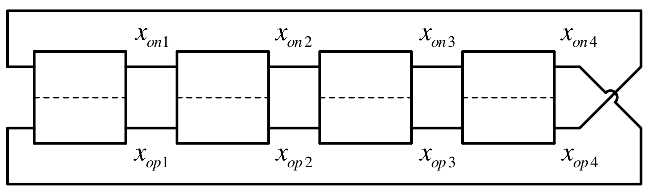

Figure 2.4: Block-diagram of the differential four-stage ring oscillator.

of the first delay cell is shown in Figure 2.5. An active biasing circuit in Figure 2.6 provides a dynamically changing voltage x_{bn} for the delay cells. We use x to denote nodal voltages (such as x_{ctrl}), and V to denote the nominal values of voltage sources (such as V_{ctrl}). The delay of a cell, and consequently, the oscillation frequency $f_0 = 1/T$ is set by the voltage at the control node x_{ctrl}. A V_{dd}-referred control voltage V_{ctrl} makes the circuit a voltage controlled oscillator (VCO).

All the simulation results for the presented sensitivity analysis were verified and are in good agreement with the results of a finite-difference based numerical sensitivity analysis method.

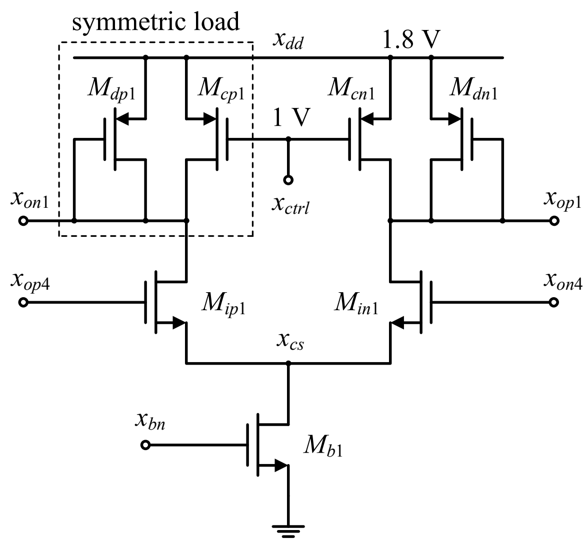

Figure 2.5: Schematic of the Maneatis delay cell with symmetric loads.

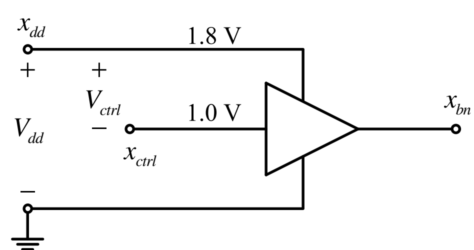

Figure 2.6: Block-diagram of the active biasing with a half-cell replica.

2.4.1 Sensitivity to the Control Voltage

In a phase-locked loop (PLL) [18], the VCO is operating at different frequencies, set by the control voltage. The oscillator sensitivities with respect to the control voltage are presented and discussed next. It is shown how these sensitivities can be postprocessed and used to compute the VCO gain, and the sensitivity of the power consumption, as well as to generate an accurate quadratic model of the VCO transfer curve $f_0(V_{ctrl})$ that maps the control voltage to the oscillation frequency.

A PSS sensitivity analysis with $\gamma_p \equiv V_{ctrl}$ finds sensitivities of the oscillation period and PSS waveforms with respect to the control voltage. The sensitivities are computed at the PSS solution with a nominal control voltage of $V^*_{ctrl} = 0.8$ V, corresponding to an oscillation period of $T = 0.7903$ ns.

The sensitivity of the oscillation period provided by the PSS sensitivity analysis is

$$\frac{dT}{dV_{ctrl}} = -3.2660 \ \frac{\text{ns}}{\text{V}}$$

This sensitivity allows us to compute the VCO gain, K_{VCO}, as

$$K_{VCO} = \frac{df_0}{dV_{ctrl}} = \frac{d\frac{1}{T}}{dV_{ctrl}} = -\frac{1}{T^2}\frac{dT}{dV_{ctrl}} = 5.2298 \ \frac{\text{GHz}}{\text{V}}$$

This is in good agreement with the VCO gain of 5.2186 GHz/V, computed based on the PPV later in this section, which validates the sensitivity of the oscillation period provided by the PSS sensitivity analysis.

Next consider the output voltages x_{op1}, x_{on1} from the first delay cell and the voltage at the control node x_{ctrl} in Figure 2.7(a). The sensitivities of these waveforms with respect to the control voltage are provided by the PSS sensitivity analysis (Figure 2.7(b)). In this example, the phase condition (2.3) is imposed by fixing the initial value of x_{op1} at 1.4 V. Consequently, the sensitivity of the initial point of dx_{op1}/dV_{ctrl} is zero.

Ideally, the outputs of a Maneatis delay cell swing between x_{ctrl} and V_{dd} as in Figure 2.7(a). The PSS sensitivities in Figure 2.7(b) predict that this property

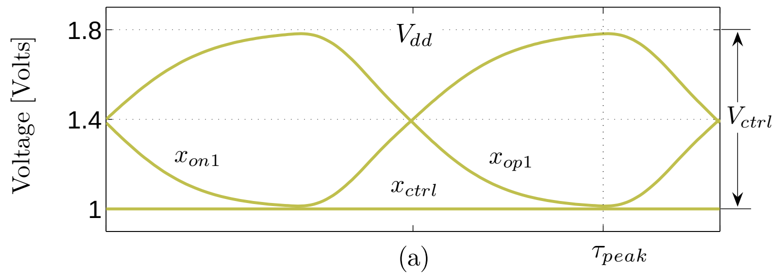

(a)

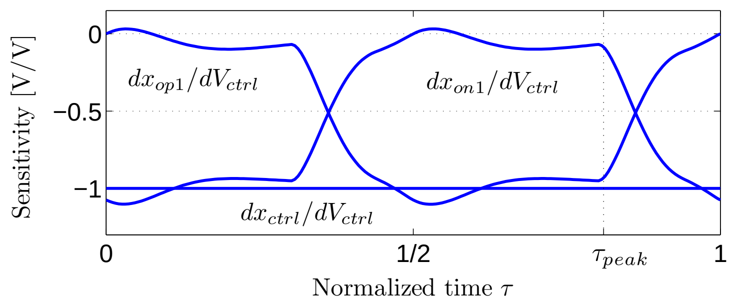

(b)

Figure 2.7: (a) The PSS solution and (b) PSS waveform sensitivities with respect to the control voltage.

is preserved while the control voltage varies around V^*_{ctrl}. For example, at time $\tau = \tau_{peak}$, shown in Figure 2.7,

$$\frac{dx_{on1}}{dV_{ctrl}} \approx 0 \qquad \text{and} \qquad \frac{dx_{op1}}{dV_{ctrl}} \approx \frac{dx_{ctrl}}{dV_{ctrl}}$$

This indicates that the highest level of x_{on1} remains nearly unchanged at V_{dd}, and the lowest level of x_{op1} follows the x_{ctrl} voltage.

The PSS sensitivities allow us to find an approximation of the PSS waveforms for any value of the control voltage that is sufficiently close to V^*_{ctrl}. For example, given the control voltage of $V^*_{ctrl} + \Delta V_{ctrl}$, the predicted steady-state waveform x

is given by

$$\underbrace{x(V_{ctrl}^* + \Delta V_{ctrl})}_{\text{predicted PSS}} \approx \underbrace{x(V_{ctrl}^*)}_{\text{original PSS}} + \underbrace{\overbrace{\Delta V_{ctrl}}^{\substack{\text{parameter}\\ \text{difference}}} \cdot \overbrace{\frac{dx}{dV_{ctrl}}}^{\substack{\text{PSS}\\ \text{sensitivity}}}}_{\text{predicted PSS difference}}$$

The accuracy of this prediction depends on how linear the dependence of the output PSS waveform on the control voltage is, and on how large ΔV_{ctrl} is.

Figure 2.8 shows the PSS waveforms and the predicted PSS waveform differences corresponding to a change of $\Delta V_{ctrl} = 50$ mV in the control voltage. This is

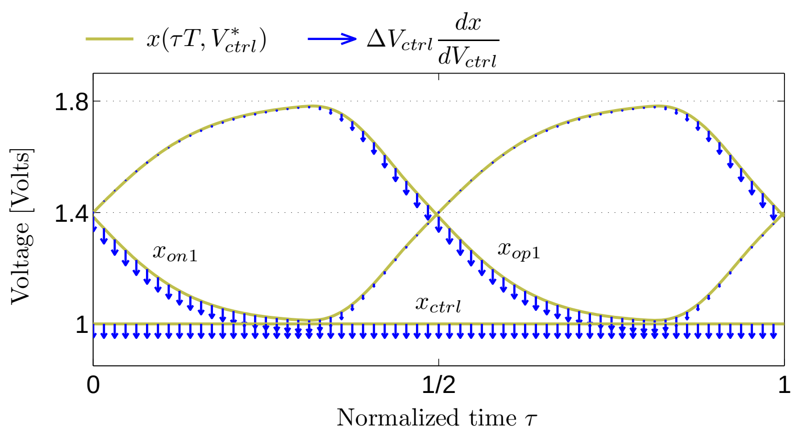

Figure 2.8: The PSS solution and the predicted PSS differences due to a difference of $\Delta V_{ctrl} = 50$ mV in the control voltage. The arrows depict how the individual PSS waveform samples are affected by the change in the control voltage.

another way of illustrating the PSS waveforms and their sensitivities in Figure 2.7. Again, it is seen that while the control voltage changes around V_{ctrl}^*, the output waveforms swing nearly between x_{ctrl} and V_{dd}.

Often it is more convenient to represent oscillator characteristics in the frequency domain. Figure 2.9 shows the magnitude spectra $|X(f)|$ of PSS waveforms.

The sensitivities of the individual magnitude spectrum components $d|X(f)|/d\gamma_p$ shown in Figure 2.9 are computed as

$$\frac{d|X|}{d\gamma_p} = \frac{\mathrm{Re}(X)\cdot\mathrm{Re}(X') + \mathrm{Im}(X)\cdot\mathrm{Im}(X')}{|X|}$$

where X' is the spectrum of $dx/d\gamma_p$.

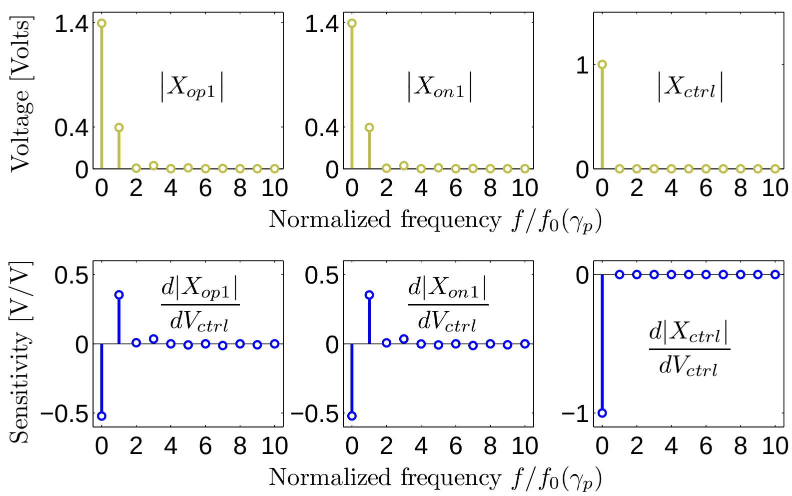

Figure 2.9: Magnitude spectra of the PSS waveforms in Figure 2.8 and their sensitivities with respect to the control voltage.

Let us take a closer look at Figure 2.9. The frequency-domain sensitivities predict that given ΔV_{ctrl}, the DC components of the output waveforms change nearly by half of ΔV_{ctrl} and stay in the middle of the ideal swing interval. The sensitivities of the magnitude components at the fundamental frequency frequency are less than 0.5 V/V. This means that the output peak-to-peak swing is going to be less than the maximum possible as V_{ctrl} increases. This is an expected result, as for higher control voltages the circuit oscillates at higher frequencies, and the output swing is limited by the rate of charging and discharging the output capacitances.

Next, consider the power consumption of the oscillator

$$P_c = -\frac{1}{T}\int_0^T V_{dd} x_{V_{dd}}(t)dt = -V_{dd} \cdot \mathrm{DC}(x_{V_{dd}}) = 6.3192 \text{ mW}$$

where $x_{V_{dd}}$ is the current flowing out of the oscillator into the power supply voltage source V_{dd} and $\mathrm{DC}(\cdot)$ denotes the DC or average value. The PSS sensitivity analysis provides data for computing the sensitivity of the power consumption to the control voltage

$$\frac{dP_c}{dV_{ctrl}} = -V_{dd} \cdot \mathrm{DC}\left(\frac{dx_{V_{dd}}}{dV_{ctrl}}\right) = 32.185 \ \frac{\text{mW}}{\text{V}}$$

In general, the voltage $x_{dd} - x_{ss}$ across a power supply voltage source V may depend on a parameter, i.e., $V = V(\gamma_p)$. In this case, a general expression for the power consumption sensitivity should be used

$$\frac{dP_c}{d\gamma_p} = -\mathrm{DC}\left(\left[\frac{dx_{dd}}{d\gamma_p} - \frac{dx_{ss}}{d\gamma_p}\right] x_V + \left[x_{dd} - x_{ss}\right]\frac{dx_V}{d\gamma_p}\right)$$

The power consumption sensitivity combined with the VCO gain results in the rate at which the power consumption changes with respect to a small change in the oscillation frequency

$$\frac{dP_c}{df_0} = \frac{dP_c}{dV_{ctrl}} \cdot \frac{1}{K_{VCO}} = 6.1543 \ \frac{\text{mW}}{\text{GHz}}$$

Next, consider the PPV $v_{1V_{ctrl}}$ in Figure 2.10 corresponding to the equation for the control source $x_{dd} - x_{ctrl} - V_{ctrl} = 0$. This PPV describes how much of a

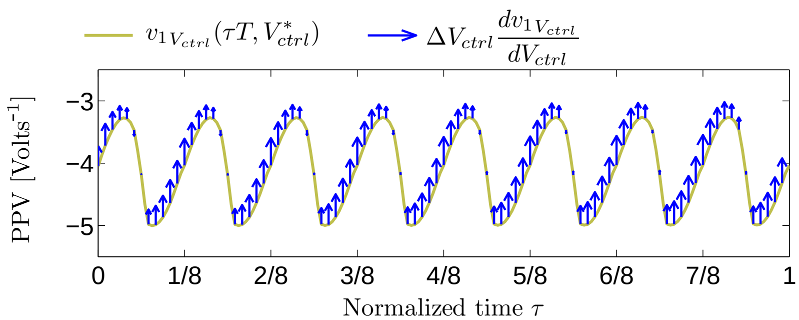

Figure 2.10: The PPV for the V_{ctrl} equation and the predicted change in the PPV due to a change $\Delta V_{ctrl} = 25$ mV in the control voltage. The arrows depict how the individual PPV waveform samples are affected by this change in the control voltage.

perturbation in the voltage at the control node projects into the oscillator phase deviation. The DC component of the PPV

$$\mathrm{DC}(v_{1V_{ctrl}}) = -4.1240 \ \mathrm{V}^{-1}$$

allows us to compute the VCO gain based on (2.6), and (2.7)

$$K_{VCO} = -f_0 \cdot \mathrm{DC}(v_{1V_{ctrl}}) = 5.2186 \ \frac{\mathrm{GHz}}{\mathrm{V}}$$

The PPV sensitivity analysis with $\gamma_p \equiv V_{ctrl}$ provides sensitivities of the PPV waveforms with respect to the control voltage. The PPV difference in Figure 2.10 shows how the PPV $v_{1V_{ctrl}}$ would change, given a change of $\Delta V_{ctrl} = 25$ mV in the control voltage. It is seen from Figure 2.10 that an increase in the control voltage decreases the magnitude of the DC component of the PPV, and therefore, the oscillator phase sensitivity to a DC voltage perturbation at the control node is decreased. The sensitivity of the DC component of the PPV is

$$\frac{d\,\mathrm{DC}(v_{1V_{ctrl}})}{dV_{ctrl}} = \mathrm{DC}\left(\frac{dv_{1V_{ctrl}}}{dV_{ctrl}}\right) = 12.202\ \frac{\mathrm{V}^{-1}}{\mathrm{V}}$$

This carries information about the curvature of the VCO transfer curve $f_0(V_{ctrl})$ around V^*_{ctrl}

$$\frac{d^2 f_0}{dV^2_{ctrl}} = \frac{dK_{VCO}}{dV_{ctrl}} = -\frac{d\big(f_0 \cdot \mathrm{DC}(v_{1V_{ctrl}})\big)}{dV_{ctrl}} = 6.0801\ \frac{\mathrm{GHz}}{\mathrm{V}^2}$$

Figure 2.11 shows that the slope and curvature descriptions, K_{VCO} and $\frac{dK_{VCO}}{dV_{ctrl}}$, allow us to generate an accurate quadratic model of the VCO transfer curve that provides a good approximation to $f_0(V_{ctrl})$ around V^*_{ctrl} for a wide range of frequencies around f^*_0.

The above analysis demonstrates that the PPV sensitivity analysis can be used to refine existing PPV-based oscillator macromodels [19], and extend their application to a wider range of control voltages around V^*_{ctrl}.

2.4.2 Sensitivity to Widths of Input Devices of Delay Cells

The geometry of individual MOSFET devices can change due to local process variations and result in mismatches in the differential structure of the oscillator, as well as in mismatches between delay cells. The effect of these mismatches on

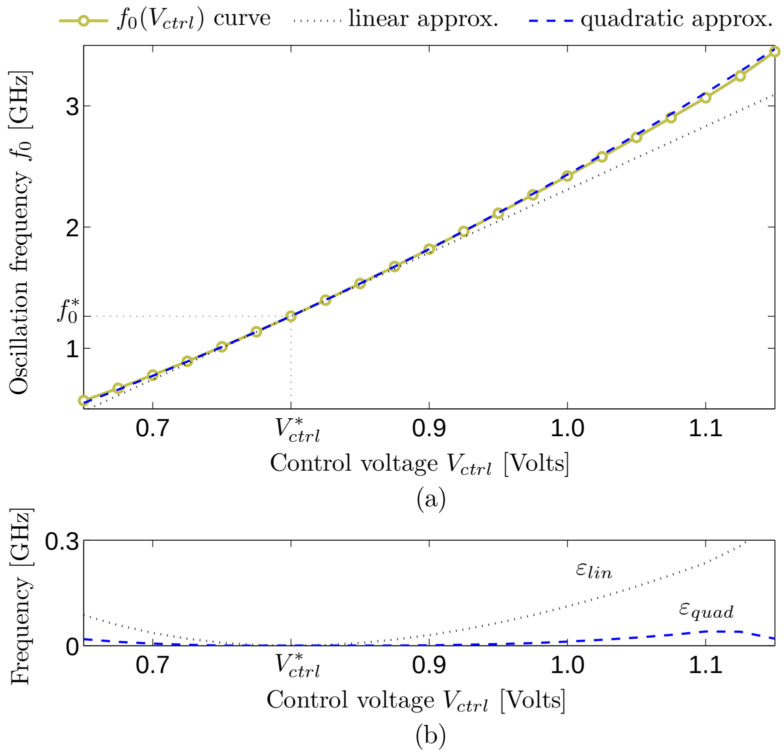

Figure 2.11: (a) VCO transfer curve $f_0(V_{ctrl})$, its linear, and quadratic approximations. (b) Errors of linear, and quadratic approximations ε_{lin}, and ε_{quad}.

oscillator signals can be predicted by an oscillator sensitivity analysis.

The PSS sensitivity analysis with respect to $\gamma_p \equiv W_{ip1}$ can be used to predict differences in PSS waveforms that correspond to a variation of $\Delta W_{ip1} = 10\ \mu$m in the width of M_{ip1}. These differences, as well as the PSS waveforms of output and common source voltages of all delay cells are shown in Figure 2.12. The sensitivity analysis shows that the mismatch between the input devices of a delay cell results in a change of the output duty cycle. It also shows an increase in the source voltage of M_{ip1} when the device is turned on.

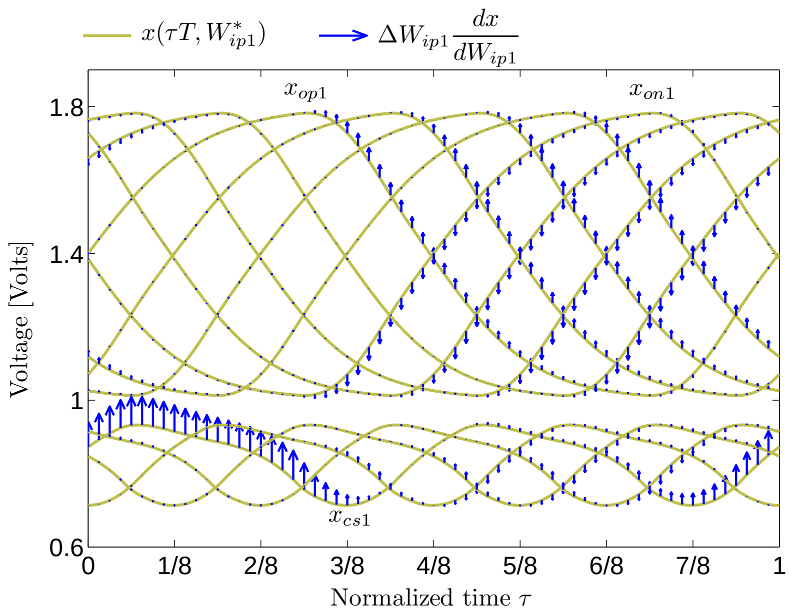

Figure 2.12: The PSS solution and the predicted PSS difference due to a difference of $\Delta W_{ip1} = 10$ μm in the width of M_{ip1}. The arrows depict how the individual PSS waveform samples are affected by the change in the width of M_{ip1}.

Next, consider the case with the parameter being the widths $\gamma_p \equiv W_{ip1} = W_{ip2}$ of both input devices of the first delay cell. The PSS waveforms and the differences corresponding to a variation of $\Delta W_{ip1} = \Delta W_{in1} = 10$ μm are shown in Figure 2.13. The PSS sensitivity analysis shows that if the input devices of the first delay cell are different than the input devices of other cells, the common source voltage x_{cs1} of the first delay cell is increased, and there is nearly no change in the output waveforms.

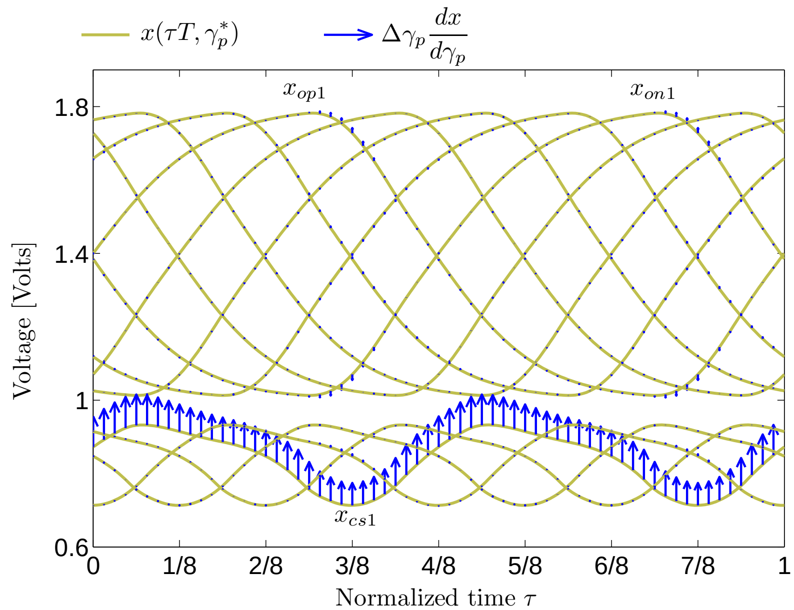

Figure 2.13: The PSS solution and the predicted PSS difference due to a difference of $\Delta\gamma_p = 10\ \mu$m in the widths of M_{ip1} and M_{in1}. The arrows depict how the individual PSS waveform samples are affected by the change in the widths of M_{ip1} and M_{in1}.

2.4.3 Sensitivity to Widths of Control Devices

One possible objective in optimizing an oscillator, is to achieve the best possible power supply noise rejection. The PPV $v_{1V_{dd}}$ corresponding to the V_{dd} equation is a measure of how much noise from the power supply is projected into the phase deviation. Therefore, a design with the smallest PPV magnitude has the best power supply noise rejection. PPV sensitivities with respect to various design parameters provide the direction of the steepest descent and lead to a design with a higher power supply noise rejection.

It is known that ring oscillators with the Maneatis delay cell reject the dynamic component of the power supply noise best when the load is symmetric, i.e., when the load devices M_c and M_d are equal. Next it will be shown that given a non-optimal oscillator design with non-symmetric loads, the PPV sensitivity analysis is able to guide a designer or an optimization loop in the direction of a better design.

Let the parameter γ_p be the widths of all control devices M_c, including M_{cp0} in the half-cell replica in Figure 2.6

$$\gamma_p \equiv W_{cp0} = W_{cp1} = \ldots = W_{cp4} = W_{cn1} = \ldots = W_{cn4}$$

These are the load devices with gate terminals connected to the control node. Figure 2.14(a) shows the PPV for the power supply voltage given symmetric loads with $\gamma_p^* = 30$ μm. As an illustration, consider a design with non-symmetric loads. Let the sizes of the control devices $\gamma_p^* = 45$ μm be 50% larger than the sizes of the diode-connected devices. The PPV for this case is presented in Figure 2.14(b). This PPV is larger than the PPV for the optimal design. The PPV sensitvity to γ_p shows that the larger widths should be decreased in order to obtain a design with a PPV of smaller magnitude. Figure 2.14(b) shows the predicted difference in the PPV corresponding to a change of -5 μm in the sizes of the larger load devices. Similarly, Figure 2.14(c) illustrates that the PPV sensitivity analysis correctly predicts that the sizes of the control devices should be increased when they are 50% smaller (15 μm) than the optimal value (30 μm).

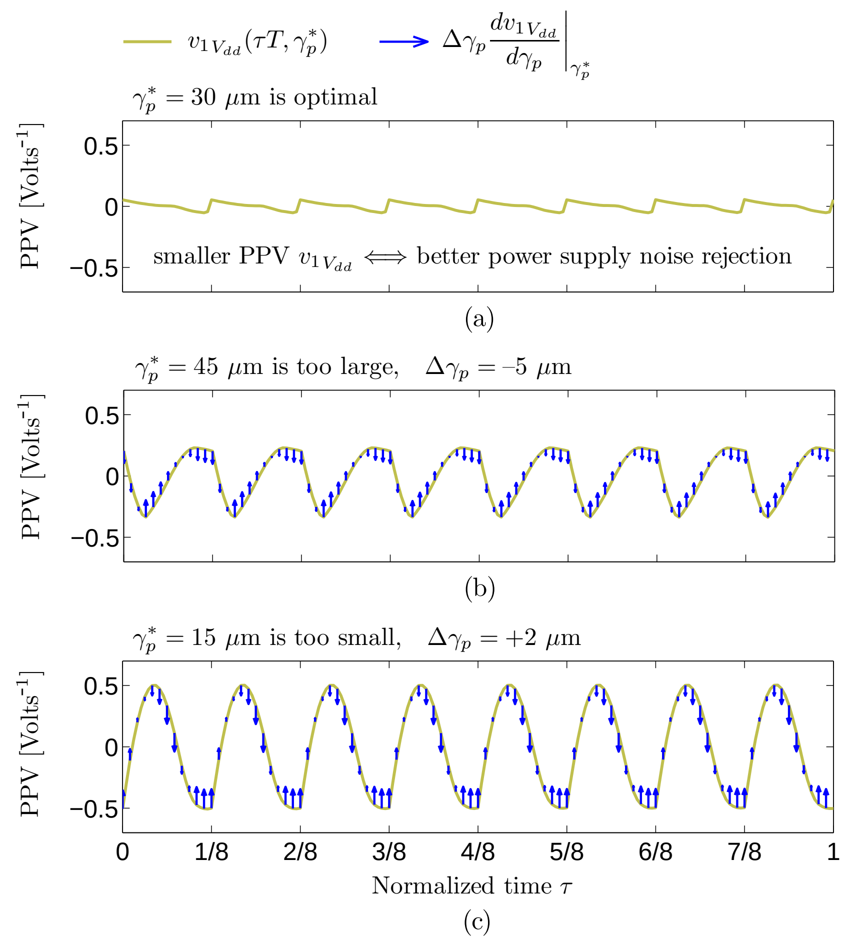

Figure 2.14: PPV for the V_{dd} equation for (a) optimal, (b) large, and (c) small values of the widths of the control devices, γ_p^*, and the predicted PPV differences for the non-optimum cases. The arrows depict how the individual PPV waveform samples are affected by a change in the widths of the load devices M_c.

Chapter 3 – Analysis of Circuits with Design Equality Constraints

In a typical design flow, a designer determines the topology and the values of circuit parameters that result in a desired circuit performance. However, conventional analyses available in circuit simulators solve the inverse problem. For a given circuit topology and parameters, these analyses determine the performance of a circuit without accounting for the design specifications. The conventional analyses have to be used in an iterative manner to improve a design in order to achieve the desired specifications.

This chapter focuses on a new design-oriented approach to circuit analysis. The capability of conventional analyses is extended to finding the values of circuit parameters such that the performance of a circuit meets a set of desired objectives. The new analyses handle specifications given by design equality constraints (DECs). The design objectives are met by performing a single analysis with constraints and circuit parameters being included in the analysis as additional equations and unknowns.

The design-oriented analysis is an elegant and efficient approach for solving problems with equality constraints, whereby nominal design specifications, or intermediate design goals can be met. The new analysis also has applications in accurately predicting the impact of parameter variations. The largest acceptable parameter variations for which the circuit performance remains within some boundaries, specified by equality constraints, can be determined.

In prior work [23], the DC operating point of an amplifier is obtained together with optimal device sizing by solving the circuit Kirchhoff laws and the design constraints as one system of equations. However, the design constraints for opamp performance are topology-specific approximations, and must be provided by an experienced designer. In [20], [21], a single oscillator parameter is tuned to obtain a desired oscillation frequency. The application of the periodic steady-state (PSS) analysis in [21] is limited to analyzing oscillators with a single constraint, i.e., a specification for the oscillation frequency.

A generalized formulation is presented in this chapter. It is capable of working with various design specifications and is independent of the circuit topology. The new analysis can simultaneously adjust multiple circuit parameters to satisfy several design specifications. Furthermore, the new design-oriented approach to circuit analysis with DECs is applicable to a range of basic analyses, such as PSS, DC and transient.

The design problem is defined as a set of nonlinear equality constraints in Section 3.1. A traditional search-based technique for solving the design problem is reviewed. The general theoretical formulation for the new design-oriented analysis is presented in Section 4.2. As an example, the PSS analysis augmented with design equality constraints (PSS-DEC) is presented. Time-domain finite-difference and shooting methods, as well as the frequency-domain harmonic balance method for the PSS-DEC analysis are described in detail in Section 3.3. In Section 3.4, the PSS-DEC analysis is used to demonstrate the efficiency of the new approach through examples. Simulation results for several circuits, including a voltage-controlled ring oscillator (VCO) and a two-stage operational amplifier, are given. The comparison of the new design-oriented analysis and the conventional search-based technique in terms of speed and convergence properties is summarized in Section 3.5. The new analysis approach is several times faster than conventional search-based techniques.

3.1 Design Problem and Search-Based Method

In this section, the design problem is defined as a set of nonlinear equality constraints. It is shown that this formulation is suitable for applications in nominal circuit design, and for analysis of marginally acceptable circuit operation. It is also shown that a conventional circuit analysis is incapable of solving this design problem. A traditional search-based technique for solving the design problem is reviewed.

3.1.1 Design Problem

For a given circuit topology, the values of circuit parameters are determined to meet the nominal design specifications, or to achieve intermediate design goals.

These design specifications are often given as equalities, such as

$$\begin{aligned} \text{duty cycle} &= 50~\% \\ \text{unity gain frequency} &= 40 \text{ MHz} \\ \text{oscillation frequency} &= 2.4 \text{ GHz} \\ \text{MOSFET drain-source voltage} &= 0.4 \text{ V} \end{aligned}$$

In the presence of process variations, different loading characteristics, and various input signals, the design performance deviates from the nominal. It is useful to find the range of parameter variations, e.g., acceptable ranges of capacitive loads or input signals, such that the performance remains within acceptable margins. The marginal circuit operation can be specified as equalities as well, e.g.,

$$\begin{aligned} \text{duty cycle} &= 50 \pm 2~\% \\ \text{phase margin} &= 60 \pm 5^\circ \end{aligned}$$

To determine the values of design or environmental parameters, such that the circuit has a desired nominal or marginal performance, we can formulate the constraint equations as

$$\begin{bmatrix} g_1\left(X_C,\ [\gamma_1, \ldots, \gamma_E]^T\right) \\ \vdots \\ g_E\left(X_C,\ [\gamma_1, \ldots, \gamma_E]^T\right) \end{bmatrix} = \begin{bmatrix} 0 \\ \vdots \\ 0 \end{bmatrix} \tag{3.1}$$

where $g_1, \ldots, g_E$ represent the individual specifications in terms of the circuit response X_C, and the tuning parameters $\gamma_1, \ldots, \gamma_E$. The circuit response X_C can be the DC operating point, the transient response, periodic steady-state waveform, its period, etc. The tuning parameters can be design parameters, such as MOSFET geometry parameters W_M, L_M, values of passive components R, L, C, process parameters, or environmental parameters, such as temperature, power supply voltage, excitation parameters, load capacitance, etc. The specifications g_e may be nonlinear.

An example of a DEC is a specification for the total harmonic distortion (THD). For a DEC that requires a THD of 1%

$$g_1\big(x(t), \Gamma_E\big) = \text{THD}\big(x(t)\big) - 1\% \tag{3.2}$$

Note that the THD is evaluated based on the harmonic content of the output signal in $x(t)$. Analytical expressions for G_E in terms of the circuit parameters Γ_E are not required.

Let $\Gamma_E = [\gamma_1, \ldots, \gamma_E]^T$ and $G_E = [g1, \ldots, g_E]^T$, then the design problem can be written using vector notation as

$$G_E(X_C, \Gamma_E) = 0 \tag{3.3}$$

In this work, we focus on the design problem in (3.3), with an equal number of parameters and constraints (E) that has an isolated solution.

3.1.2 Conventional Circuit Analyses

Conventional circuit analyses are not capable of solving the design problem in (3.3). Only the circuit performance X_C is determined without incorporating the design specifications.

$$\Gamma_E \rightarrow \boxed{\text{Analysis}} \rightarrow X_C(\Gamma_E) \tag{3.4}$$

For example, a PSS analysis may find the PSS solution $x(t)$ with an output duty cycle of 40%, while the design specification is 50%.

A conventional circuit analysis finds the circuit response X_C based on the analysis equations

$$F_C(X_C, \Gamma_E) = 0 \tag{3.5}$$

Given the values of circuit parameters in Γ_E, these equations are solved numerically for the circuit response X_C. With a Newton-based method, an initial guess $X_C^{(0)}$ is iteratively refined $X_C^{(1)}, \ldots, X_C^{(N_C)}$ until convergence is achieved. At iteration $k+1$, the equations that are solved are

$$\left.\frac{\partial F_C}{\partial X_C}\right|_{X_C^{(k)}} \cdot \left[X_C^{(k+1)} - X_C^{(k)}\right] = -F_C\left(X_C^{(k)}, \Gamma_E\right) \tag{3.6}$$

3.1.3 Conventional Search-Based Technique

In a traditional design approach, the solution to the design problem in (3.3) is obtained by searching for a suitable set of parameters Γ_E. Given an initial design $\Gamma_E^{(0)}$, the values of circuit parameters are updated manually by a designer, or automatically, in an iterative manner $\Gamma_E^{(1)}, \ldots, \Gamma_E^{(K)}$. At each search iteration $k = 0, \ldots, K$ a conventional circuit analysis provides the circuit response $X_C(\Gamma^{(k)})$ necessary to evaluate the DECs G_E

$$\begin{array}{c} \Gamma_E^{(0)} \to \boxed{\text{Analysis}} \to X_C(\Gamma_E^{(0)}) \\ \Gamma_E^{(1)} \to \boxed{\text{Analysis}} \to X_C(\Gamma_E^{(1)}) \\ \vdots \\ \Gamma_E^{(K)} \to \boxed{\text{Analysis}} \to X_C(\Gamma_E^{(K)}) \end{array} \tag{3.7}$$

The search process stops when $G_E\left(X_C(\Gamma_E^{(K)}), \Gamma_E^{(K)}\right) = 0$, and the desired specifications are met.

In case of an automated design, the Newton-Raphson method is applied directly to the DECs in (3.3). The values of the circuit parameters are obtained from

$$\left.\frac{dG_E}{d\Gamma_E}\right|_{\Gamma_E^{(k)}} \cdot \left[\Gamma_E^{(k+1)} - \Gamma_E^{(k)}\right] = -G_E\left(X_C(\Gamma_E^{(k)}), \Gamma_E^{(k)}\right) \tag{3.8}$$

where

$$\frac{dG_E}{d\Gamma_E} = \frac{\partial G_E}{\partial X_C} \cdot \frac{dX_C}{d\Gamma_E} + \frac{\partial G_E}{\partial \Gamma_E} \tag{3.9}$$

and the sensitivity of the circuit unknowns $dX_C/d\Gamma_E$ with respect to the circuit parameters $\gamma_1, \ldots, \gamma_E$ is obtained from E sensitivity analyses

$$\left.\frac{\partial F_C}{\partial X_C}\right|_{\Gamma_E^{(k)}} \cdot \left.\frac{dX_C}{d\Gamma_E}\right|_{\Gamma_E^{(k)}} = -\left.\frac{\partial F_C}{\partial \Gamma_E}\right|_{\Gamma_E^{(k)}} \tag{3.10}$$

This system of equation is obtained by differentiation of (3.5) with respect to Γ_E

at the current Newton iteration where $\Gamma_E = \Gamma_E^{(k)}$.

A good initial guess $X_C^{(k+1)}$ for the next analysis can be predicted using the sensitivity information $dX_C/d\Gamma_E$

$$X_C^{(k+1)} = X_C^{(k)} + \left.\frac{dX_C}{d\Gamma_E}\right|_{\Gamma_E^{(k)}} \cdot \left[\Gamma_E^{(k+1)} - \Gamma_E^{(k)}\right] \tag{3.11}$$

3.2 Design-Oriented Circuit Analysis

In this section, an elegant and efficient solution to the design problem in (3.3) is proposed. A general formulation of the new design-oriented analysis, that handles the design specifications, is described first. Then, the design-oriented PSS-DEC analysis is presented as an example.

3.2.1 General Formulation

A design-oriented circuit analysis is formulated by combining the conventional analysis equations in (3.5) and DECs in (3.3) together, while having X_C, and Γ_E as the unknowns of the new system of equations

$$\begin{bmatrix} F_C\left(X_C, \Gamma_E\right) \\ \hdashline G_E(X_C, \Gamma_E) \end{bmatrix} = \begin{bmatrix} 0 \\ \hdashline 0 \end{bmatrix} \tag{3.12}$$

Once the design goals are specified as equality constraints, and a suitable set of circuit parameters is defined, a single design-oriented analysis adjusts the values of the parameters Γ_E, such that the design goals are met, while simultaneously finding the corresponding circuit response X_C that satisfies the specifications

$$\begin{array}{|c|}\hline \text{Analysis} \\ \hline g_1 = 0 \\ \vdots \\ g_E = 0 \\ \hline \end{array} \quad \begin{array}{c} X_C \\ \gamma_1 \\ \vdots \\ \gamma_E \end{array} \qquad (3.13)$$

A Newton method is applied to (3.12). An initial guess $[X_C^{(0)}, \Gamma_E^{(0)}]^T$ is iteratively refined until convergence, $k = 1, \ldots, N_{\text{DEC}}$ according to

$$J \cdot \begin{bmatrix} X_C^{(k+1)} - X_C^{(k)} \\ \hdashline \Gamma_E^{(k+1)} - \Gamma_E^{(k)} \end{bmatrix} = - \begin{bmatrix} F_C\left(X_C^{(k)}, \Gamma_E^{(k)}\right) \\ \hdashline G_E\left(X_C^{(k)}, \Gamma_E^{(k)}\right) \end{bmatrix} \qquad (3.14)$$

with the Jacobian matrix

$$J = \left. \left[\begin{array}{c:c} \frac{\partial F_C}{\partial X_C} & \frac{\partial F_C}{\partial \Gamma_E} \\ \hdashline \frac{\partial G_E}{\partial X_C} & \frac{\partial G_E}{\partial \Gamma_E} \end{array} \right] \right|_{X_C^{(k)},\ \Gamma_E^{(k)}} \qquad (3.15)$$

The upper-left square block of (3.15) is the same as the Jacobian of the conventional analysis in (3.6). The upper-right columns of J are the same as the right-hand side for the sensitivity analysis in (3.10). These sensitivities are obtained from the device models. The bottom rows of J are obtained by differentiating the expressions for the equality constraints G_E with respect to the conventional analysis variables X_C, and the circuit parameters Γ_E. These derivatives are the same as the components for the Jacobian of the search-based method in (3.9).

The solution of (3.12) $[X_C, \Gamma_E]^T$ simultaneously satisfies the equations of the conventional analysis in (3.5), and the design problem in (3.3).

Newton method has local convergence, and therefore, the initial guess must be close enough to the solution. The values of the tuning parameters Γ_E, and the response $X_C(\Gamma_E)$ of the original circuit is a reasonable initial guess for the new design-oriented analysis with DECs.

There may be no solution to the design problem with DECs in (3.3), which means that the design specifications can not be satisfied by tuning the values of the selected parameters. Selection of a suitable set of parameters requires a good understanding of the design, and is delegated to a designer.

Numerical methods that are employed in the conventional analysis for solving (3.5), are also applicable to the augmented system of equations in (3.12). As shown in Section 3.5 a single analysis augmented with DECs solves the design problem faster than a conventional search-based technique.

It is important to note the following features of the new analysis. First, the design specifications must be expressed as equalities that can be nonlinear. Second, the specifications must be expressed in terms of the solution of the conventional analysis X_C, and parameters Γ_E. Performance specifications that are not directly available from a conventional analysis, can not be handled by the design-oriented analysis. For example, specifications for noise performance can not be handled by the PSS-DEC analysis, as the noise performance is not directly available from a conventional PSS analysis.

The design-oriented circuit analysis approach is applicable to conventional analyses, such as DC, transient, and PSS. In this chapter we focus on the PSS analysis.

3.2.2 Design-Oriented Periodic Steady-State Analysis

As an example, we present a detailed description of the design-oriented periodic steady-state analysis augmented with design equality constraints. We call it the PSS-DEC analysis.

Any nonlinear circuit can be modeled as a set of m differential-algebraic equations (DAEs) given by

$$\frac{d}{dt}q\big(x(t),\Gamma_E\big) + f\big(x(t),\Gamma_E\big) + b(t,\Gamma_E) = 0 \tag{3.16}$$

where

$$\begin{aligned}
t \in \mathbb{R} \quad &: \text{ time, independent variable,}\\
x : \mathbb{R} \to \mathbb{R}^m &: \text{ circuit variables,}\\
q : \mathbb{R}^m \times \mathbb{R}^E \to \mathbb{R}^m &: \text{ contribution of reactive components,}\\
f : \mathbb{R}^m \times \mathbb{R}^E \to \mathbb{R}^m &: \text{ contribution of resistive components,}\\
b : \mathbb{R} \times \mathbb{R}^E \to \mathbb{R}^m &: \text{ excitations and independent sources.}
\end{aligned}$$

The T-periodic solution $x(t)$ of the DAEs in (3.16) is called the PSS solution if it satisfies $x(t) = x(t+T)$. This periodicity constraint can be expressed as

$$x(0) = x(T) \tag{3.17}$$

For oscillators, the excitation b does not vary with time, and the period T is an unknown. If $x(t)$ is a PSS solution, then $x(t + \Delta t)$, $\forall \Delta t$ is also a valid PSS solution, whereby there are several possible phase-shifted solutions. A unique isolated solution can be selected by imposing a phase condition

$$\varphi\big(x(0)\big) = 0, \quad \varphi : \mathbb{R}^m \to \mathbb{R} \tag{3.18}$$

One possible phase condition is to let a component of $x(0)$ be a fixed value.

The PSS $x(t)$ and the oscillation period T of an oscillator are uniquely defined by (3.16), (3.17), and (3.18)

$$\begin{cases} \frac{d}{dt} q\big(x(t), \Gamma_E\big) + f\big(x(t), \Gamma_E\big) + b(\Gamma_E) = 0 \\ x(0) = x(T) \\ \varphi\big(x(0)\big) = 0 \end{cases} \tag{3.19}$$

The description in (3.19) is a periodic boundary value problem (BVP) in $x(t)$ and T, a special case of a two-point BVP [15].

A design-oriented PSS-DEC analysis is based on the PSS formulation in (3.19) augmented with the DECs

$$\left[\begin{array}{c} \frac{d}{dt}q\big(x(t),\Gamma_E\big) + f\big(x(t),\Gamma_E\big) + b(\Gamma_E) \\ x(0) - x(T) \\ \varphi\big(x(0)\big) \\ \hdashline G_E\left(x(t), T, \Gamma_E\right) \end{array}\right] = \left[\begin{array}{c} 0 \\ 0 \\ 0 \\ \hdashline 0 \end{array}\right] \tag{3.20}$$

Note that Γ_E is now included in the list of unknowns.

In forced circuits, a T_{in}-periodic excitation $b(t, \Gamma_E)$ uniquely defines the initial phase and the steady-state period. As shown in [22], the PSS-DEC analysis for forced circuits is based on a simplified version of (3.20) with the initial phase condition equation removed and T set to the known period T_{in}. Here we focus on a PSS-DEC analysis for autonomous circuits.

3.3 Numerical Methods for the PSS-DEC Analysis

The numerical methods applicable to the DAEs in (3.19) are also applicable to the PSS-DEC formulation in (3.20). In this section, finite difference, shooting and the harmonic balance methods for computing the periodic steady-state in the presence of design equality constraints are presented.

3.3.1 Discrete-Time Circuit Description

For numerical time-domain PSS analysis, time is discretized and the time-derivative operator is replaced by a finite-difference approximation. As an example, using uniformly spaced timepoints $t_i = ih$, $i \in \mathbb{N}$ and applying the backward Euler method, a simple discrete counterpart of (3.20) for $t \in (0, T]$ is

$$\begin{bmatrix} \dot{q}_1 + f_1 + b \\ \vdots \\ \dot{q}_n + f_n + b \\ x_0 - x_n \\ \varphi(x_0) \\ \hdashline G_E\left(x_0, \ldots, x_n, T, \Gamma_E\right) \end{bmatrix} = \begin{bmatrix} 0 \\ \vdots \\ 0 \\ 0 \\ 0 \\ \hdashline 0 \end{bmatrix} \tag{3.21}$$

where

$$\begin{aligned} \dot{q}_i &= \tfrac{1}{h}(q_i - q_{i-1}), & x_i &\equiv x(t_i), \\ q_i &= q(x_i, \Gamma_E), & t_i &= ih, \\ f_i &= f(x_i, \Gamma_E), & h &= h(T) = T/n, \\ b_i &= b(t_i, \Gamma_E). \end{aligned}$$

The discrete-time description in (3.21) is a square system of $nm + m + 1 + E$ nonlinear algebraic equations. The equations are written in terms of $(n + 1)m$ PSS waveform samples $x_0, \ldots, x_n$, the oscillation period T and E circuit parameters

$\gamma_1, \ldots, \gamma_E$.

3.3.2 Finite Difference Method for the PSS-DEC Analysis

$$
J_{fd} = \left[\begin{array}{ccccc:c}
\frac{1}{h}C_1 + G_1 & & & -\frac{1}{h}C_n & -\frac{1}{h}\left(\frac{q_1}{T} - \frac{q_n}{T}\right) & \frac{1}{h}\left(\frac{\partial q_1}{\partial \Gamma_E} - \frac{\partial q_n}{\partial \Gamma_E}\right) + \frac{\partial f_1}{\partial \Gamma_E} + \frac{\partial b}{\partial \Gamma_E} \\
-\frac{1}{h}C_1 & \frac{1}{h}C_2 + G_2 & & & -\frac{1}{T}\dot{q}_2 & \frac{1}{h}\left(\frac{\partial q_2}{\partial \Gamma_E} - \frac{\partial q_1}{\partial \Gamma_E}\right) + \frac{\partial f_2}{\partial \Gamma_E} + \frac{\partial b}{\partial \Gamma_E} \\
& \ddots & \ddots & & \vdots & \vdots \\
& & -\frac{1}{h}C_{n-1} & \frac{1}{h}C_n + G_n & -\frac{1}{T}\dot{q}_n & \frac{1}{h}\left(\frac{\partial q_n}{\partial \Gamma_E} - \frac{\partial q_{n-1}}{\partial \Gamma_E}\right) + \frac{\partial f_n}{\partial \Gamma_E} + \frac{\partial b_n}{\partial \Gamma_E} \\
& & & & \left.\frac{d\varphi}{dx}\right|_{x_n} & \Big) + \\
\hdashline
\frac{\partial g_1}{\partial x_1} & \frac{\partial g_1}{\partial x_2} & \cdots & \frac{\partial g_1}{\partial x_n} & \frac{\partial g_1}{\partial T} & \frac{\partial g_1}{\partial \Gamma_E} \\
\vdots & \vdots & & \vdots & \vdots & \vdots \\
\frac{\partial g_E}{\partial x_1} & \frac{\partial g_E}{\partial x_2} & \cdots & \frac{\partial g_E}{\partial x_n} & \frac{\partial g_E}{\partial T} & \frac{\partial g_E}{\partial \Gamma_E}
\end{array}\right] \tag{3.22}
$$

The equations in (3.21) can be written in the following form

$$\left[\begin{array}{c} \frac{1}{h}(q_1 - q_n \quad) + f_1 + b \\ \frac{1}{h}(q_2 - q_1 \quad) + f_2 + b \\ \vdots \\ \frac{1}{h}(q_n - q_{n-1}) + f_n + b \\ \varphi(x_n) \\ \hdashline G_E\left(x_1, \ldots, x_n, T, \Gamma_E\right) \end{array}\right] = \left[\begin{array}{c} 0 \\ 0 \\ \vdots \\ 0 \\ 0 \\ \hdashline 0 \end{array}\right] \tag{3.23}$$

Note that the periodicity constraint $x_0 = x_n$ is not explicitly present in the above system. The periodicity constraint equation was used to eliminate x_0 from the list of unknowns. The remaining $nm + 1 + E$ equations represent a finite-difference formulation of the PSS-DEC analysis.

The Jacobian matrix of the finite-difference method for the PSS analysis augmented with DECs is given by (3.22),

$$J_{fd} : \underbrace{\mathbb{R}^m \times \ldots \times \mathbb{R}^m}_{n} \times \mathbb{R} \times \mathbb{R}^E \rightarrow \mathbb{R}^{(nm+1+E)\times(nm+1+E)}.$$

The Jacobian matrix is defined in terms of C_i and G_i, the capacitance and conductance matrices

$$C_i = \frac{\partial q_i}{\partial x_i} = \left.\frac{\partial q(x, \Gamma_E)}{\partial x}\right|_{x_i}, \; C_i : \mathbb{R}^m \times \mathbb{R}^E \rightarrow \mathbb{R}^{m\times m} \tag{3.24}$$

$$G_i = \frac{\partial f_i}{\partial x_i} = \left.\frac{\partial f(x, \Gamma_E)}{\partial x}\right|_{x_i}, \; G_i : \mathbb{R}^m \times \mathbb{R}^E \rightarrow \mathbb{R}^{m\times m} \tag{3.25}$$

3.3.3 Shooting Method for the PSS-DEC Analysis

The last $m+1+E$ equations in (3.21) represent a shooting formulation of the PSS analysis

$$\left[\begin{array}{c} x_n(x_0, T, \Gamma_E) - x_0 \\ \varphi(x_0) \\ \hdashline G_E\left(x_0, T, \Gamma_E\right) \end{array}\right] = \left[\begin{array}{c} 0 \\ 0 \end{array}\right] \tag{3.26}$$

where the unknowns are x_0, T, and Γ_E.

Given Γ_E, x_n is obtained from a transient analysis for the interval $t \in [0, T]$ with an initial condition x_0 using the first nm equations in (3.21). After the solution x_0 and T are found, the remaining PSS waveform samples x_i, $i = 1, \ldots, n$ are obtained from an additional transient analysis.

The Jacobian matrix of the shooting method for the PSS analysis augmented with DECs is given by (3.27), $J_{sh} : \mathbb{R}^m \times \mathbb{R} \times \mathbb{R}^E \to \mathbb{R}^{(m+1+E)\times(m+1+E)}$,

$$J_{sh} = \left[\begin{array}{cc:cccc} \frac{\partial x_n}{\partial x_0} - I & \frac{\partial x_n}{\partial T} & \frac{\partial x_n}{\partial \gamma_1} & \cdots & \frac{\partial x_n}{\partial \gamma_E} \\ \frac{\partial \varphi}{\partial x}\Big|_{x_0} & & & & \\ \hdashline \frac{dg_1}{dx_0} & \frac{\partial g_1}{dT} & \frac{dg_1}{d\gamma_1} & \cdots & \frac{dg_1}{d\gamma_E} \\ \vdots & \vdots & \vdots & \ddots & \vdots \\ \frac{dg_E}{dx_0} & \frac{dg_E}{dT} & \frac{dg_E}{d\gamma_1} & \cdots & \frac{dg_E}{d\gamma_E} \end{array}\right] \tag{3.27}$$

where I is the identity matrix.

Computation of the Jacobian requires differentiation of the first nm equations in (3.21) with respect to x_0, T and Γ_E

$$\left[\frac{1}{h}C_i + G_i\right]\frac{\partial x_i}{\partial x_0} = \frac{1}{h}C_{i-1}\frac{\partial x_{i-1}}{\partial x_0} \tag{3.28}$$

$$\left[\frac{1}{h}C_i + G_i\right]\frac{\partial x_i}{\partial T} = \frac{1}{h}C_{i-1}\frac{\partial x_{i-1}}{\partial T} + \frac{1}{T}\dot{q}_i \tag{3.29}$$

$$\begin{aligned}\left[\frac{1}{h}C_i + G_i\right]\frac{\partial x_i}{\partial \Gamma_E} = {} & \frac{1}{h}C_{i-1}\frac{\partial x_{i-1}}{\partial \Gamma_E} \\ & -\frac{1}{h}\left(\frac{\partial q_i}{\partial \Gamma_E} - \frac{\partial q_{i-1}}{\partial \Gamma_E}\right) - \frac{\partial f_i}{\partial \Gamma_E} - \frac{db}{d\Gamma_E}\end{aligned} \tag{3.30}$$

The derivatives $\partial x_n/\partial x_0$, $\partial x_n/\partial T$, and $\partial x_n/\partial \Gamma_E$ are obtained from (3.28), (3.29), and (3.30) iteratively for $i = 1, \ldots, n$ starting from the initial conditions $\partial x_0/\partial x_0 = I$, $\partial x_0/\partial T = 0$, and $\partial x_0/\partial \Gamma_E = 0$.

Note that the constraints G_E are written in terms of x_0. The rest of the PSS waveform samples $x_1, \ldots, x_n$ are expressed in terms of x_0 as, e.g., $x_n(x_0, T, \Gamma_E)$, and they can still be used in specifying the DECs, such as the amplitude of oscillation. Therefore, the total sensitivities of the DECs with respect to x_0, T, and Γ_E in (3.27) are computed with the use of the chain rule and the sensitivities dx_i/dx_0, dx_i/dT, and $dx_i/d\Gamma_E$ from (3.28), (3.29), and (3.30), respectively

$$\frac{dG_E}{dx_0} = \frac{\partial G_E}{\partial x_0} + \sum_{i=1}^{n}\frac{\partial G_E}{\partial x_i}\cdot\frac{dx_i}{dx_0} \tag{3.31}$$

$$\frac{dG_E}{dT} = \frac{\partial G_E}{\partial T} + \sum_{i=1}^{n} \frac{\partial G_E}{\partial x_i} \cdot \frac{dx_i}{dT} \tag{3.32}$$

$$\frac{dG_E}{d\Gamma_E} = \frac{\partial G_E}{\partial \Gamma_E} + \sum_{i=1}^{n} \frac{\partial G_E}{\partial x_i} \cdot \frac{dx_i}{d\Gamma_E} \tag{3.33}$$

3.3.4 Harmonic Balance Method for the PSS-DEC Analysis

$$J_{hb} = \left[\begin{array}{cccccccc|c}
\multicolumn{7}{c}{j\Omega\Gamma \begin{bmatrix} C_0 & & \\ & \ddots & \\ & & C_{n-1} \end{bmatrix} \Gamma^{-1} + \Gamma \begin{bmatrix} G_0 & & \\ & \ddots & \\ & & G_{n-1} \end{bmatrix} \Gamma^{-1}} & j\frac{\Omega}{f_0}\Gamma \begin{bmatrix} q_0 \\ \vdots \\ q_{n-1} \end{bmatrix} & j\Omega\Gamma \begin{bmatrix} \frac{\partial q_0}{\partial \Gamma_E} \\ \vdots \\ \frac{\partial q_{n-1}}{\partial \Gamma_E} \end{bmatrix} + \Gamma \begin{bmatrix} \frac{\partial f_0}{\partial \Gamma_E} \\ \vdots \\ \frac{\partial f_{n-1}}{\partial \Gamma_E} \end{bmatrix} + \begin{bmatrix} 0 \\ \frac{\partial b}{\partial \Gamma_E} \\ 0 \end{bmatrix} \\
\cdots & \frac{\partial \varphi_{hb}}{\partial X_{-2}} & \frac{\partial \varphi_{hb}}{\partial X_{-1}} & \frac{\partial \varphi_{hb}}{\partial X_{0}} & \frac{\partial \varphi_{hb}}{\partial X_{1}} & \frac{\partial \varphi_{hb}}{\partial X_{2}} & \cdots & 0 & 0 \\
\hline
\cdots & \frac{\partial g_1}{\partial X_{-2}} & \frac{\partial g_1}{\partial X_{-1}} & \frac{\partial g_1}{\partial X_{0}} & \frac{\partial g_1}{\partial X_{1}} & \frac{\partial g_1}{\partial X_{2}} & \cdots & \frac{\partial g_1}{\partial f_0} & \frac{\partial g_1}{\partial \Gamma_E} \\
 & \vdots & \vdots & \vdots & \vdots & \vdots & & \vdots & \vdots \\
\cdots & \frac{\partial g_E}{\partial X_{-2}} & \frac{\partial g_E}{\partial X_{-1}} & \frac{\partial g_E}{\partial X_{0}} & \frac{\partial g_E}{\partial X_{1}} & \frac{\partial g_E}{\partial X_{2}} & \cdots & \frac{\partial g_E}{\partial f_0} & \frac{\partial g_E}{\partial \Gamma_E}
\end{array}\right] \tag{3.34}$$

The n-periodic discrete-time waveforms x_i can be uniquely represented as an n-

periodic sequence of impulses in the frequency domain at multiples of the oscillation frequency $f_0 = 1/T$. Given the DECs, the harmonic balance method for the PSS-DEC analysis finds the oscillation frequency f_0, parameters Γ_E, and n Fourier coefficients X_k, $X_k \in \mathbb{C}^m$, $k = \ldots, -1, \quad 0, +1, \ldots$ of the PSS solution waveform

$$\begin{bmatrix} \vdots \\ X_{-1} \\ X_0 \\ X_1 \\ \vdots \end{bmatrix} = \Gamma \begin{bmatrix} x_0 \\ \vdots \\ x_{n-1} \end{bmatrix} \tag{3.35}$$

where $\Gamma : \underbrace{\mathbb{R}^m \times \ldots \times \mathbb{R}^m}_{n} \to \underbrace{\mathbb{C}^m \times \ldots \times \mathbb{C}^m}_{n}$ represents the discrete-time Fourier transform operator, defined by

$$X_k = \frac{1}{n} \sum_{i=0}^{n-1} x_i e^{-j2\pi ki/n} \tag{3.36}$$

After the Fourier coefficients X_k are found, the inverse Fourier transform Γ^{-1} is used to get the time-domain PSS solution

$$x_i = \sum_{k=0}^{n-1} X_k e^{j2\pi ki/n} \tag{3.37}$$

where n-periodicity of X_k was used.

The harmonic balance method for the PSS-DEC analysis can be formulated as a system of $nm + 1 + E$ nonlinear equations

$$\left[\begin{array}{c} j\Omega\Gamma \begin{bmatrix} q_0 \\ \vdots \\ q_{n-1} \end{bmatrix} + \Gamma \begin{bmatrix} f_0 + b \\ \vdots \\ f_{n-1} + b \end{bmatrix} \\ \varphi_{hb}(\ldots, X_{-1}, X_0, X_1, \ldots) \\ \hdashline G_E\left(\ldots, X_{-1}, X_0, X_1, \ldots, f_0, \Gamma_E\right) \end{array}\right] = \left[\begin{array}{c} 0 \\ \vdots \\ 0 \\ 0 \\ \hdashline 0 \end{array}\right] \tag{3.38}$$

where the unknowns are $X_k,\ k = \ldots, -1,\ \ 0, +1, \ldots,\ f_0$, and Γ_E. The first nm equations in (3.38) correspond to the first nm equations in (3.21). Notice that the equations in (3.38) are algebraic. The time-domain differentiation in (3.21) is replaced by a frequency domain multiplication with $j\Omega$,

$$j\Omega : \underbrace{\mathbb{C}^m \times \ldots \times \mathbb{C}^m}_{n} \to \underbrace{\mathbb{C}^m \times \ldots \times \mathbb{C}^m}_{n}$$

such that

$$\begin{bmatrix} \dot{q}_0 \\ \vdots \\ \dot{q}_{n-1} \end{bmatrix} = \Gamma^{-1} j\Omega\Gamma \begin{bmatrix} q_0 \\ \vdots \\ q_{n-1} \end{bmatrix} \tag{3.39}$$

with

$$\Omega = 2\pi f_0 \begin{bmatrix} \ddots & & & & \\ & -I & & & \\ & & 0 & & \\ & & & I & \\ & & & & \ddots \end{bmatrix} \tag{3.40}$$

where I is the identity matrix, $I \in R^{m \times m}$, and $0 \in R^{m \times m}$.

The periodicity constraint of (3.21) $x_n = x_0$ is not explicitly present in (3.38). It is enforced by the periodic nature of the complex exponential basis functions of the inverse Fourier transform in (3.37).

Similar to the phase condition equation in (3.21), the equation $\varphi_{hb} = 0$ in (3.38),

$$\varphi_{hb} : \underbrace{\mathbb{C}^m \times \ldots \times \mathbb{C}^m}_{n} \to \mathbb{R}$$

is used to select a unique isolated solution among an infinite set of valid phase-shifted solutions. A commonly used phase condition is to let the imaginary part of the first Fourier coefficient of a component of the PSS solution be zero.

The Jacobian matrix of the harmonic balance method for the PSS analysis augmented with DECs

$$J_{hb} : \underbrace{\mathbb{C}^m \times \ldots \times \mathbb{C}^m}_{n} \times \mathbb{R} \to \mathbb{C}^{(nm+1+E)\times(nm+1+E)}$$

requires the sensitivities of the Fourier coefficients of q_i and f_i with respect to

X_k. These sensitivities can be calculated analytically for linear circuit components and for devices which are defined in the frequency domain, such as delays and transmission lines. The sensitivities of the nonlinear resistive device contributions can be computed as

$$\frac{\partial \Gamma \begin{bmatrix} f_0 \\ \vdots \\ f_{n-1} \end{bmatrix}}{\partial \begin{bmatrix} \vdots \\ X_{-1} \\ X_0 \\ X_1 \\ \vdots \end{bmatrix}} = \Gamma \frac{\partial \begin{bmatrix} f_0 \\ \vdots \\ f_{n-1} \end{bmatrix}}{\partial \Gamma \begin{bmatrix} x_0 \\ \vdots \\ x_{n-1} \end{bmatrix}} = \Gamma \begin{bmatrix} G_0 & & \\ & \ddots & \\ & & G_{n-1} \end{bmatrix} \Gamma^{-1} \tag{3.41}$$

and require time domain evaluations of the conductance matrices G_i. The sensitivities due to the nonlinear reactive devices require the capacitance matrices C_i and can be computed in a manner similar to (3.41). The harmonic balance Jacobian matrix J_{hb} is given by (3.34).

3.4 Examples and Results

We have implemented the PSS-DEC analysis in a Matlab-based circuit simulator. In this section, a differential four-stage ring VCO, a two-stage operational amplifier [25], and a feedback circuit are used to demonstrate the application of the new design-oriented analysis.

The design-oriented PSS-DEC is used to adjust the device sizes in a ring VCO for a desired duty cycle, output waveform symmetry, oscillation frequency, and other specifications. The PSS-DEC is also applied to a nominal VCO design to compute the effect of mismatches on the duty cycle. It is then shown how the PSS-DEC analysis can handle commonly used op amp specifications. Constraints for harmonic distortion, unity gain bandwidth, phase margin, and power consumption are considered.

3.4.1 Design of a Ring Oscillator

The oscillator under consideration is a differential four-stage ring oscillator in Figure 3.1 that consists of four identical Lee-Kim delay cells [27]. The schematic of

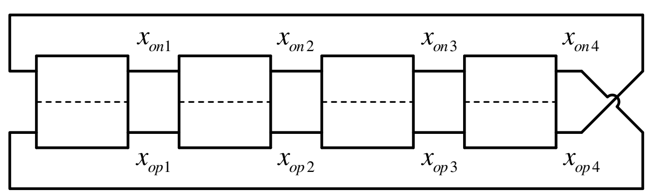

Figure 3.1: Block-diagram of the differential four-stage ring oscillator.

the first delay cell is shown in Figure 3.2. A feed forward duty cycle corrector in Figure 3.3 utilizes the 180° shifted output signals x_{op1} and x_{on1} to produce a 50% duty cycle output x_{out} [27].

In the original design, the widths of all p-channel and n-channel devices are 60 μm and 20 μm, respectively. An analysis is performed at the upper limit of the

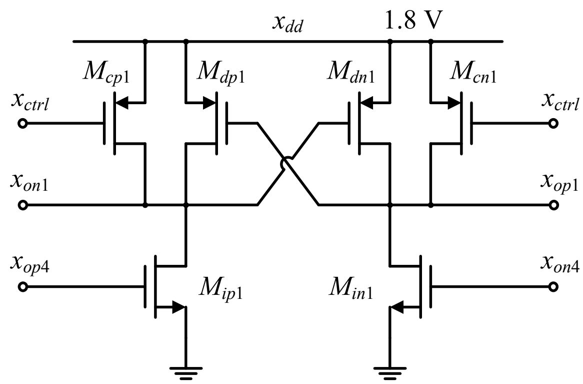

Figure 3.2: Schematic of the Lee-Kim delay cell [27].

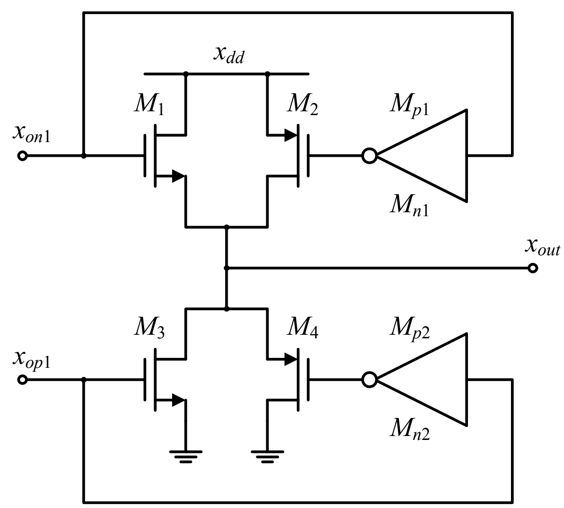

Figure 3.3: Schematic of the feed forward duty cycle corrector.

tuning range (the oscillation frequency is 1 GHz), where the performance is the most critical. The steady-state performance of the original design is obtained from a conventional PSS analysis

$$
\begin{array}{rl}
V_c = & 1.47\ \mathrm{V} \\
W_{\mathrm{pMOS}} = & 60.00\ \mu\mathrm{m} \\
W_{\mathrm{nMOS}} = & 20.00\ \mu\mathrm{m}
\end{array}
\rightarrow \boxed{\mathrm{PSS}} \rightarrow
\begin{array}{rl}
 & x(t) \\
T = & 1.00\ \mathrm{ns} \\
P_c = & 25.38\ \mathrm{mW} \\
D_{out} = & 49.23\% \\
S_{up}/S_{dn} = & -3.97 \\
\left|X_{op1_1}\right| = & 0.63\ \mathrm{V} \\
L_X = & 1.11\ \mathrm{V}
\end{array}
$$

where P_c is the power consumption, D_{out} is the duty cycle, L_X is the intersect level of the output voltages of the first delay cell x_{op1} and x_{on1}, as shown in Figure 3.4(a). S_{up} and S_{dn} are the slopes of the transition edges of the output of the duty cycle corrector x_{out}, as shown in Figure 3.4(b).

It is seen that for a control voltage of 1.47 V, the oscillation frequency is 1 GHz, and the power consumption P_c, for both the oscillator and the duty cycle corrector, is 25.38 mW. Note that the rising edge of x_{out} is almost 4 times steeper than its falling edge, resulting in asymmetric rise/fall times and higher phase noise [26].

Next it is shown that the PSS-DEC analysis can efficiently adjust the sizes of all transistors to meet the following design specifications. The output waveform x_{out} should have a 50% duty cycle, as well as a symmetric rise and fall slopes S_{up} and S_{dn}. The power consumption P_c should be reduced from 25.38 to 8 mW. The oscillation period T should be kept at 1 ns while the control voltage V_c is reduced from 1.47 to 1.4 V. The amplitude of the fundamental component of the delay cell outputs should be increased from 0.63 to 0.7 V. Note that the delay cell topology

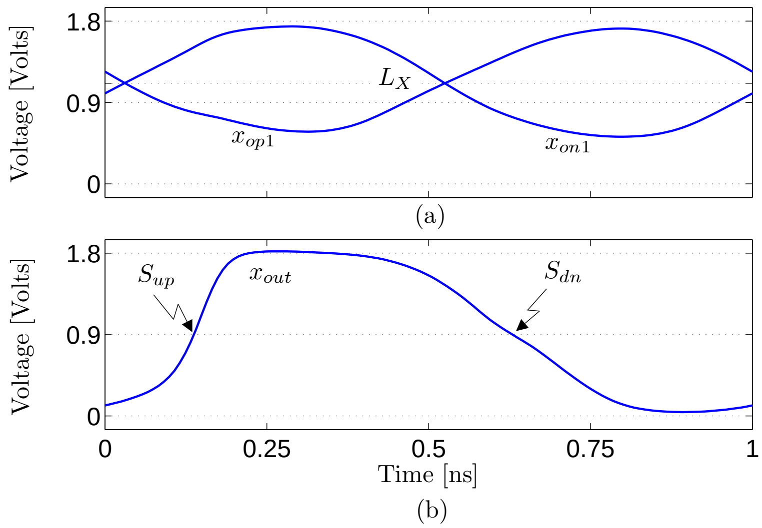

Figure 3.4: (a) Output voltages of the first delay cell, and (b) the output voltage of the duty cycle corrector for the original design. The output waveform x_{out} has asymmetric rise/fall times that result in higher phase noise [26].

provides higher swing for lower frequencies. Finally, the voltage intersect level L_X should be shifted from 1.11 V to the mid-supply at 0.9 V.

These specifications are achieved by adjusting the device sizes. To preserve the differential structure of the cell, as well as to keep the cells identical, the sizes of certain devices must be kept equal, e.g., $W_{ip1} = \ldots = W_{ip4} = W_{in1} = \ldots = W_{in4}$. The parameters for the PSS-DEC analysis are the width of eight input devices W_i, eight controlling devices W_c, and eight cross-coupled devices W_d in the delay cells, as well as the widths $W_2 = W_4$, $W_{p1} = W_{p2}$, and $W_{p1} = W_{p2} = W_1 = W_3$ in the duty cycle correction circuit. All devices have the same length of 0.5 μm.

These six tuning parameters are adjusted by the PSS-DEC analysis to satisfy six design constraints

$$
V_c = 1.40\text{ V} \rightarrow \boxed{\begin{array}{c}\text{PSS}\\ \hline g_1 = 0\\ \vdots\\ g_6 = 0\end{array}} \rightarrow
\begin{array}{lrl}
 & x(t) & \\
 & T = & 1.00\text{ ns}\\
 & P_c = & 8.00\text{ mW}\\
 & S_{up}/S_{dn} = & -1.00\\
 & L_X = & 0.90\text{ V}\\
 & \left|X_{op1_1}\right| = & 0.70\text{ V}\\
 & D_{out} = & 50.00\%\\
\gamma_1: & W_i = & 8.19\ \mu\text{m}\\
\gamma_2: & W_d = & 12.06\ \mu\text{m}\\
\gamma_3: & W_c = & 20.08\ \mu\text{m}\\
\gamma_4: & W_2 = W_4 = & 30.92\ \mu\text{m}\\
\gamma_5: & W_{p1} = W_{p2} = & 20.83\ \mu\text{m}\\
\gamma_6: & W_{n1,n2} = W_{1,3} = & 9.12\ \mu\text{m}
\end{array}
$$

$$
\begin{aligned}
g_1(T) &= T - 1\text{ ns} & g_4(x) &= S_{up} + S_{dn}\\
g_2(x) &= P_c - 8\text{ mW} & g_5(x) &= \left|X_{op1_1}\right| - 0.7\text{ V}\\
g_3(x) &= D_{out} - 50\% & g_6(x,T) &= L_X - 0.9\text{ V}
\end{aligned}
$$

The steady-state waveforms of the new design obtained from the PSS-DEC analysis are shown in Figure 3.5. It is seen that the PSS solution has the specified properties.

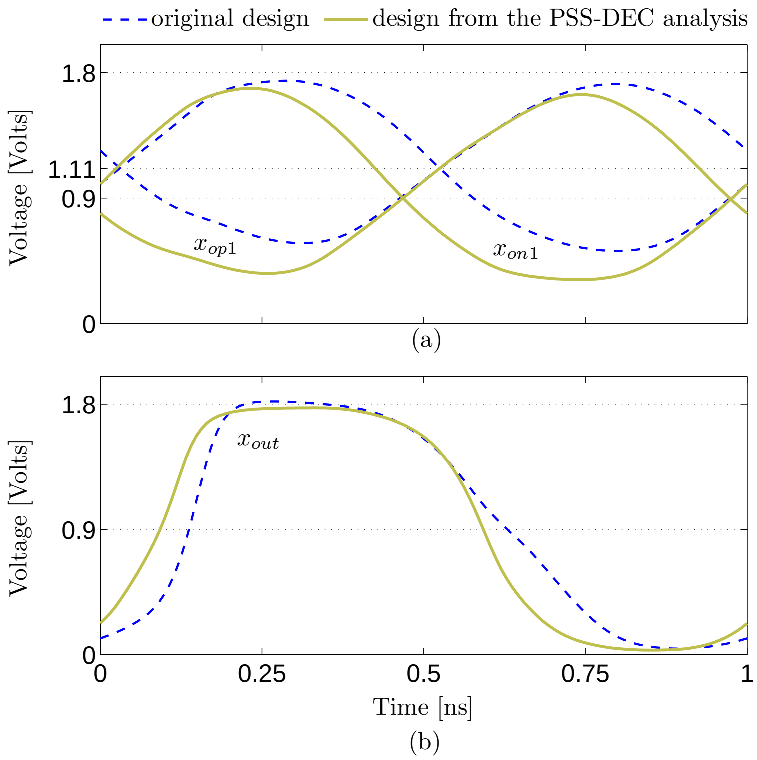

Figure 3.5: (a) Output voltages of the first delay cell, and (b) the output voltage of the duty cycle corrector for the original design, and the design obtained from the PSS-DEC analysis. The PSS-DEC analysis improves the symmetry and the duty-cycle of the output waveform x_{out} by adjusting the device sizes.

3.4.2 Mismatch Analysis for Ring Oscillator

In the ring oscillator of Section 3.4.1, parameter variations cause mismatch in device sizes that result in deviation of the circuit performance from the nominal. In case parameter variations cause the oscillation frequency to change, the feedback in a phase-locked loop (PLL) can adjust the control voltage and bring the frequency to the desired value. However, the feed forward type duty cycle corrector in Figure 3.3 can not compensate for device mismatches, and therefore, the duty cycle may change. It is important to verify the performance of the VCO in the presence of mismatches.

A traditional Monte-Carlo approach generates random parameter variations and provides their effect on circuit performance. This is done by performing a conventional PSS analysis for each combination of parameter variations. However, the Monte-Carlo analysis does not identify which devices are the most critical.

A sensitivity analysis for oscillators [5] can predict how individual devices affect the duty cycle. However, this prediction is only suitable for small parameter variations. For large parameter variations, the PSS-DEC analysis can be used.

PSS-DEC analysis is a large-signal analysis and therefore, it is accurate for arbitrarily large parameter variations. It can be used to provide acceptable ranges for individual parameter variations, such that the circuit performance remains within the specified boundaries. For example, the PSS-DEC analysis finds the smallest acceptable value for W_2, such that the duty cycle is 48% as

$$
\begin{array}{rc|c|cl}
\cline{3-3}
 & & \text{PSS} & & x(t) \\
\cline{3-3}
W_4 = 30.92\ \mu\text{m} & \rightarrow & g_1 = 0 & \rightarrow & \gamma_1 : W_2 = 21.71\ \mu\text{m} \\
 & & g_2 = 0 & & \gamma_2 : \ V_c = \ 1.39995\ \text{V} \\
\cline{3-3}
\end{array}
$$

$$
\begin{aligned}
g_1(T, x) &= D_{out} - 48\% \\
g_2(T) &= T - 1\ \text{ns}
\end{aligned}
$$

The PSS-DEC analysis is setup to adjust the control voltage V_c to compensate for possible frequency deviations caused by a change in W_2, as in the PLL operation.

In a similar manner, the upper boundary for W_2 is found, such that the duty cycle is less than 52%. A pair of the PSS-DEC analyses indicates that the duty cycle $D_{out} \in [48, 52]\%$ if $W_2 \in [21.71, 38.51]$ μm. Note that the sensitivity analysis for oscillators results in an optimistic lower bound of 18.52 μm indicating the need for a large-signal variational analysis.

The output waveforms x_{out} with 48% and 52% duty cycles due to individual variations in W_2, W_3, W_{cn1}, and W_{in1} are shown in Figures 3.6(a), (b), (c), and (d), respectively. The PSS-DEC analysis indicates that variations in W_{in1} are the most

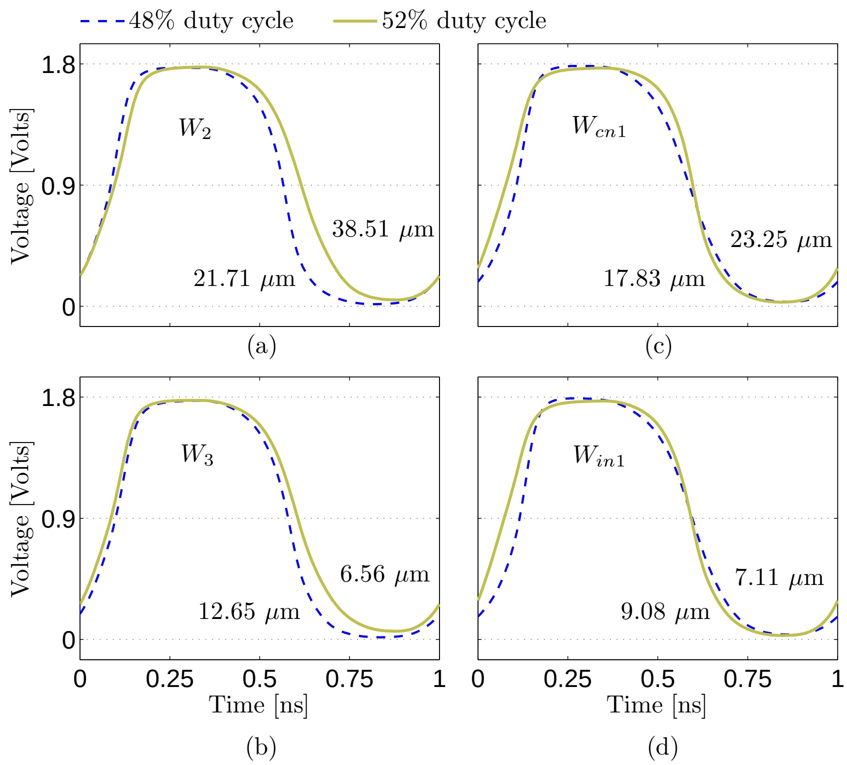

Figure 3.6: Output voltages x_{out} with 48 and 52 % duty cycles, due to a variation in (a) W_2, (b) W_3, (c) W_{cn1}, and (d) W_{in1}. Each range of parameter variations is obtained from a pair of PSS-DEC analyses.

critical, as the acceptable range for W_{in1} is the smallest for the four parameters under consideration.

3.4.3 Harmonic Distortion

Consider a two-stage operational amplifier in Figure 3.7 connected in a feedback arrangement as shown in Figure 3.8.

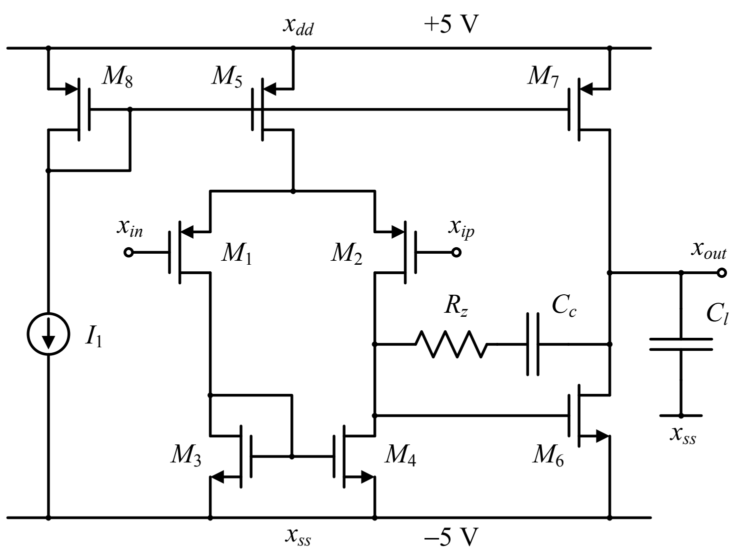

Figure 3.7: Two-stage operational amplifier.

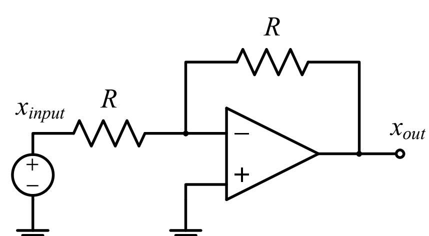

Figure 3.8: Operational amplifier in a unity gain negative feedback.

Amplifiers cause unwanted distortion of an input signal due to inherent nonlinearities. For example, given a sinusoidal input $x_{input}(t) = A_{in}\sin(2\pi f_{in}t)$, the output voltage contains complex harmonics $X_{out_2}, X_{out_3}, \ldots$. Harmonic distortion is a measure of the signal distortion, and depends on both the input amplitude A_{in} and the frequency f_{in} [24]. The N^{th} harmonic distortion HD_N is defined as the ratio of the magnitude of the N^{th} harmonic to the magnitude of the 1^{st} harmonic (the fundamental) at the output $\mathrm{HD}_N = |X_{out_N}| \,/\, |X_{out_1}|$.

Given an input frequency and amplitude, harmonic distortion can be found by a conventional PSS analysis that provides the output waveform $x_{out}(t)$ or its frequency spectrum. An example is shown below for the op amp in Figure 3.8.

$$\begin{array}{c} f_{in} = 1.00 \text{ MHz} \\ A_{in} = 4.00 \text{ V} \end{array} \rightarrow \boxed{\text{PSS}} \rightarrow \begin{array}{l} x(t) \\ \mathrm{HD}_2 = 7.39\% \end{array}$$

Alternatively, given a frequency f_{in}, a designer is often interested in finding the input amplitude A_{in} for which the harmonic distortion reaches a certain specified level, e.g., $\mathrm{HD}_2 = 1\%$. A single PSS-DEC analysis with one DEC and one parameter, A_{in}, can solve this problem efficiently. An appropriate amplitude A_{in} is found directly as depicted below.

$$f_{in} = 1.00 \text{ MHz} \rightarrow \begin{array}{|c|} \hline \text{PSS} \\ \hline g_1 = 0 \\ \hline \end{array} \rightarrow \begin{array}{c} x(t) \\ \mathrm{HD}_2 = 1.00\% \\ \gamma_1\!: \; A_{in} = 3.28 \text{ V} \end{array}$$

$$g_1(x) \;=\; |X_{out_2}| \,/\, |X_{out_1}| - 1\%$$

The PSS-DEC solution $x(t)$ satisfies the DEC equation, $|X_{out_2}| \,/\, |X_{out_1}| \;=\; 1\%$, which ensures that HD_2 is exactly 1%. As expected, at a given frequency, a smaller input signal exhibits less distortion.

The DEC g_1 is written in terms of the output voltage $x_{out}(t)$. The derivatives $\partial g_1/\partial x_i$ must appear in the last row of the finite difference or harmonic balance Jacobian matrices J_{fd} and J_{hb}, respectively. If the shooting method is used, these derivatives are used in (3.31), (3.32), and (3.33). The derivatives of the excitation $\partial b_i/\partial \gamma_1$ must appear in the last column of J_{fd} andJ_{hb}, or in (3.30) in case of the shooting method.

The PSS-DEC analysis with constraints on harmonic distortion has applications in analog filter design. The signal-to-noise ratio (SNR) of analog filters is normally defined for the input level that results in a specified harmonic distortion. This input level can be found efficiently from the PSS-DEC analysis as illustrated in the above example.

3.4.4 Unity Gain Frequency and Phase Margin

Small-signal frequency-domain characteristics of an op amp are the gain $A(f) = X_{out}(f)/X_{in}(f)$and the unity gain frequency f_u, $|A(f_u)| = 1$. Another characteristic is the phase margin (PM), a measure of amplifier stability. The phase difference between the input and output signals $\angle X_{in}(f) - \angle X_{out}(f)$ must be less than 180° for all $f \in [0, f_u]$. Otherwise in a feedback configuration, the system may become unstable, and unwanted oscillations occur. The phase margin is defined as

$$\mathrm{PM} = 180^\circ - \left[\angle X_{in}(f_u) - \angle X_{out}(f_u)\right] \tag{3.42}$$

The frequency response $A(f)$ is traditionally computed by a fast small-signal AC sweep, rather than by a large-signal PSS analysis. However, small-signal characteristics can be verified by a conventional large-signal PSS analysis as well, given a sufficiently small input amplitude, such that the output harmonics are negligible. The harmonic-balance method for PSS analysis can handle this problem efficiently by representing the PSS waveforms $x(t)$ by a DC component and one complex harmonic. Thus a PSS-DEC analysis with DECs for the phase margin and the unity gain frequency is employed. Such a problem can not be handled by a traditional small-signal AC analysis.

The op amp in Figure 3.7 is designed with the use of a compensation capacitor C_c for a typical PM of 60°, and a unity gain frequency of 40 MHz. The PM and f_u can be verified by a conventional large-signal PSS analysis.

$$\begin{array}{rl} f_{in} = & 40.00\ \text{MHz} \\ A_{in} = & 1.00\ \text{mV} \\ C_c = & 2.84\ \text{pF} \end{array} \;\rightarrow\; \boxed{\text{PSS}} \;\rightarrow\; \begin{array}{rl} |A(f_{in})| = & 1.00 \\ f_u = & 40.00\ \text{MHz} \\ \text{PM} = & 60.00^\circ \end{array}$$

In practice, due to parameter variations, the value of the on-chip compensation capacitor C_c is not exactly the same as the nominal value of 2.84 pF. Consequently, the phase margin and unity gain frequency deviate from the ideal values. Let the design specifications allow the PM and f_u to vary from their ideal values by at most $\pm 5°$ and ± 10 MHz, respectively. It is useful to know the bounds for acceptable capacitor variations, and what design specification is violated first as the C_c variation increases.

This problem can be solved by several PSS-DEC analyses. The C_c value that results in $f_u = 30$ MHz is found from a PSS-DEC analysis with one DEC and one parameter.

$$
\begin{array}{rcc|c|cr}
 & & & & & |A(f_{in})| = \;\; 1.00 \\
f_{in} = 30.00 \text{ MHz} & & & \text{PSS} & & f_u = 30.00 \text{ MHz} \\
 & \rightarrow & & & \rightarrow & \\
A_{in} = \;\; 1.00 \text{ mV} & & & g_1 = 0 & & \text{PM} = 67.27° \\
 & & & & & \gamma_1\!: \quad C_c = \;\; 3.99 \text{ pF}
\end{array}
$$

$$g_1(x) \;=\; |X_{out}| - |X_{in}|$$

The design equality constraint used in this example, $|X_{out}| = |X_{in}|$, ensures that the output and input magnitudes are equal, and therefore, the gain is unity. The value of 3.99 pF obtained from the PSS-DEC analysis corresponds to the upper limit of the compensation capacitor, for the unity gain frequency to stay in the specified bounds. The PSS-DEC analysis finds the lower limit $C_c = 2.12$ pF that corresponds to $f_u = 50$ MHz in a similar fashion. It can be seen from the above results, as well as from Figure 3.9, that the phase margin specification is violated first as C_c variation increases.

A tighter region of capacitor variations that simultaneously results in acceptable f_u and PM is found based on two PSS-DEC analyses, one for PM $= 55°$ and one for PM $= 65°$. The upper limit for C_c is found from a PSS-DEC analysis with two DECs and two parameters.

$$A_{in} = 1.00 \text{ mV} \rightarrow \begin{array}{|c|} \hline \text{PSS} \\ \hline g_1 = 0 \\ g_2 = 0 \\ \hline \end{array} \rightarrow \begin{array}{rl} |A(f_{in})| = & 1.00 \\ f_u = & 33.08 \text{ MHz} \\ \text{PM} = & 65.00° \\ \gamma_1: \quad C_c = & 3.56 \text{ pF} \\ \gamma_2: \quad f_{in} = & 33.08 \text{ MHz} \end{array}$$

$$\begin{aligned} g_1(x) &= |X_{out}| - |X_{in}| \\ g_2(x) &= \angle X_{in} - \angle X_{out} - 115° \end{aligned}$$

The lower limit for C_c is found from an additional PSS-DEC analysis. Figure 3.9 shows that if $C_c \in [2.30 \text{ pF},\ 3.56 \text{ pF}]$, then PM $\in [55°,\ 65°]$, and the unity gain frequency is within the acceptable range as well.

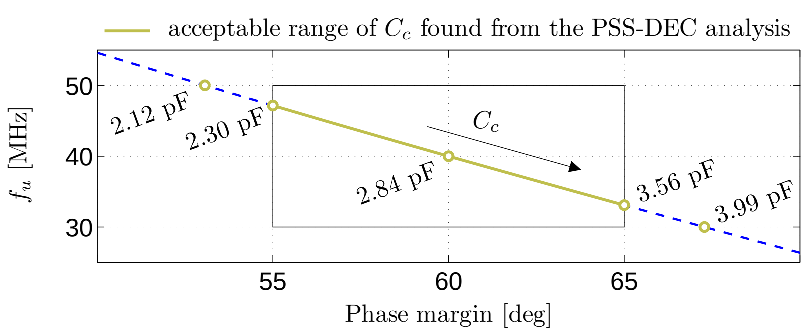

Figure 3.9: Values of the compensation capacitor C_c that correspond to the upper and lower limits of the unity gain frequency, and phase margin, obtained from four PSS-DEC analyses, and the region of acceptable values of C_c.

Note that in the previous PSS-DEC setup, the second parameter γ_2 is the input frequency f_{in}, and the steady-state period is not known beforehand. This example shows the flexibility of the PSS-DEC analysis, and its ability to simulate forced circuits in a similar manner to oscillators where the period of oscillation is one of the PSS unknowns.

3.4.5 Power Consumption and Other Design Constraints

Next, consider an op amp at an intermediate stage of a design process. At this design stage the response is computed by a conventional PSS analysis.

$$\begin{array}{r@{\,=\,}l} f_{in} & 38.90 \text{ MHz} \\ A_{in} & 1.00 \text{ mV} \\ W_1 & 75.00\ \mu\text{m} \\ W_6 & 17.00\ \mu\text{m} \\ R_z & 591.22\ \Omega \\ I_1 & 200.00\ \mu A \end{array} \rightarrow \boxed{\text{PSS}} \rightarrow \begin{array}{r@{\,=\,}l} |A(f_{in})| & 1.00 \\ f_u & 38.90 \text{ MHz} \\ \text{PM} & 52.07^\circ \\ P_c & 10.11 \text{ mW} \end{array}$$

In this example, the power consumption P_c is computed as

$$P_c = -\left[V_{dd} \cdot \text{DC}(x_{V_{dd}}) + V_{ss} \cdot \text{DC}(x_{V_{ss}})\right] \tag{3.43}$$

where DC$(\cdot)$ denotes the DC or average value, V_{dd}, V_{ss} are the values of the power supply voltage sources, and $x_{V_{dd}}$, $x_{V_{ss}}$ are the currents through these voltage sources.

Let the design goal be to achieve a 60° phase margin at 40 MHz unity gain frequency, as well as to reduce the power consumption by 20% to 8 mW by tuning the design parameters. Other design considerations must be taken into account, such as keeping the input pair devices same $W_1 = W_2$, preserving the width ratio $W_6 = kW_3 = kW_4,\ k = 17/5$, as well as adjusting the zero cancellation resistor according to $R_z = 1/g_{m6}$ if the size of M_6 changes.

This problem can be solved by a PSS-DEC analysis with four DECs and four parameters.

$$
\begin{array}{rl} f_{in} = & 40.00\text{ MHz} \\ A_{in} = & 1.00\text{ mV} \end{array}
\;\rightarrow\;
\begin{array}{|c|}\hline \text{PSS} \\ \hline g_1 = 0 \\ g_2 = 0 \\ g_3 = 0 \\ g_4 = 0 \\ \hline \end{array}
\;\rightarrow\;
\begin{array}{rrl}
 & |A(f_{in})| = & 1.00 \\
 & f_u = & 40.00\text{ MHz} \\
 & \text{PM} = & 60.00^\circ \\
 & P_c = & 8.00\text{ mW} \\
\gamma_1: & R_z = & 361.02\ \Omega \\
\gamma_2: & W_1 = & 74.73\ \mu\text{m} = W_2 \\
\gamma_3: & W_6 = & 57.66\ \mu\text{m} = kW_{3,4} \\
\gamma_4: & I_1 = & 156.48\ \mu\text{A}
\end{array}
$$

$$
\begin{aligned}
g_1(x) &= |X_{out}| - |X_{in}| \\
g_2(x) &= \angle X_{in} - \angle X_{out} - 120^\circ \\
g_3(x) &= -\big[V_{dd} \cdot \text{DC}(x_{V_{dd}}) + V_{ss} \cdot \text{DC}(x_{V_{ss}})\big] - 8\text{ mW} \\
g_4(x, \gamma_1, \gamma_3) &= R_z - 1/g_{m6}\big(x, W_6\big)
\end{aligned}
$$

The circuit parameters and performance measurements of the original design, and the design obtained by the PSS-DEC analysis are shown in Table 3.1.

Describing W_6, W_3, and W_4 by only one parameter γ_3 results in a more compact PSS-DEC problem, without including the relationships $W_6 = kW_3$ and $W_6 = kW_4$

Table 3.1: Parameters and performance comparison of the original design and the design obtained from the PSS-DEC analysis.

	Units	PSS	PSS-DEC
f_u	[MHz]	38.90	40.00
PM	[deg]	52.07	60.00
P_c	[mW]	10.11	8.00
R_z	[Ω]	591.22	361.02 (γ_1)
$W_1 = W_2$	[μm]	75.00	74.73 (γ_2)
$W_6 = kW_3 = kW_4$	[μm]	17.00	57.66 (γ_3)
I_1	[μA]	200.00	156.48 (γ_4)

as DECs. Note that the entries of the corresponding column of the Jacobian matrices J_{fd}, J_{sh}, or J_{hb} must be computed as, e.g.,

$$\frac{\partial q}{\partial \gamma_3} = \frac{\partial q}{\partial W_6} + k\frac{\partial q}{\partial W_3} + k\frac{\partial q}{\partial W_4} \tag{3.44}$$

The relation for the input pair devices $W_1 = W_2$ is treated in a similar fashion.

The DEC $g_4(x, \gamma_1, \gamma_3)$ is written not only in terms of $x(t)$ but also in terms of γ_1 and γ_3. Partial derivatives $\partial g_4/\partial \gamma_1$, and $\partial g_4/\partial \gamma_3$ must appear in the bottom-right block of J_{fd} and J_{hb}, or in (3.33) in case of the shooting method.

The PSS-DEC analysis can also handle specifications for transient operation, such as slew rate and settling time [22].

3.5 Convergence of the Design-Oriented Analysis

In this section, the performance of the new analysis augmented with DECs, is compared to the performance of the search method with a Newton update rule for Γ_E that employs a sequence of conventional analyses. It is shown that the new analysis is several times faster, than a carefully implemented search-based method, while having a comparable region of convergence (ROC). Finally, a globally-convergent method for the design problem is proposed, that can be utilized in both techniques.

3.5.1 Computational Cost

The speed of the two approaches is compared based on the number of iterations N_{DEC} of the analysis with DECs (3.14) and the sum $N_{\text{S}} = \Sigma N_{\text{C}}^{(k)}$ of the conventional analysis iterations (3.6) $N_{\text{C}}^{(k)}$ at every iteration $k = 0, \ldots, N$ of the search-based method. The analysis with DECs solves the linear system (3.14) that contains E more equations than the system (3.6) of the conventional analysis. This cost is balanced by E sensitivity analyses in (3.10) at each search iteration.

Both of the computation costs N_{DEC} and N_{C} account for evaluation of the DECs in (3.8) and (3.14), their sensitivities in (3.9) and (3.15), and the sensitivities of the conventional analysis equations with respect to the tuning parameters in (3.10) and (3.15).

Next it will be shown that the new analysis with DECs is faster than the search-based method. The speed improvement is expressed as the ratio

$$\text{speedup} = \frac{N_{\text{S}}}{N_{\text{DEC}}} = \frac{\Sigma N_{\text{C}}^{(k)}}{N_{\text{DEC}}} \tag{3.45}$$

The simulation results are summarized in Table 3.2. For a given relative tol-

Circuit	Specifications	N_{DEC}	$N_{\text{S}} = \Sigma N_{\text{C}}^{(k)}$	$\frac{\Sigma N_{\text{C}}^{(k)}}{N_{\text{DEC}}}$
OA	HD_2	6	$13 = {\scriptstyle 3+3+3+2+2}$	2.17
	f_u	6	$16 = {\scriptstyle 4+3+3+3+3}$	2.67
	PM	5	$13 = {\scriptstyle 4+3+3+3}$	2.60
	P_c, f_u, PM, $R_z = 1/g_{m6}$	8	$25 = {\scriptstyle 4+6+5+4+3+3}$	3.13
	P_c, f_u, PM, $R_z = 1/g_{m6}$ ${\scriptstyle (W_{1,2}^{(0)} = 75\,\mu\text{m})}$	7	$31 = {\scriptstyle 3+6+7+5+4+3+3}$	4.43
VCO	T, P_c, D_{out}, $S_{up/dn}$, $\lvert X_{op1_1} \rvert$, L_X ${\scriptstyle (\lambda = \frac{1}{3})}$	6	$20 = {\scriptstyle 4+4+4+3+3+2}$	3.33
	D_{out}	6	$16 = {\scriptstyle 5+4+4+3}$	2.67

Table 3.2: Summary of speed performance of the DEC analysis and a Newton-based search method.

erance of $\epsilon_{rel} = 10^{-3}$, the new analyses with DECs are 2 to 4 times faster than a carefully implemented Newton-based search method. The solutions obtained by the two techniques agree within the simulation tolerance.

It is also shown that the new analysis has an adequate region of convergence.

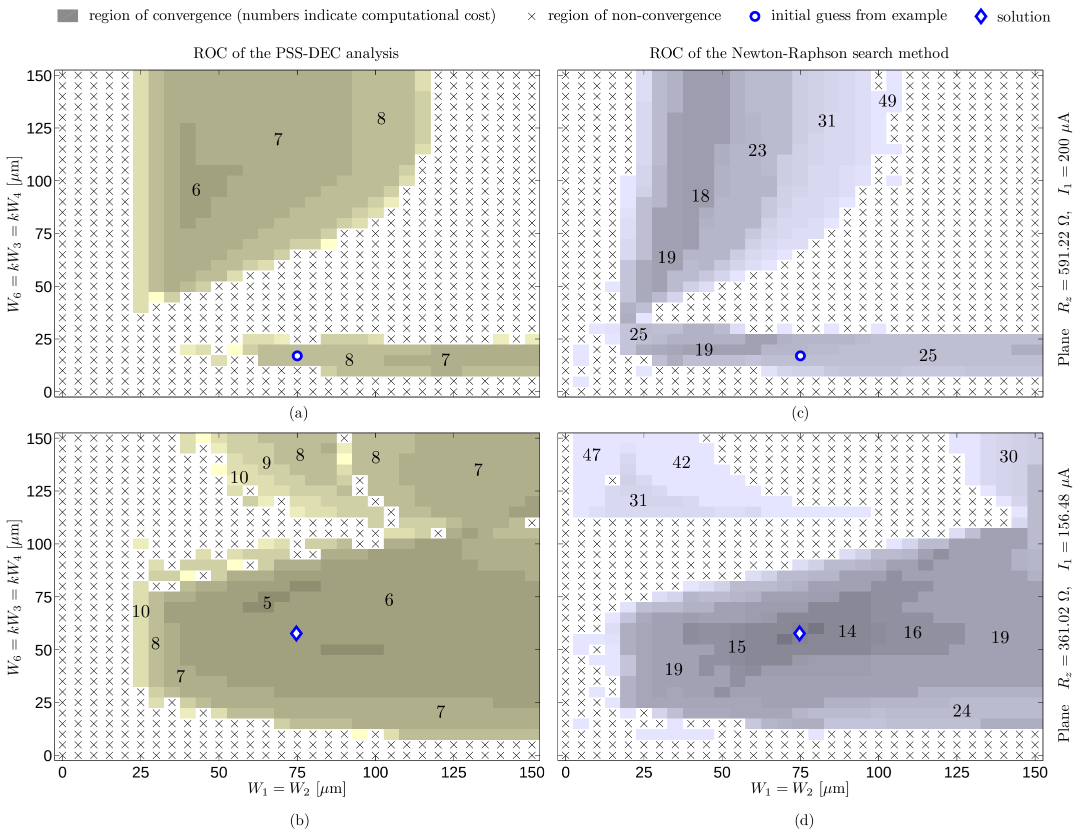

Figure 3.10: (a) The ROC of the PSS-DEC analysis, and (c) the ROC of the Newton-Raphson search method for the plane $W_1 \times W_6$ that corresponds to an initial guess $R_z = 591.22\ \Omega$, and $I_1 = 200\ \mu$m from Table 3.1. The corresponding ROCs for the solution plane where $R_z = 361.02\ \Omega$, and $I_1 = 156.48\ \mu$m are shown in (b) and (d). The numbers are the iteration count N_{DEC} and N_{S} of the PSS-DEC analysis and the search-based method, respectively. The darker regions indicate the initial guesses that converge to the solution in fewer iterations.

3.5.2 Region of Convergence (ROC)

Both techniques under consideration employ the Newton-Raphson method, and therefore have quadratic convergence in close proximity with the solution. The convergence far from the solution depends on the type of the circuit and the nonlinearities in the DECs G_E. Since the equality constraints are handled differently in the new analysis augmented with DECs than in a search-based analysis, it is important to ensure that the new method converges to the solution from various initial guesses.

An iterative method converges to a solution if the initial guess lies in the region of convergence (ROC) of that solution. Given a nonlinear problem, different numerical methods may have different ROCs. While looking for the values of circuit parameters Γ_E, a method with a larger ROC may find a well-performing design even when the initial design is far from meeting the specifications.

The ROCs of the PSS-DEC and search-based analyses are studied for the operational amplifier in Figure 3.7. As described in Section 3.4.5, the amplifier is tuned to comply with four design specifications using four circuit parameters. The region of convergence for the circuit parameters $\Gamma_E \equiv [R_z, W_1, W_6, I_1]^T$ lies in the four-dimensional space $\mathbb{R}^4$.

Figures 3.10(a) and (b) show the ROC of the PSS-DEC analysis, and Figures 3.10(c) and (d) show the ROC of the Newton-based search method. For each analysis method, a pair of planes $W_1 \times W_6$ that slice through a four-dimensional space are shown. Figures 3.10(a) and (c) show the plane corresponding to the initial guess $R_z = 591.22\ \Omega$, and $I_1 = 200\ \mu$m for the example in Table 3.1. The plane in Figures 3.10(b) and (d) corresponds to the solution $R_z = 361.02\ \Omega$, and $I_1 = 156.48\ \mu$m.

The data in Figure 3.10 is obtained from a number of PSS-DEC and search-based analyses with various initial guesses for Γ_E. For every value of Γ_E, a DC solution is taken as the initial guess for the circuit state unknowns $x(t)$. The numbers in Figure 3.10 are the iteration counts N_{DEC} and N_{S} of the PSS-DEC analysis and the search-based method, respectively. The darker regions indicate the initial guesses that converge to the solution in fewer iterations. It is seen that for a given example, the PSS-DEC and the search-based analyses have comparable regions of convergence, while the new PSS-DEC analysis is several times faster.

In this example, both techniques use the classical Newton-Raphson method. In practice, the convergence properties of both techniques can be improved by employing globally convergent continuation methods.

3.5.3 Globally Convergent Continuation Method

In the ring VCO example in Section 3.4.1, the initial design is far from meeting the specifications. Particularly, the initial power consumption P_c is 25.38 mW, while the desired value is 8 mW. Neither the PSS-DEC analysis, nor the search-based method can converge to the solution with a classical Newton method.

One way to meet the tight specifications is to improve the design performance gradually [23]. In the VCO design example, the circuit is first tuned to consume 20 mW, then 14 mW, and finally 8 mW. Each of the three steps enroute to the final design are easily handled by both the PSS-DEC analysis, and the search-based method.

Mathematically, this approach can be described as a continuation method.

Consider the design problem in (3.3) rewritten in the following form

$$G_E(X_C, \Gamma_E) = (1 - \lambda)G_E^{(0)} \tag{3.46}$$

where $\lambda \in [0, 1]$ is the continuation parameter, and $G_E^{(0)} \in \mathbb{R}^E$ is the residual DEC error in (3.3) corresponding to the initial design. For the VCO example, $g_2^{(0)} = 25.38 - 8 = 17.38$ mW. Therefore, the initial design satisfies (3.46) with $\lambda = 0$, and when $\lambda = 1$, (3.46) is the same as (3.3). The intermediate values of λ represent relaxed design specifications that are tighter for larger λ.

Figure 3.11 illustrates the continuation method applied to the ring VCO example in Section 3.4.1. The specifications are met as λ is increased from 0 to 1 in three equal steps.

Given the initial design, a single PSS-DEC (Figure 3.11(a)) or a single search-based method (Figure 3.11(d)) can only solve a design problem with relaxed design specifications for any $\lambda \leq 0.5$. For larger λ, both techniques fail. However, the design problem with $\lambda = 1/3$ can be solved easily as a first step towards the desired performance. After the first step, the relaxed specifications (3.46) with $\lambda = 1/3$ are satisfied, and an additional PSS-DEC analysis (Figure 3.11(b)) or search-based method (Figure 3.11(e)) is performed to meet a tighter set of specifications with $\lambda = 2/3$. Finally, the desired performance with $\lambda = 1$ is within the reach of a single PSS-DEC analysis (Figure 3.11(c)) or search method (Figure 3.11(f)).

Note that both techniques are comparable in converging to a given relaxed specification, while the new design-oriented PSS-DEC analysis is about 3 times

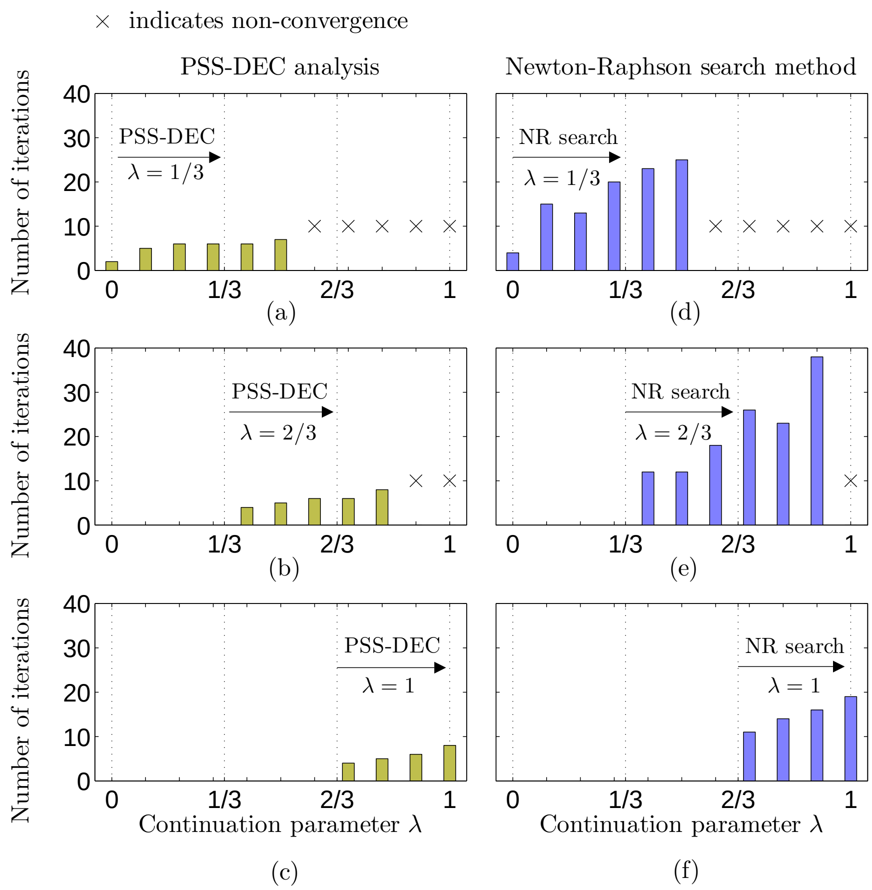

Figure 3.11: Continuation method for the ring VCO design problem from Section 3.4.1 finds the solution from a remote initial guess, for which both the PSS-DEC and Newton-Raphson search approaches fail. Starting from the original design, $\lambda = 0$, the desired design, $\lambda = 1$, is found by gradually tightening the design specifications, $\lambda = 1/3,\ \lambda = 2/3,\ \lambda = 1$.

faster.

A similar constraint stepping technique can be employed to solve a minimization problem. For example, the power consumption constraint can be gradually tightened. This power minimization process is continued until a local minimum is found, the values of circuit parameters become non-physical, or some other consideration, such as power tradeoff for noise performance becomes important.

Chapter 4 – Automated Design and Optimization of Low Noise Oscillators

Oscillators are autonomous systems that require no external excitation to produce a periodic output. They are commonly used to generate stable frequency references that translate data to the desired frequency band in transceivers, and clock signals that trigger events in digital circuits. Noise in oscillators appears in the form of phase noise or timing jitter and limits the number of non-interfering channels in communication systems, or the speed of digital systems. Therefore, the design and optimization of low-noise oscillators is an important aspect of circuit design for a wide range of applications [4].

The large-signal operation of oscillators causes noise translation to different frequencies due to circuit nonlinearities. This makes the modeling and simulation of noise in oscillators a difficult problem. Simplified noise models for hand calculations use approximations that degrade accuracy. Circuit simulators with RF capabilities can account for all noise frequency translation mechanisms and can predict oscillator noise performance with high accuracy. Accurate phase noise computations are based on a perturbation projection vector (PPV) analysis [3] that describes how the oscillator converts the noise from circuit components and power supply into phase noise. The impulse sensitivity function (ISF) [4] is similar to the PPV in describing the conversion of noise.

Several techniques for automated oscillator optimization have been developed in recent years. Geometric programming (GP) has been applied to optimize LC oscillators in [29]. This approach is fast, and finds the global optimum. However, the GP method is topology-dependent, requires an expert designer to formulate the problem in a special form suitable for optimization, and relies on an approximation of the phase noise performance. The CYCLONE tool [30] employs simulated annealing (SA) for synthesis of optimal LC oscillators. This approach uses a circuit simulator to accurately evaluate phase noise and relies on an electromagnetic simulator [31] for accurate estimation of the on-chip inductor losses. However, SA is a heuristic that is stochastic in nature as it relies on random decisions. It requires high computational power to perform extensive simulations. Gradient-based methods for automated circuit design and optimization [32], [33], [34] take advantage of circuit sensitivity information that describes directions for design improvement. The gradient-based methods find a local optimum and require a reasonably good initial design. The initial design can be provided by a designer, or obtained after several steps from a stochastic technique.

Recent advances in the sensitivity analysis for oscillators [5] pave the way for efficient gradient-based oscillator optimization. The optimization technique proposed in this dissertation relies on a comprehensive phase noise sensitivity computation. The periodic steady-state (PSS) sensitivity guides minimization of the oscillator noise intensities, and the PPV sensitivity provides directions for improving an oscillator's immunity to noise. No closed-form expressions for phase noise performance are needed, and therefore, the new optimization technique is general and applicable to all types of oscillators, independent of the circuit topology.

A new design-oriented approach to circuit analysis [22], [21] is employed in the proposed optimization technique to handle the design constraints. The PSS-DEC analysis [22], a design-oriented PSS analysis augmented with design equality constraints (DEC), is used to find the values of circuit parameters, such that several design constraints are satisfied. This analysis encapsulates the PSS constraints and reduces the optimization problem to an optimization problem. A new design-oriented modification of the sensitivity analysis for oscillators [5] provides tradeoffs between circuit parameters that define feasible directions for design improvement. This sensitivity analysis is a generalization of the sensitivity analysis for oscillators with a specification for the oscillation frequency [21], [35]. The design-oriented approach to circuit analysis facilitates gradient-based oscillator design and optimization in the presence of design constraints. Design specifications that can not be included in the PSS-DEC analysis [22] are handled by general-purpose methods for constrained optimization.

In Section 4.1 a technique for phase noise computation in oscillators that employs the perturbation projection vector (PPV) is reviewed. Section 4.2 presents design-oriented periodic steady-state and sensitivity analyses that facilitate automated oscillator optimization. In Section 4.3 a simple optimization example is considered to highlight the key ideas of the proposed optimization technique. A general formulation of the optimization method is given in Section 4.4. Phase noise optimization examples are given in Section 4.5.

4.1 Phase Noise Computation in Oscillators

Computation of phase noise in oscillators relies on the perturbation projection vector (PPV). The PPV quantitatively describes how noise generated by circuit components at the periodic steady-state (PSS) or noise from a power supply is converted by an oscillator into a phase deviation. An understanding of the PSS, PPV, and phase noise is crucial for oscillator design and optimization. An *LC* oscillator in Figure 4.1 is used to illustrate the contribution of transistor M_1 to the phase noise. First, a brief overview of the PSS solution and the PPV calculation is provided.

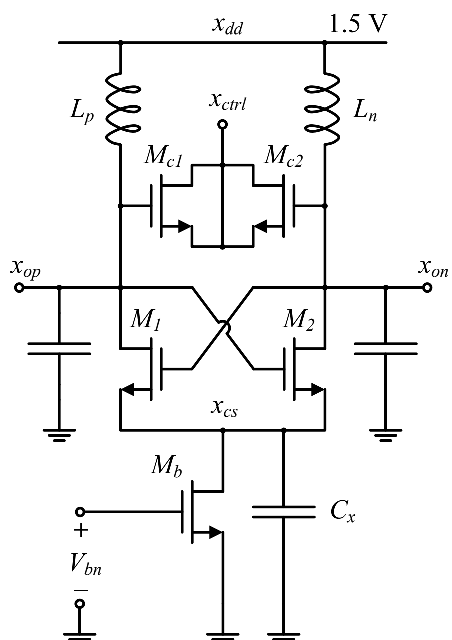

Figure 4.1: Schematic of a differential *LC* VCO.

4.1.1 Periodic Steady State (PSS) Solution

Any nonlinear oscillator circuit can be modeled as a set of m differential-algebraic equations (DAEs) in $x(t)$ given by

$$\frac{d}{dt}q\big(x(t)\big) + f\big(x(t)\big) + b = 0 \tag{4.1}$$

where

$$\begin{aligned} t \in \mathbb{R} \quad &: \text{ time, independent variable,} \\ x : \mathbb{R} \to \mathbb{R}^m &: \text{ circuit unknowns,} \\ q : \mathbb{R}^m \to \mathbb{R}^m &: \text{ contribution of reactive components,} \\ f : \mathbb{R}^m \to \mathbb{R}^m &: \text{ contribution of resistive components,} \\ b \in \mathbb{R}^m &: \text{ independent sources.} \end{aligned}$$

The T-periodic solution $x(t)$ of the DAEs in (4.1) is called the PSS solution if it satisfies $x(t) = x(t + T)$. This periodicity constraint can be expressed as

$$x(0) = x(T) \tag{4.2}$$

Notice that if $x(t)$ is a PSS solution, then $x(t + \Delta t)$, $\forall \Delta t$ is also a valid PSS solution. A unique isolated solution can be selected by imposing a phase condition

$$\varphi\big(x(0)\big) = 0, \quad \varphi : \mathbb{R}^m \to \mathbb{R} \tag{4.3}$$

One possible phase condition is to let a component of $x(0)$ be a fixed value.

The oscillator PSS is uniquely defined by (4.1), (4.2), and (4.3), resulting in continuous-time equations for the oscillator in the steady-state

$$\begin{cases} \frac{d}{dt}q\big(x(t)\big) + f\big(x(t)\big) + b = 0 \\ x(0) = x(T) \\ \varphi\big(x(0)\big) = 0 \end{cases} \tag{4.4}$$

This is a periodic boundary value problem (BVP) in $x(t)$ and T, a special case of a two-point BVP [15]. The PSS solution $x_s(t)$ can be found by solving (4.4) in the time domain by the finite difference, or shooting methods, as well as in the frequency domain by the harmonic balance method [2] as depicted below

$$\boxed{\text{PSS}} \;\rightarrow\; \begin{matrix} x_s \\ T \end{matrix} \tag{4.5}$$

The steady-state voltages x_{op}, x_{on}, and x_{cs} of the LC oscillator in Figure 4.1 are shown in Figure 4.2 (a) for one period, $t \in [0, T]$.

4.1.2 Perturbation Projection Vector (PPV)

The oscillator perturbed by a small time-dependent noise $b_n(t) : \mathbb{R} \rightarrow \mathbb{R}^p$ modulated by a state-dependent function $B(x) : \mathbb{R}^m \rightarrow \mathbb{R}^{m \times p}$ can be modeled by a set

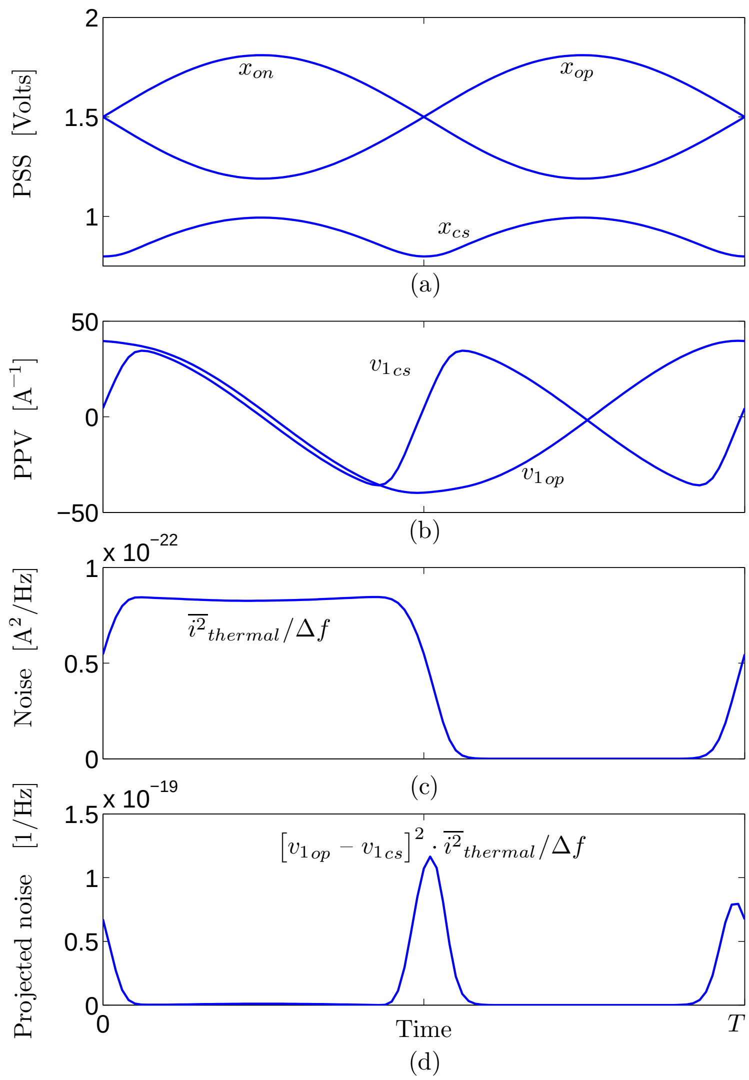

Figure 4.2: (a) The PSS solution for terminal voltages of M_1, (b) the PPV at the drain and source nodes of M_1, (c) spectral density of the channel thermal noise of M_1, and (d) the thermal noise of M_1 projected into the phase noise for one oscillation period.

of m DAEs

$$\frac{d}{dt}q\big(x(t)\big) + f\big(x(t)\big) + b + B\big(x(t)\big)b_n(t) = 0 \tag{4.6}$$

The noisy solution x_n of (4.6) can be expressed in terms of the noiseless PSS solution x_s of (4.1) as [3]

$$x_n(t) = x_s\big(t + \alpha(t)\big) + a(t) \tag{4.7}$$

where

$$\begin{aligned} a : \mathbb{R} \to \mathbb{R}^m &: \text{ orbital deviation that remains small,} \\ \alpha : \mathbb{R} \to \mathbb{R} \quad &: \text{ phase deviation that can grow unbounded.} \end{aligned}$$

The phase deviation $\alpha(t)$ is the solution of the following nonlinear DAE

$$\frac{d}{dt}\alpha(t) = v_1^T\big(t + \alpha(t)\big)B\Big(x_s\big(t + \alpha(t)\big)\Big)b_n(t) \tag{4.8}$$

where $v_1 : \mathbb{R} \to \mathbb{R}^m$ is a T-periodic vector, known as the perturbation projection vector. The time-dependent PPV quantitatively describes how additive noise is converted by the oscillator into phase deviation.

Consider a system of m linear DAEs in $x(t)$

$$\frac{d}{dt}\big(C(t)x(t)\big) + G(t)x(t) = 0 \tag{4.9}$$

with T-periodic coefficients

$$C(t) \equiv C\big(x_s(t)\big) = \left.\frac{dq(x)}{dx}\right|_{x_s(t)}, \;\; C : \mathbb{R} \to \mathbb{R}^{m\times m} \tag{4.10}$$

and

$$G(t) \equiv G\big(x_s(t)\big) = \left.\frac{df(x)}{dx}\right|_{x_s(t)}, \; G : \mathbb{R} \to \mathbb{R}^{m \times m} \tag{4.11}$$

known as the capacitance and conductance matrices, respectively. The system in (4.9) is obtained by differentiation of (4.1) with respect to x at the PSS solution. The corresponding adjoint system of m linear DAEs in $y(t)$ is given by

$$C^T(t)\frac{d}{dt}y(t) - G^T(t)y(t) = 0 \tag{4.12}$$

The adjoint system is satisfied by any linear combination of its eigenmodes $v_k(t)e^{-\mu_k t}$, $k = 1, \ldots, r$, where $r = \text{rank}(C)$, μ_k are the characteristic exponents, and $\lambda_k = e^{\mu_k T}$ are characteristic multipliers of the original linear system in (4.9). Assuming that the oscillator circuit has one asymptotic orbitally stable PSS solution, the PPV $v_1(t)$ is the only periodic and nonzero eigenmode. It corresponds to the oscillatory characteristic multiplier $\lambda_1 = 1$. The rest of the eigenmodes are either zero, or decay quickly as time decreases, as $|\lambda_k| < 1$, $k = 2, \ldots, r$, and $\lambda_{r+1} = \ldots = \lambda_m = 0$.

Any scaled version of the PPV satisfies the adjoint system. A properly scaled PPV is selected by requiring that

$$-v_1^T(t)C(t)\dot{x}_s(t) = 1, \quad \forall t \tag{4.13}$$

where $\dot{x}_s \equiv dx_s/dt$.

The oscillator PPV is defined by the system of linear DAEs in y which ensures that the solution $v_1(t)$ satisfies the adjoint system, is periodic, and is properly scaled

$$\begin{cases} C^T \frac{d}{dt} y - G^T y = 0 \\ y(0) = y(T) \\ -y^T C \dot{x}_s = 1, \quad t = 0 \end{cases} \tag{4.14}$$

The PPV is found by solving (4.14) directly [8], or by reducing it to an initial value problem (IVP) [7].

The PPV components v_{1op} and v_{1cs} along one oscillation period, $t \in [0, T]$, are shown in Figure 4.2 (b). They describe how the currents injected into the nodes *op* and *cs* of the *LC* oscillator are projected into the phase deviation at different time instances in one period.

4.1.3 Phase Noise

In the frequency domain, the spectrum of a purely periodic x_s is given by a sequence of impulses at DC, the oscillation frequency $f_0 = 1/T$, and its harmonics. In practice, noise from circuit components, substrate, and power supply cause frequency instabilities. The spectrum of a noisy oscillator has sidebands around the oscillation frequency f_0. These are generally referred as the phase noise sidebands. In the frequency domain an oscillator's instabilities are characterized by a single sideband (SSB) noise spectral density, phase noise, $\mathcal{L}(f_m) : \mathbb{R} \to \mathbb{R}$ in dBc/Hz as a function of an offset frequency f_m. $\mathcal{L}(f_m)$ is the power in a 1 Hz band around $f_0 + f_m$ frequency, normalized to the total power around the frequency of oscillation. Phase noise depends on the noise intensities of circuit components, substrate and power supply, as well as the susceptibility of an oscillator to the noise.

A simple expression for the oscillator phase noise $\mathcal{L}(f_m)$ due to all white noise sources for a range of offset frequencies $\pi f_0^2 c_w \ll f_m \ll f_0$ is given by [3]

$$\mathcal{L}(f_m) \approx 10 \log_{10}\left(\left(\frac{f_0}{f_m}\right)^2 c_w\right) \tag{4.15}$$

where c_w is the white noise constant. It captures the contributions of all white noise sources to the phase noise

$$c_w = \frac{1}{T}\int_0^T v_1^T(\tau) B\big(x_s(\tau)\big) B^T\big(x_s(\tau)\big) v_1(\tau) d\tau \tag{4.16}$$

where $B(x) : \mathbb{R}^m \rightarrow \mathbb{R}^{m \times p}$ represents the connectivity and state-dependent modulation of p uncorrelated white Gaussian noise sources $b_n(t) : \mathbb{R} \rightarrow \mathbb{R}^p$ with rms values of 1 A/$\sqrt{\text{Hz}}$ at all frequencies. The phase noise due to colored noise sources is computed in a similar manner [36].

Consider the device M_1 of the LC oscillator and its channel thermal noise source in Figure 4.3. The thermal noise intensity of M_1 depends on the device width W_1 and length L_1, as well as on the voltages x_{op}, x_{on}, and x_{sc} in Figure 4.2 (a). The T-periodic voltages result in a T-periodic noise current spectral density $\overline{i^2}_{thermal}/\Delta f$ in Figure 4.2 (c). During circuit operation, the channel resistance and transconductances of M_1 vary with time, and therefore, the spectral density of the channel noise $\overline{i^2}_{thermal}/\Delta f$ varies with time as well [37].

The channel noise sources of M_1 inject equal and opposite amounts of current

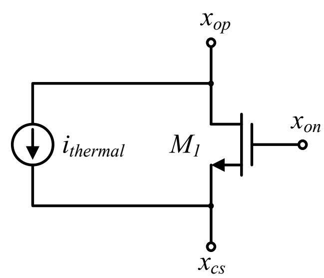

Figure 4.3: MOSFET M_1 and its channel thermal noise source.

into the drain and source nodes. Therefore, the amount of channel noise projected into phase noise is described by the difference between the drain and source PPV in Figure 4.2 (b). The thermal noise modulated by the drain-source PPV difference is shown in Figure 4.2 (d). It is seen that a large amount of thermal noise does not contribute to phase noise when the drain-source PPV difference is small. The spikes near $t = 1/T$ and $t = T$ in Figure 4.2 (d) correspond to the time instances when both the noise intensity and the PPV difference are large.

The contribution of the M_1 thermal noise to phase noise is described by a noise constant

$$c_{w1} = \frac{1}{T} \int_0^T \left(v_{1op} - v_{1cs}\right)^2 \cdot \overline{i^2}_{thermal} \, d\tau \tag{4.17}$$

The white noise constant in (4.16) can be expressed as a sum of the noise constants of p individual noise sources

$$c_w = \sum_{i=1}^{p} c_{wi} \tag{4.18}$$

Form this discussion it follows that for phase noise minimization, not only the individual noise intensities but also the PPV needs to be shaped in such a way that the resulting phase noise is reduced.

4.2 Design-Oriented Analysis for Oscillators

In the constrained oscillator optimization, the PSS specifications that can be written as equalities can be efficiently handled by a design-oriented PSS-DEC analysis [22]. In this section, the PSS-DEC analysis is reviewed, and the sensitivity analysis for oscillators [5] is generalized to account for design constraints, similar to [35]. The new design-oriented formulation of the sensitivity analysis, in conjunction with the PSS-DEC analysis, facilitates gradient-based oscillator design and optimization. These analyses can guide oscillator improvement while ensuring that additional performance specifications are not compromised during the optimization.

4.2.1 PSS Analysis with Design Equality Constraints

The oscillator specifications can often be given as equalities [22]

$$\begin{aligned} \text{power consumption} &= 5.0 \text{ mW} \\ \text{oscillation frequency} &= 2.4 \text{ GHz} \\ \text{duty cycle} &= 50 \ \% \\ \text{output amplitude} &= 1 \text{ V} \end{aligned}$$

These design equality constraints (DECs) can be written in a vector form as

$$G_E(x, T, \Gamma_E) = 0 \tag{4.19}$$

where G_E represents E PSS-based design specifications, and $\Gamma_E \in \mathbb{R}^E$ is a vector of E circuit parameters, such as the MOSFET geometry parameters W_M, L_M, values of passive components R, L, C, process parameters, or environmental parameters, such as temperature, power supply voltage, etc.

The PSS-DEC analysis finds the PSS waveform $x_s(t)$ and the oscillation period T while adjusting the values of E circuit parameters in Γ_E, such that a set of E design specifications in (4.19) are satisfied [22], as depicted below

$$\begin{array}{|c|}\hline \text{PSS} \\ \hline G_E = 0 \\ \hline \end{array} \rightarrow \begin{array}{c} x_s \\ T \\ \Gamma_E \end{array} \tag{4.20}$$

The mathematical description of the PSS-DEC analysis is obtained by augmenting the PSS equations in (4.4) by E additional DECs in (4.19). The PSS unknowns are augmented by E circuit parameters in Γ_E. This results in a square system of equations that has an isolated solution [22]

$$\begin{cases} \frac{d}{dt} q\big(x(t)\big) + f\big(x(t)\big) + b = 0 \\ x(0) = x(T) \\ \varphi\big(x(0)\big) = 0 \\ G_E(x, T, \Gamma_E, \Gamma_P) = 0 \end{cases} \tag{4.21}$$

The solution x_s, T, and Γ_E obtained by solving the periodic BVP in (4.21) simultaneously satisfies the equations of the PSS analysis in (4.4), and the design constraints in (4.19). There may be no solution to (4.19) and (4.21), which means that the design specifications can not be satisfied by tuning the values of the parameters in Γ_E. For instance, a specification for the oscillation frequency of an LC oscillator can be achieved by tuning the tank parameters. Other circuit parameters have very little or no control on the oscillation frequency, and result in a singular or badly conditioned PSS-DEC Jacobian matrix. Selection of a suitable set of parameters requires a good understanding of the design, and is delegated to a designer.

4.2.2 Sensitivity Analysis with Design Equality Constraints

An oscillator's PSS, PPV, and phase noise can change in response to a change in the design, process, or environmental parameters of the oscillator. Let $\gamma_p \in \mathbb{R}$ be a design parameter. The PSS sensitivity $dx_s/d\gamma_p$ can assist in minimizing the noise intensities, and predict the change in the oscillation period $dT/d\gamma_p$. The PPV sensitivity $dv_1/d\gamma_p$ can guide the improvement of an oscillator's noise rejection, and predict the change in the VCO gain [5].

In this section, a modification of the sensitivity analysis for oscillators is proposed. It is a generalization of the sensitivity analysis for oscillators with a specification for the oscillation frequency [21], [35]. The new design-oriented sensitivity analysis accounts for DECs in (4.19) and provides feasible directions for design improvement. The tradeoffs between two or more circuit parameters can be made, such that one or more design feasibility conditions remain satisfied.

It is shown in [5] that the impact of a parameter change on an oscillator can be decomposed into a change in the oscillation period T and a change in the PSS and PPV amplitudes. The change in x_s and v_1 is computed in a normalized time τ,

$$\tau \equiv t/T(\gamma_p), \quad \tau \in \mathbb{R} \tag{4.22}$$

such that $dx_s/d\gamma_p$ and $dv_1/d\gamma_p$ are small and periodic in τ with a period of 1. The normalized time τ is the independent variable in the sensitivity analysis for oscillators. The absolute time t, and the d/dt operator in the PSS-DEC and PPV descriptions in (4.21) and (4.14) are redefined as

$$t \equiv \tau T(\gamma_p) \tag{4.23}$$

and

$$\frac{d}{dt} \equiv \frac{1}{T(\gamma_p)} \frac{d}{d\tau} \tag{4.24}$$

The design-oriented PSS sensitivity analysis for oscillators finds the sensitivity of the PSS-DEC solution with respect to a circuit parameter $\gamma_p \notin \Gamma_E$. For a given value of parameter γ_p^*, the PSS-DEC analysis finds the solution as

$$\gamma_p^* \;\rightarrow\; \boxed{\begin{array}{c} \text{PSS} \\ \hline G_E = 0 \end{array}} \;\rightarrow\; \begin{array}{r} x_s(\gamma_p^*) \\ T(\gamma_p^*) \\ \Gamma_E(\gamma_p^*) \end{array} \tag{4.25}$$

A small change $\Delta\gamma_p$ can be compensated by a corresponding change $\Delta\Gamma_E$, such that the design constraints remain satisfied

$$\gamma_p^* + \Delta\gamma_p \quad \rightarrow \quad \boxed{\begin{array}{c} \text{PSS} \\ \hline G_E = 0 \end{array}} \quad \rightarrow \quad \begin{array}{r} x_s(\gamma_p^*) + \left.\dfrac{dx_s}{d\gamma_p}\right|_{G_E,\gamma_p^*}\Delta\gamma_p \\ T(\gamma_p^*) + \left.\dfrac{dT}{d\gamma_p}\right|_{G_E,\gamma_p^*}\Delta\gamma_p \\ \Gamma_E(\gamma_p^*) + \underbrace{\left.\dfrac{d\Gamma_E}{d\gamma_p}\right|_{G_E,\gamma_p^*}\Delta\gamma_p}_{\Delta\Gamma_E} \end{array} \tag{4.26}$$

where the three sensitivities $dx_s/d\gamma_p|_{G_E}$, $dT/d\gamma_p|_{G_E}$, and $d\Gamma_E/d\gamma_p|_{G_E}$ in (4.26) represent the oscillator PSS sensitivities in the presence of design equality constraints. The presence of the DECs is indicated by the subscript G_E as in $dT/d\gamma_p|_{G_E}$.

Though $\Delta\gamma_p$ and $\Delta\Gamma_E$ compensate for each other to keep the constraints satisfied, the PSS solution changes. The PSS solution sensitivities $dx_s/d\gamma_p|_{G_E}$ and $dT/d\gamma_p|_{G_E}$ in (4.26) are different from the conventional PSS solution sensitivities $dx_s/d\gamma_p$ and $dT/d\gamma_p$ in [5]. For instance, if the value for the oscillation period T is specified as a DEC, then $dT/d\gamma_p|_{G_E} = 0$, while the conventional period sensitivity may not be zero. The proposed sensitivities are related to the conventional sensitivities with respect to Γ_E and γ_p as

$$\left.\frac{dx_s}{d\gamma_p}\right|_{G_E} = \frac{dx_s}{d\gamma_p} + \frac{dx_s}{d\Gamma_E} \cdot \left.\frac{d\Gamma_E}{d\gamma_p}\right|_{G_E} \tag{4.27}$$

with similar expressions for $dT/d\gamma_p|_{G_E}$ and $dv_1/d\gamma_p|_{G_E}$.

Let us combine the parameters as $\Gamma \equiv [\gamma_p \quad \Gamma_E^T]^T$. Then the design-oriented sensitivity can be interpreted as the rate at which the oscillator characteristics change given a small change in circuit parameters Γ along a feasible direction s_p,

$$\left.\frac{dx_s}{d\gamma_p}\right|_{G_E} = \lim_{\Delta\gamma_p = 0} \frac{x_s\big(\Gamma^* + s_p \cdot \Delta\gamma_p\big) - x_s\big(\Gamma^*\big)}{\Delta\gamma_p} \tag{4.28}$$

where the feasible direction is given by

$$s_p = \begin{bmatrix} 1 \\ \frac{d\Gamma_E}{d\gamma_p} \end{bmatrix} \tag{4.29}$$

A small change in the parameters Γ along s_p preserves the design feasibility, i.e., the design constraints remain satisfied, $dG_E/d\gamma_p|_{G_E} = 0$.

Therefore, the design-oriented sensitivity analysis provides the feasible direction, and the sensitivities of the oscillator characteristics along this direction. These sensitivities, such as phase noise sensitivity $d\mathcal{L}(f_m)/d\gamma_p|_{G_E}$, can guide design improvement, while meeting the design constraints. This makes the design-oriented sensitivity analysis well-suited for constrained oscillator optimization.

In further discussions, the subscript G_E is omitted, and the presence of DECs is implied.

4.2.3 PSS Sensitivity Analysis with DECs

The PSS sensitivity in the presence of DECs is obtained by a differentiation of the PSS-DEC equations in (4.21) with respect to the parameter γ_p at the steady-state solution where $x = x_s$. Note that according to (4.23) and (4.24) t and d/dt must be treated as functions of γ_p during the differentiation.

The contribution of the resistive circuit components to (4.21) at the steady-state x_s

$$f\Big(x_s\big(\tau T(\gamma_p), \gamma_p\big), \Gamma_E(\gamma_p), \gamma_p\Big) \tag{4.30}$$

depends on γ_p directly, as well as indirectly through the PSS waveform x_s, period T, and parameters Γ_E that are affected by γ_p. Therefore, the total derivative of f with respect to γ_p is composed of four terms

$$\begin{aligned}
&\frac{d}{d\gamma_p}\bigg[f\Big(x\big(\tau T(\gamma_p), \gamma_p\big), \Gamma_E(\gamma_p), \gamma_p\Big)\bigg] \\
&= \frac{\partial f}{\partial \gamma_p} + \frac{\partial f}{\partial \Gamma_E} \cdot \frac{d\Gamma_E}{d\gamma_p} + \frac{\partial f}{\partial x} \cdot \frac{dx}{d\gamma_p} + \underbrace{\frac{\partial f}{\partial x} \cdot \frac{dx}{dT} \cdot \frac{dT}{d\gamma_p}}_{4} \\
&= \underbrace{\frac{\partial f}{\partial \gamma_p}}_{1} + \underbrace{\frac{\partial f}{\partial \Gamma_E} \cdot \frac{d\Gamma_E}{d\gamma_p}}_{2} + \underbrace{G \cdot \frac{dx}{d\gamma_p}}_{3} + \underbrace{0}_{4}
\end{aligned} \tag{4.31}$$

which have the following interpretations:

1. Direct effect of parameter γ_p on f. Resistive circuit components that directly depend on γ_p, such as a resistor with resistance being the parameter $\gamma_p \equiv R$, contribute to this term.

2. Chain effect of parameter γ_p on f caused by a change in the PSS waveform x_s. Resistive circuit components, such as a resistor, or a MOSFET, contribute to this term.

3. Chain effect of parameter γ_p on f caused by a change in parameters Γ_E. The change in Γ_E compensates for the change in the parameter γ_p to keep the DECs satisfied.

4. Chain effect of parameter γ_p on f caused by a change in the oscillation period T. This term is zero because a change in the period alone causes the PSS waveform x_s to stretch or shrink in the absolute time t, without affecting the value of x in the normalized time

$$\frac{dx_s(\tau T, \gamma_p)}{dT} = 0 \tag{4.32}$$

Consequently, f is not affected in the normalized time.

The contribution of the reactive circuit components to (4.21) at the steady-state is

$$\frac{1}{T(\gamma_p)} \frac{d}{d\tau} q\Big(x_s\big(\tau T(\gamma_p), \gamma_p\big), \Gamma_E(\gamma_p), \gamma_p\Big) \tag{4.33}$$

and its total derivative with respect to γ_p is composed of four terms as well

$$\begin{aligned} &\frac{d}{d\gamma_p}\left[\frac{1}{T(\gamma_p)} \frac{d}{d\tau} q\Big(x\big(\tau T(\gamma_p), \gamma_p\big), \Gamma_E(\gamma_p), \gamma_p\Big)\right] \\ &= \frac{d}{dt}\left(\frac{\partial q}{\partial \gamma_p} + \frac{\partial q}{\partial \Gamma_E} \cdot \frac{d\Gamma_E}{d\gamma_p} + C \cdot \frac{dx}{d\gamma_p}\right) - \underbrace{\frac{1}{T}\frac{dq}{dt} \cdot \frac{dT}{d\gamma_p}}_{4} \end{aligned} \tag{4.34}$$

where (4.32) was used. The interpretation of the first three terms in (4.34) is similar to the corresponding terms in (4.31), and term 4 represents the chain effect of parameter γ_p on dq/dt caused by a change in the oscillation period T.

A change in the period causes the waveform x_s and, consequently, q to stretch or shrink in the absolute time t. As a result, the slope dq/dt is decreased or increased accordingly.

Therefore, the oscillator PSS-DEC sensitivity equations are given by a system of linear DAEs that represent a periodic BVP in $dx/d\gamma_p$, $dT/d\gamma_p$, and $d\Gamma_E/d\gamma_p$

$$\begin{cases} \frac{d}{dt}\left(C\frac{dx}{d\gamma_p}\right) + G\frac{dx}{d\gamma_p} - \frac{1}{T}\frac{dq}{dt}\frac{dT}{d\gamma_p} \\ \quad + \frac{\partial}{\partial \Gamma_E}\left[\frac{dq}{dt} + f + b\right]\frac{d\Gamma_E}{d\gamma_p} = -\frac{\partial}{\partial \gamma_p}\left[\frac{dq}{dt} + f + b\right] \\ \frac{dx(0,\gamma_p)}{d\gamma_p} - \frac{dx(T,\gamma_p)}{d\gamma_p} = 0 \\ \frac{\partial}{\partial x}\varphi(x)\Big|_{x(0,\gamma_p)}\frac{d}{d\gamma_p}x(0,\gamma_p) = 0 \\ \frac{\partial G_E}{\partial x}\cdot\frac{dx}{d\gamma_p} + \frac{\partial G_E}{\partial T}\cdot\frac{dT}{d\gamma_p} + \frac{\partial G_E}{\partial \Gamma_E}\cdot\frac{d\Gamma_E}{d\gamma_p} = -\frac{\partial G_E}{\partial \gamma_p} \end{cases} \tag{4.35}$$

which reduces to the conventional PSS sensitivity formulation [5] when there are no additional DECs and $d\Gamma_E/d\gamma_p = 0$.

The new PSS sensitivity analysis requires a PSS-DEC analysis to be first performed to obtain the PSS waveforms x_s, the oscillation period T, parameters Γ_E, and dq/dt. Assuming that the underlying PSS-DEC analysis is based on the Newton-Raphson method, the periodic matrix coefficients C, and G are also available. The partial derivatives of q, f, and b with respect to Γ_E and γ_p are obtained from the device models at the steady-state x_s.

Once assembled, the continuous-time PSS-DEC sensitivity equations in (4.35) can be solved in the time domain by the finite-difference, or shooting methods, as well as in the frequency domain by the harmonic balance method for $dx_s/d\gamma_p$, $dT/d\gamma_p$, and $d\Gamma_E/d\gamma_p$.

In optimization problems, the gradient of an objective function ∇F_{obj} with respect to a P-vector of design parameters $\Gamma_P = [\gamma_1, \ldots, \gamma_P]^T$ is often needed. In this case, (4.35) must be solved P times with different right-hand side terms to compute PSS sensitivities with respect to all optimization parameters γ_p, $p = 1, \ldots, P$. The left-hand side coefficients G, C, dq/dt, $\partial\left[\frac{dq}{dt} + f + b\right]/\partial\Gamma_E$, and T in (4.35) are properties of the periodic steady-state, and do not depend on the choice of parameter γ_p.

4.2.4 PPV Sensitivity Analysis with DECs

A PPV sensitivity analysis with design equality constraints is based on differentiation of the PPV description in (4.14) with respect to the parameter γ_p at the steady-state where $y = v_1$, in the normalized time τ. The PPV sensitivity $dv_1/d\gamma_p$ is the solution of the linear system of DAEs in $dy/d\gamma_p$

$$\begin{cases} C^T \frac{d}{dt}\frac{dy}{d\gamma_p} - G^T \frac{dy}{d\gamma_p} = -\left[\frac{dC^T}{d\gamma_p}\frac{dv_1}{dt} - \frac{dG^T}{d\gamma_p} v_1\right] \\ \frac{dy(0,\gamma_p)}{d\gamma_p} - \frac{dy(T,\gamma_p)}{d\gamma_p} = 0 \\ \left[C\dot{x}_s\right]^T \frac{dy}{d\gamma_p} = -\left[\frac{dC}{d\gamma_p}\dot{x}_s + C\frac{d\dot{x}_s}{d\gamma_p} - \frac{1}{T}\frac{dT}{d\gamma_p}C\dot{x}_s\right]^T v_1 \end{cases} \tag{4.36}$$

where the last equation is written for time $t = 0$. The total derivative of the capacitance matrix with respect to parameter γ_p is given by

$$\frac{d}{d\gamma_p}C(x, \Gamma_E, \gamma_p) = \frac{\partial C}{\partial \gamma_p} + \frac{\partial C}{\partial x} \cdot \frac{dx}{d\gamma_p} + \frac{\partial C}{\partial \Gamma_E} \cdot \frac{d\Gamma_E}{d\gamma_p} \tag{4.37}$$

with

$$\frac{\partial C}{\partial x} \cdot \frac{dx}{d\gamma_p} \equiv \sum_{j=1}^{m} \left(\frac{\partial C}{\partial x_j} \cdot \frac{dx_j}{d\gamma_p} \right) \tag{4.38}$$

where x_j is the j-th entry of x. The expression for the total derivative of the conductance matrix with respect to γ_p is similar to (4.37). These derivatives are obtained from device models at the steady-state x_s.

The PPV sensitivity analysis requires the PSS-DEC solution, its sensitivity, and the PPV. These provide elements of the PPV sensitivity equations such as C, and G at the steady-state x_s, as well as $dx_s/d\gamma_p$, $dT/d\gamma_p$, $d\Gamma_E/d\gamma_p$, and v_1. If $d\Gamma_E/d\gamma_p = 0$ and the conventional PSS sensitivities are used, the PPV sensitivity description in (4.36) reduces to the conventional PPV sensitivity formulation in [5].

Once the BVP in (4.36) is assembled, the PPV sensitivity $dv_1/d\gamma_p$ is obtained by solving it directly in the time or frequency domains, or by reducing it to an initial value problem (IVP) [5].

4.2.5 Phase Noise Sensitivity Analysis

As shown in Section 4.1.3, the single-sideband phase noise $\mathcal{L}(f_m)$ can be determined based on the PPV and the oscillator noise source intensities computed at the steady-state x_s. The sensitivity analysis for oscillators provides all the necessary components for accurate computation of the phase noise sensitivity $d\mathcal{L}/d\gamma_p$.

The sensitivity of the white noise constant in (4.16) with respect to the parameter γ_p is given by

$$\frac{dc_w}{d\gamma_p} = \frac{1}{T}\int_0^T \frac{d}{d\gamma_p}\Big(v_1^T B B^T v_1\Big) d\tau \tag{4.39}$$

The PPV sensitivity $dv_1/d\gamma_p$ is available from Section 4.2.4, and the sensitivity of noise contributions is

$$\begin{aligned} &\frac{d}{d\gamma_p}\Big[B\big(x(t,\gamma_p),\Gamma_E(\gamma_p),\gamma_p\big)\Big] \\ &= \frac{\partial B}{\partial \gamma_p} + \frac{\partial B}{\partial \Gamma_E}\cdot\frac{d\Gamma_E}{d\gamma_p} + \frac{\partial B}{\partial x}\cdot\frac{dx}{d\gamma_p} \end{aligned} \tag{4.40}$$

where the PSS waveform sensitivity $dx_s/d\gamma_p$ and parameter sensitivity $d\Gamma_E/d\gamma_P$ from Section 4.2.3 are used. This phase noise sensitivity consists of the direct effect of the parameter γ_p on B, chain effect of parameter γ_p on B caused by a change in the PSS waveform x_s, and chain effect of γ_p on B caused by a change in Γ_E, such that the DECs are satisfied.

The sensitivity of the phase noise expression in (4.15) is given by

$$\frac{d\mathcal{L}(f_m)}{d\gamma_p} \approx \frac{10}{f_0 c_w \ln(10)}\left(2c_w\frac{df_0}{d\gamma_p} + f_0\frac{dc_w}{d\gamma_p}\right) \tag{4.41}$$

which reduces to

$$\frac{d\mathcal{L}(f_m)}{d\gamma_p} \approx \frac{10}{\ln(10)}\cdot\frac{dc_w}{d\gamma_p} \tag{4.42}$$

for oscillators with a specified oscillation frequency [21] as $df_0/d\gamma_p = 0$ in this case. Note that the sensitivity of the phase noise due to white noise sources is independent of the offset frequency f_m. The sensitivity of the phase noise with a contribution from colored noise sources [36] is obtained in a similar manner.

The sensitivity $d\mathcal{L}/d\gamma_p$ accurately captures the impact of a circuit parameter alteration on the phase noise through the change in the PSS-dependent noise intensities, and also through the change in the PPV. It describes the change in the phase noise given a small change in the circuit parameters γ_p and Γ_E along the feasible direction s_p.

4.3 Phase Noise Minimization Example

In this section, a phase noise minimization example in the presence of specifications for the oscillation frequency and power consumption is considered. This highlights the key ideas of a new optimization method. The theoretical formulation of the new optimization technique for oscillators is presented in Section 4.4.

The oscillator under consideration is a differential four-stage ring oscillator in Figure 4.4 that consists of four identical Maneatis delay cells [16]. The schematic

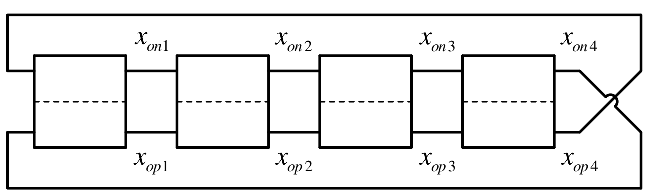

Figure 4.4: Block-diagram of the differential four-stage ring oscillator.

of the first delay cell is shown in Figure 4.5. An active biasing circuit in Figure 4.6 provides a dynamically changing voltage x_{bn} for the delay cells. We use x to denote

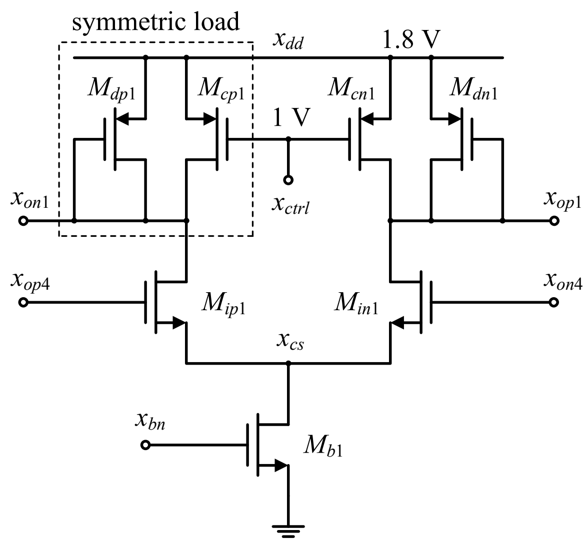

Figure 4.5: Schematic of the Maneatis delay cell with symmetric loads.

nodal voltages (such as x_{ctrl}), and V to denote the nominal values of voltage sources (such as V_{ctrl}).

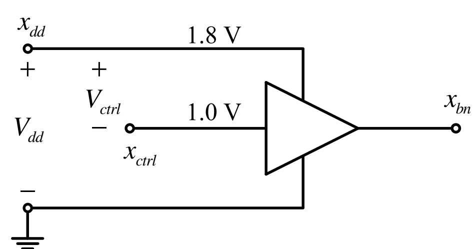

Figure 4.6: Block-diagram of the active biasing with a half-cell replica.

Let the design objective be minimization of the phase noise $F_{obj} \equiv \mathcal{L}(f_m)$ at an offset frequency of $f_m = 1$ MHz for an oscillation frequency of $f_0 = 1$ GHz. The power consumption is limited to be at most 6 mW. This limitation can be represented as an equality constraint $P_c = 6$mW as higher power consumption results in lower phase noise.

To preserve the symmetry of the loads, and keep the delay cells identical during optimization, the sizes of several transistors are described by a single circuit parameter. The widths of all tail bias, input, and load devices, including those in the half-cell replica, are represented by three circuit parameters, W_b, W_i, and W_l, respectively.

This phase noise minimization problem is written as

$$\min_{\Gamma} \{F_{obj}(\Gamma) : \ T = 1 \text{ ns}, \ P_c = 6 \text{ mW}\} \tag{4.43}$$

where Γ is the three-dimensional design space

$$\Gamma \equiv [W_b, W_i, W_l]^T \tag{4.44}$$

Figure 4.7 shows that all designs with the desired oscillation frequency, and all designs with the desired power consumption are given by two surfaces in the three-dimensional design space. The intersection of the two surfaces is a feasible design curve representing all designs that meet both specifications.

Instead of exploring the entire three-dimensional design space space Γ, the optimum point along a single dimension of the feasible curve $H_{feasible}$ is searched, as shown in Figure 4.7. Starting from an infeasible design $\Gamma = [20, 45, 30]$ μm with $P_c = 6.73$ mW and $T = 0.89$ ns the PSS-DEC analysis [22] is used first to adjust

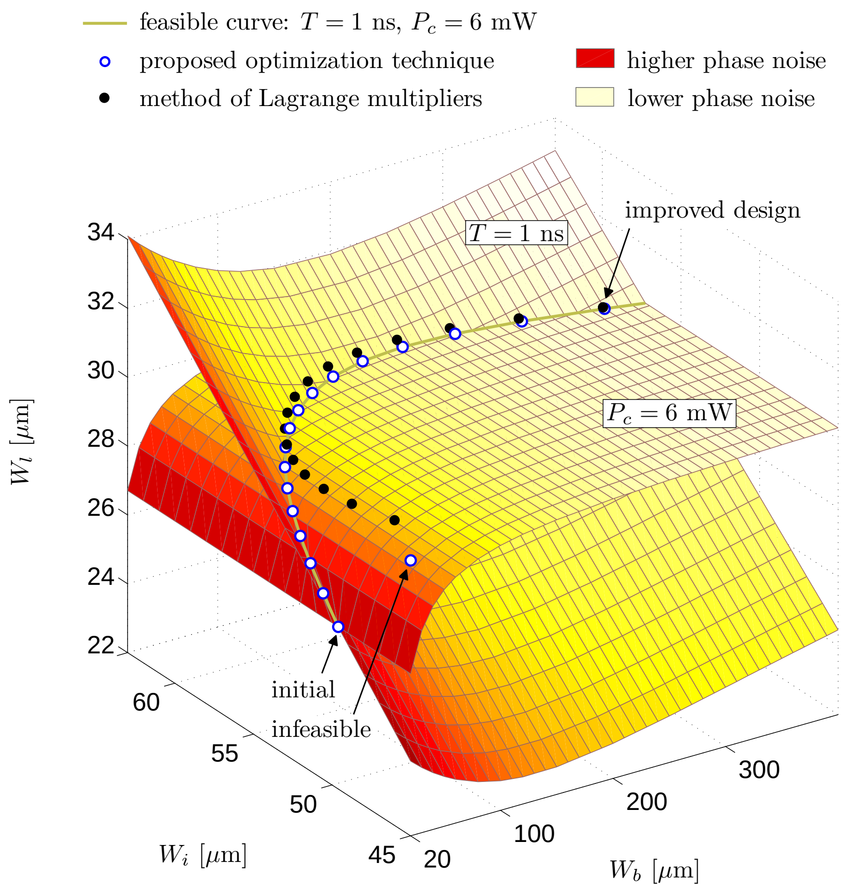

Figure 4.7: Design space $\Gamma \equiv [W_b, W_i, W_l]^T$ with two surfaces that represent designs with $T = 1$ ns and $P_c = 6$ mW. Darker areas indicate higher phase noise. The feasible curve is given by the intersection of the two surfaces, where both the specifications for oscillation period T and power consumption P_c are met. When applied to an infeasible design $\Gamma = [20, 45, 30]$ μm with $P_c = 6.73$ mW and $T = 0.89$ ns, the method of Lagrange multipliers improves the phase noise while gradually meeting the feasibility criteria. In contrast, the proposed optimization technique first employs the PSS-DEC analysis [22] to make the design feasible, and then proceeds along the feasible curve in the direction of lower phase noise. Therefore, the design feasibility is maintained at all optimization steps.

W_i and W_l, such that the design specifications are met,

$$W_b \;\rightarrow\; \boxed{\begin{array}{c} \text{PSS} \\ \hline T\text{=1 ns} \\ P_c\text{=6 mW} \end{array}} \;\rightarrow\; \begin{array}{l} W_i(W_b) \\ W_l(W_b) \end{array} \tag{4.45}$$

In further discussions, the feasible design obtained in this manner is referred to as the initial design. It serves as a reference for monitoring the phase noise improvement for equal P_c and T that meet the specifications.

As seen from (4.45), the PSS-DEC analysis encapsulates the specifications for T and P_c, and makes W_b the only independent optimization parameter that determines $W_i(W_b)$ and $W_l(W_b)$. Thus, the problem in (4.43) is simplified to an unconstrained optimization problem in a single variable, W_b

$$\min_{W_b} \{F_{obj}(W_b)\} \tag{4.46}$$

The independent optimization parameter W_b is updated iteratively, such that the phase noise is improved, while W_i and W_l are changed accordingly to maintain the design feasibility, as shown in Figure 4.8. At optimization step k, the design point moves along the tangent to the feasible curve $dW_i/dW_b^{(k)}$ in the direction of lower phase noise. The design deviates from the feasible curve due to its curvature. It is then shifted back onto the feasible curve by adjusting W_i. The PSS-DEC analysis uses the predicted value $\hat{W}_i^{(k+1)}$ as the initial guess and produces the corrected value $W_i^{(k+1)}$. Parameter W_l is predicted/corrected in a manner similar to W_i.

The PSS-DEC analysis also provides the steady-state solution for the PPV-based phase noise computation and the sensitivity analysis for the subsequent optimization step $k+1$. The new design-oriented sensitivity analysis for oscillators described in Section 4.2.2 computes the feasible search direction s_p, tangent to the feasible

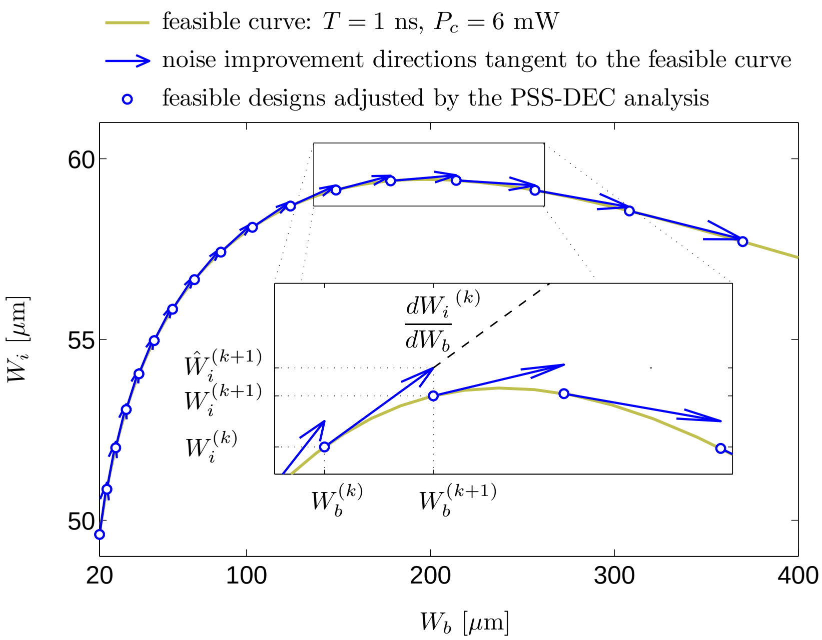

Figure 4.8: Optimization trajectory for W_b and W_i is shown. The search directions are tangent to the feasible curve. After a step is taken, the design point slightly deviates from the feasible curve due to its curvature. A subsequent PSS-DEC analysis [22] adjusts W_i to shift the design point back onto the feasible curve.

curve

$$s_p = \begin{bmatrix} 1 & \frac{dW_i}{dW_b} & \frac{dW_l}{dW_b} \end{bmatrix}^T \tag{4.47}$$

The sensitivity analysis also provides the sensitivity of the objective function

$$\begin{aligned} \left.\frac{dF_{obj}}{dW_b}\right|_{\substack{T=1\text{ ns}\\ P_c=6\text{ mW}}} &= \lim_{\Delta W_b \to 0} \frac{F_{obj}(\Gamma^* + s_p \cdot \Delta W_b) - F_{obj}(\Gamma^*)}{\Delta W_b} \\ &= \frac{\partial F_{obj}}{\partial W_b} + \frac{\partial F_{obj}}{\partial W_i} \cdot \frac{dW_i}{dW_b} + \frac{\partial F_{obj}}{\partial W_l} \cdot \frac{dW_l}{dW_b} \\ &= \nabla F_{obj} \cdot s_p \end{aligned} \tag{4.48}$$

which describes the rate at which the phase noise F_{obj} changes given a small change in the design parameters along the feasible curve, at the point where $\Gamma = \Gamma^*$. This sensitivity provides the direction along the feasible curve in which the design point Γ should be moved to reduce the phase noise. The sensitivity in (4.48) is computed by a single sensitivity analysis directly, as described in Section 4.2.5, without the need to compute the three entries of the gradient

$$\nabla F_{obj} = \begin{bmatrix} \frac{\partial F_{obj}}{\partial W_b} & \frac{\partial F_{obj}}{\partial W_i} & \frac{\partial F_{obj}}{\partial W_l} \end{bmatrix} \tag{4.49}$$

The step ΔW_b can be determined from a range of optimization methods, such as the steepest descent method, or quasi-Newton method, based on (4.48). The corresponding prediction step in the three-dimensional space is obtained as shown in Figure 4.8 according to

$$\Delta\Gamma = s_p \cdot \Delta W_b \tag{4.50}$$

The described technique enables fast gradient-based optimization of low noise oscillators that can efficiently handle the design equality constraints. To emphasize the role of the new design-oriented sensitivity and PSS-DEC analyses, consider the method of Lagrange multipliers [38]. This method for constrained optimization can be applied to (4.43) with conventional PSS and sensitivity [5] analyses for oscillators.

The optimization steps of the method of Lagrange multipliers implemented with a BFGS quasi-Newton method are also shown in Figure 4.7. Given the same infeasible design $\Gamma = [20, 45, 30]$ μm, the method of Lagrange multipliers improves the phase noise while gradually meeting the feasibility criteria. It does not guarantee a feasible design when far from optimum point. In contrast, the proposed technique achieves feasibility at the first step and allows the designer to terminate the optimization at any time after the phase noise has been sufficiently improved. In both methods, the change in the design parameters $\Delta\Gamma$ is limited to 20 % of Γ to ensure fast PSS/PSS-DEC convergence at all optimization steps.

The proposed technique searches for the optimum point in a single dimension of the feasible curve, while the method of Lagrange multipliers performs the optimization in five parameters $[W_b, W_i, W_l, \lambda_{P_c}, \lambda_T]^T$, where the latter two are the Lagrange multipliers that handle the two design specifications. At each optimization point, the method of Lagrange multipliers performs three PSS and PPV sensitivity analyses to compute the gradient in (4.49). The proposed technique requires one PSS and PPV sensitivity calculation with respect to W_b, while the sensitivities of device contributions to W_i and W_l are used in the underlying PSS-DEC analysis.

Table 4.1 shows the parameters and performance characteristics of the infeasible design, the initial feasible design provided by the PSS-DEC analysis, and the improved design. The optimization results in a 4.59 dBc/Hz improvement in phase noise at a 1 MHz offset frequency over the initial feasible design. Figure 4.9 shows the phase noise performance of the initial feasible and improved oscillator designs.

Table 4.1: Parameters and performance of the infeasible design, initial design from the PSS-DEC analysis, and improved design.

	Units	Infeasible	Initial	Improved
f_0	[GHz]	1.12	1.00	1.00
P_c	[mW]	6.73	6.00	6.00
$\mathcal{L}$(1 MHz)	[dBc/Hz]	−83.45	−83.87	−88.46
W_b	[μm]	20.00	20.00	369.77
W_i	[μm]	45.00	49.61	57.71
W_l	[μm]	30.00	26.71	30.31

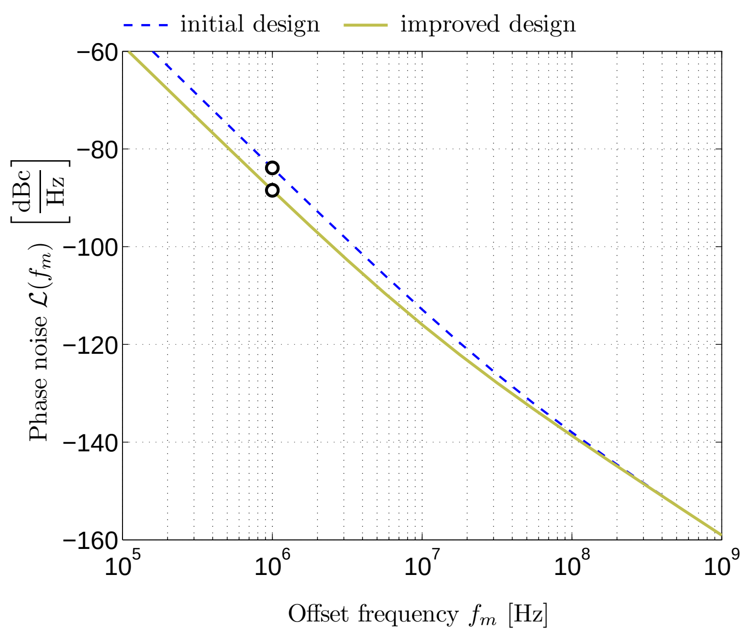

Figure 4.9: Optimization applied to the four-stage differential ring oscillator with Maneatis delay cell results in a 4.59 dBc/Hz phase noise improvement at 1 MHz offset frequency.

4.4 New Optimization Technique

Based on the example presented in the previous section, we can generalize the new optimization method.

Consider a constrained optimization problem

$$\min_{\Gamma} \{F_{obj}(\Gamma) : \; G_E(\Gamma) = 0\} \tag{4.51}$$

where

$$\begin{aligned} \Gamma &\in \mathbb{R}^{P+E} && : \text{ vector of circuit parameters,} \\ F_{obj} &: \mathbb{R}^{P+E} \to \mathbb{R} && : \text{ objective function,} \\ G_E &: \mathbb{R}^{P+E} \to \mathbb{R}^E && : \text{ design equality constraints (DECs),} \end{aligned}$$

where E is the number of equality constraints, and $P + E$ is the number of circuit parameters that are adjusted during optimization. The objective function F_{obj} represents the oscillator's performance, such as phase noise, sensitivity to power supply or substrate noise, etc. The DECs G_E can represent PSS-based design specifications [22] for power consumption, oscillation frequency, duty cycle, or oscillation amplitude. The parameters Γ can be design parameters, such as MOSFET geometry parameters W_M, L_M, values of passive components R, L, C, process parameters, or environmental parameters, such as temperature, power supply voltage, load capacitance.

A design is feasible if the specifications given by the DECs are met. A space of all feasible designs is given by

$$H_{feasible} \equiv \{\Gamma : \; G_E(\Gamma) = 0\} \tag{4.52}$$

Let us split the parameters into two groups, Γ_P and Γ_E,

$$\Gamma = \begin{bmatrix} \Gamma_P \\ \hdashline \Gamma_E \end{bmatrix} = \begin{bmatrix} \gamma_1 \cdots \gamma_P & \vdots & \gamma_{P+1} \cdots \gamma_{P+E} \end{bmatrix}^T \tag{4.53}$$

such that the E design specifications in G_E can be satisfied by adjusting E parameters in Γ_E. This adjustment is done by the PSS-DEC analysis [22] in the following manner

$$\Gamma_P \;\; \rightarrow \;\; \boxed{\begin{array}{c} \text{PSS} \\ \hline G_E = 0 \end{array}} \;\; \rightarrow \;\; \Gamma_E(\Gamma_P) \tag{4.54}$$

such that

$$\Gamma(\Gamma_P) = \begin{bmatrix} \Gamma_P \\ \hdashline \Gamma_E(\Gamma_P) \end{bmatrix} \in H_{feasible} \tag{4.55}$$

Parameters Γ_P are now the independent optimization variables, and Γ_E is defined by the PSS-DEC analysis for a given value of Γ_P. Therefore, while handling the equality constraints, the PSS-DEC analysis reduces the dimensionality of the design space from $P + E$ to P, and the optimization is performed in the space of all feasible designs $H_{feasible}$, rather than in the space of all designs. Therefore, the minimization problem in (4.51) is simplified to an unconstrained optimization in a space of reduced dimensionality

$$\min_{\Gamma_P} \left\{ F_{obj}\big(\Gamma(\Gamma_P)\big) \right\} \tag{4.56}$$

The proposed optimization technique performs optimization in P variables. It explores P dimensions of the feasible space.

The design-oriented sensitivity analysis for oscillators, described in Section 4.2.2, provides feasible directions for design improvement. The feasible directions are obtained from P sensitivity analyses with respect to the independent optimization variables in Γ_P and are used to construct the matrix $S = [s_1, \ldots, s_P]$,

$$S = \frac{\partial \Gamma}{\partial \Gamma_P} = \begin{bmatrix} I \\ \hdashline \frac{\partial \Gamma_E}{\partial \Gamma_P} \end{bmatrix} = \begin{bmatrix} 1 & & \\ & \ddots & \\ & & 1 \\ \hdashline \frac{\partial \gamma_{P+1}}{\partial \gamma_1} & \cdots & \frac{\partial \gamma_{P+1}}{\partial \gamma_P} \\ \vdots & & \vdots \\ \frac{\partial \gamma_{P+E}}{\partial \gamma_1} & \cdots & \frac{\partial \gamma_{P+E}}{\partial \gamma_P} \end{bmatrix} \tag{4.57}$$

where each column represents a direction tangent to the feasible space $H_{feasible}$, and orthogonal to the gradient of the DECs,

$$\begin{bmatrix} \frac{\partial G_E}{\partial \gamma_1} \cdots \frac{\partial G_E}{\partial \gamma_{P+E}} \end{bmatrix} \cdot S = \nabla G_E \cdot S = 0 \tag{4.58}$$

The columns of S represent P degrees of freedom for the feasible design space exploration while searching for the optimum point.

The new sensitivity analysis also computes the PSS and PPV sensitivities $dT/d\Gamma_P|_{G_E}$, $dx_s/d\Gamma_P|_{G_E}$, $dv_1/d\Gamma_P|_{G_E}$ which are postprocessed to obtain the gradient of the objective function in presence of the DECs

$$\begin{aligned}\left.\frac{\partial F_{obj}}{\partial \Gamma_P}\right|_{G_E} &= \left[\left.\frac{\partial F_{obj}}{\partial \gamma_1}\right|_{G_E} \cdots \left.\frac{\partial F_{obj}}{\partial \gamma_P}\right|_{G_E} \right] \\ &= \left[\frac{\partial F_{obj}}{\partial \gamma_1} \cdots \frac{\partial F_{obj}}{\partial \gamma_P} \right] \cdot S \\ &= \nabla F_{obj} \cdot S \end{aligned} \tag{4.59}$$

where an individual entry

$$\left.\frac{\partial F_{obj}}{\partial \gamma_p}\right|_{G_E} = \lim_{\Delta\gamma_p \to 0} \frac{F_{obj}(\Gamma^* + s_p \cdot \Delta\gamma_p) - F_{obj}(\Gamma^*)}{\Delta\gamma_p} \tag{4.60}$$

is the rate at which F_{obj} changes given a small change in the circuit parameters along a feasible direction s_p for $p = 1, \ldots, P$. Note that the gradient in (4.59) is computed directly from P sensitivity analyses in the presence of DECs, and there is no need for computing ∇F_{obj} itself, which would require $P + E$ conventional sensitivity analyses [5].

The proposed technique enables gradient-based oscillator optimization and handles the design equality constraints efficiently. It can be integrated with any gradient-based optimization method. For example, the optimization step $\Delta\Gamma_P$

for the steepest descent method is given by

$$\Delta\Gamma_P = -\alpha \cdot \left.\frac{\partial F_{obj}}{\partial \Gamma_P}\right|_{G_E} \tag{4.61}$$

where $\alpha > 0$ is the step size.

Once the method-specific change in the optimization variable $\Delta\Gamma_P$ is determined, the corresponding change in the space of all design parameters is computed as a linear combination of the feasible directions in (4.57)

$$\Delta\Gamma = S \cdot \Delta\Gamma_P \tag{4.62}$$

It is seen from (4.59) and (4.62) that $\Delta\Gamma_P$ from (4.61) results in the steepest feasible descent direction step $\Delta\Gamma$, given by the projection of the objective function gradient onto the feasible space

$$\Delta\Gamma = -\alpha S S^T \nabla F_{obj}^T \tag{4.63}$$

Figure 4.10 shows the algorithm of the proposed optimization technique. Note that in Step 3, the PSS-DEC analysis converges in a few iterations, since a good initial guess $\hat{\Gamma}_E^{(k)}$ is provided from Step 8. A good initial guess for the PSS solution T and $x(t)$ is computed based on the PSS sensitivity to Γ_P. Also, note that only P sensitivity analyses are performed at each optimization iteration at Step 5, as there is no need for computing the gradient ∇F_{obj} in $P + E$ variables. The PSS-DEC analysis in Step 3 also ensures that a feasible design that meets the spec-

1. provide initial design $\left[\Gamma_P^{(0)} \;\; \hat{\Gamma}_E^{(0)}\right]^T$
2. initialize the counter $k = 0$
3. correct the design $\hat{\Gamma}_E^{(k)} \rightarrow \Gamma_E^{(k)}$ by PSS-DEC analysis
4. evaluate $F_{obj}^{(k)}$ and exit if performance is sufficiently improved
5. compute $S^{(k)}$ and $\left.\frac{\partial F_{obj}}{\partial \Gamma_P}\right|_{G_E}^{(k)}$ from P sensitivity analyses
6. compute $\Delta\Gamma_P^{(k)}$ and corresponding $\Delta\Gamma_E^{(k)}$
7. update optimization parameters $\Gamma_P^{(k+1)} = \Gamma_P^{(k)} + \Delta\Gamma_P^{(k)}$
8. predict feasible design $\hat{\Gamma}_E^{(k+1)} = \Gamma_E^{(k)} + \Delta\Gamma_E^{(k)}$
9. increase the counter $k = k + 1$ and proceed to Step 3

Figure 4.10: Algorithm of the proposed optimization technique.

ifications is available at each optimization iteration, and therefore the optimization process can be stopped at any time after the objective function F_{obj} is sufficiently improved. One possible strategy is to exit when an additional optimization step insignificantly reduces the objective function, compared to the improvement from the initial design, and does not justify the simulation time or change in the circuit parameters.

The proposed optimization technique is general, and applicable to any oscillator, independent of the type and topology. Accurate PPV-based evaluation of phase noise performance and fast sensitivity computation form a foundation for automated low-noise oscillator design and optimization. The PSS-DEC analysis and the new sensitivity analysis efficiently handle the PSS-based design specifications given by equalities. Those design specifications that can not be included in the PSS-DEC analysis can be handled by general-purpose methods for constrained optimization.

4.5 Examples and Results

We have implemented the above optimization technique in our Matlab-based circuit simulator. In this section, phase noise optimization examples are presented for the LC oscillators in Figures 4.1 and 4.11.

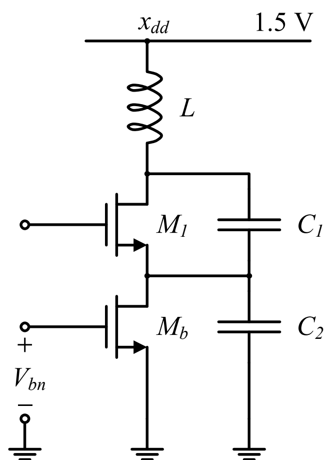

Figure 4.11: Schematic of a Colpitts LC VCO.

Consider a Colpitts oscillator in Figure 4.11. As shown [28] and [39], there exists an optimum capacitive divider ratio $n = C_1/(C_1 + C_2)$, for which the phase noise is minimized. The described optimization technique is applied to find the values of circuit parameters

$$\Gamma \equiv \left[W_1 \; C_2 \;\vdots\; C_1 \; V_{bn}\right]^T \tag{4.64}$$

such that the phase noise at 100 kHz offset frequency is minimized,

$$F_{obj} \equiv \mathcal{L}(f_m), \quad f_m = 100 \text{ kHz} \tag{4.65}$$

Parameters $\Gamma_E \equiv [C_1 \; V_{bn}]^T$ are chosen to be adjusted by the PSS-DEC analysis to meet the specifications for power consumption and oscillation period,

$$G_E \equiv \begin{bmatrix} P_c - 40 \text{ mW} \\ T - 1.1 \text{ ns} \end{bmatrix} \tag{4.66}$$

Figure 4.12 shows the phase noise as a function of independent optimization parameters $\Gamma_P \equiv [W_1 \; C_2]^T$, as well as the initial feasible design, and the design improved by the optimization. As seen from Figure 4.13 the phase noise at $f_m = 100$ kHz is reduced by 5.22 dBc/Hz. The values of circuit parameters and performance of the infeasible, initial, and improved designs are summarized in Table 4.2. The optimum capacitive divider ratio for this circuit is $n = 0.31$.

Next, consider the LC VCO of Figure 4.1. A capacitor C_x in parallel with the tail current source M_b can be used to improve oscillator noise performance [40], [41]. In [40] is is shown that C_x shorts noise from M_b at frequencies around $2f_0$ to ground, while in [41] the capacitor C_x is used to shape the tail current such that noise injection from M_1 and M_2 occurs when the oscillator is less sensitive to noise. As shown in Figure 4.14, adding $C_x = 1$ pF reduces the phase noise at 10 kHz offset frequency by 6.65 dBc/Hz.

It is shown next that the new optimization technique can further reduce the

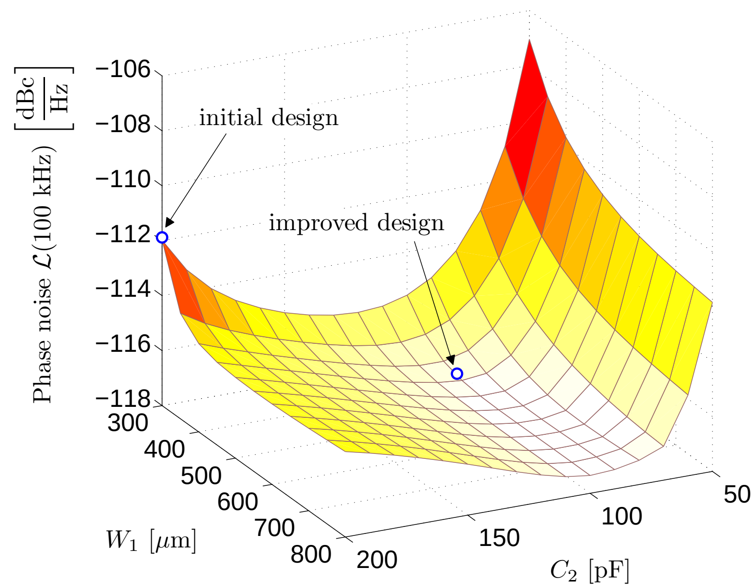

Figure 4.12: Phase noise at a 100 kHz offset frequency of the Colpitts oscillator is shown as a function of independent optimization parameters C_2 and W_1. The specifications for the power consumption and oscillation frequency are satisfied by adjusting V_{bn} and C_1 in the PSS-DEC analysis. The optimization results in 5.22 dBc/Hz phase noise improvement.

phase noise by adjusting transistor sizes. Let the objective be minimization of phase noise

$$F_{obj} \equiv \mathcal{L}(f_m), \quad f_m = 10 \text{ kHz} \tag{4.67}$$

subject to constraints for the power consumption and oscillation frequency

$$G_E \equiv \begin{bmatrix} P_c - 1.5 \text{ mW} \\ f_0 - 4.0 \text{ GHz} \end{bmatrix} \tag{4.68}$$

Consider an example where the phase noise optimization is performed by ad-

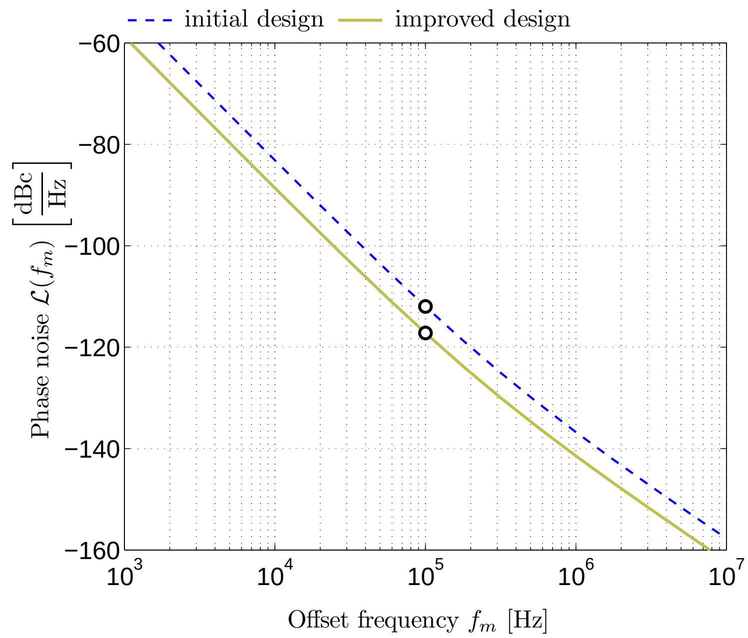

Figure 4.13: Optimization applied to the Colpitts LC oscillator results in a 5.22 dBc/Hz phase noise improvement at 100 kHz offset frequency.

justing six circuit parameters

$$\Gamma \equiv \left[W_b \ L_b \ W_{1,2} \ L_{1,2} \ \vdots \ V_{bn} \ W_{c1,c2}\right]^T \tag{4.69}$$

where the bias voltage and the width of tank varactors $\Gamma_E \equiv [V_{bn} \ W_{c1,c2}]^T$ are chosen to be adjusted by the PSS-DEC analysis to satisfy the design constraints. The sizes of the tail current source and the cross-coupled pair $\Gamma_P \equiv [W_b \ L_b \ W_{1,2} \ L_{1,2}]^T$ are independent optimization parameters.

As shown in Figure 4.14 the optimization results in the lowest phase noise from 1 kHz to 10 MHz with significantly reduced flicker noise and nearly unchanged white noise contributions. The phase noise at 10 kHz offset frequency is reduced

Table 4.2: Parameters and performance of the infeasible Colpitts LC oscillator design, initial design from the PSS-DEC analysis, and improved design.

	Units	Infeasible	Initial	Improved
T	[ns]	1.13	1.10	1.10
P_c	[mW]	39.64	40.00	40.00
$\mathcal{L}$(1 MHz)	[dBc/Hz]	−111.76	−111.98	−117.20
W_1	[μm]	300.00	300.00	438.01
C_2	[pF]	200.00	200.00	100.20
C_1	[pF]	40.00	37.22	45.85
V_{bn}	[mV]	700.00	702.55	703.05

by 4.91 dBc/Hz.

Table 4.3 shows the parameter values and performance characteristics of the infeasible design without C_x, initial designs without and with C_x obtained from the PSS-DEC analysis, and the improved design with C_x and optimized values of circuit parameters.

The corresponding change in the PSS and PPV waveforms is shown in Figures 4.15 and 4.16. It is seen that with the introduction of the tail capacitor C_x, the variation in the x_{cs} voltage is reduced, and the magnitude of the PPV v_{1sc} is substantially decreased. This leads to an improvement of the oscillator's rejection of the noise from the tail current source M_b. Adjusting the circuit parameters in Γ_P and Γ_E insignificantly changes the PSS and PPV.

Figure 4.17 shows the contributions of white and flicker noise from the tail current source M_b, the transistors M_1, M_2, and the tank inductors L_p and L_n to

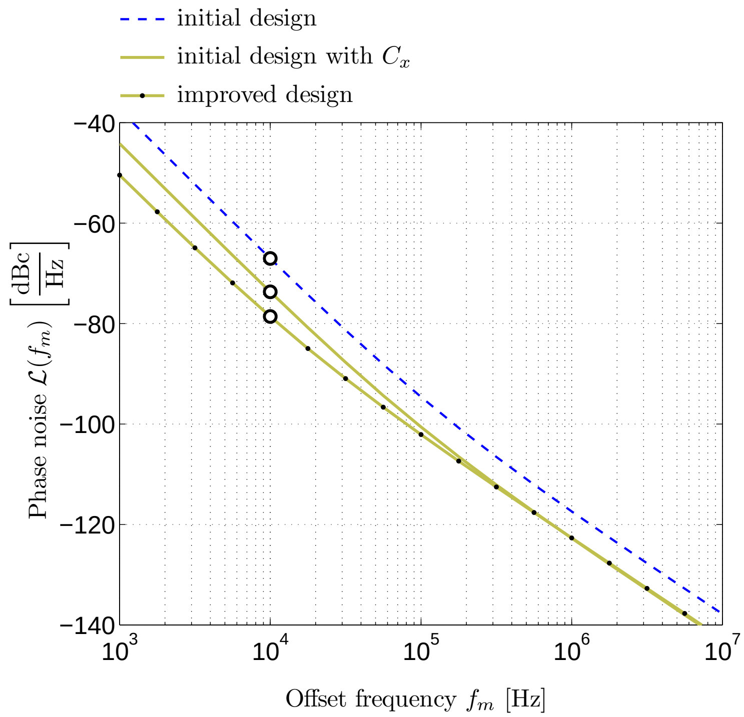

Figure 4.14: Adding a capacitor $C_x = 1$ pF to the differential LC VCO results in a 6.65 dBc/Hz phase noise improvement at 10 kHz offset frequency. Optimization that adjusts device sizes results in an additional 4.91 dBc/Hz phase noise improvement.

the phase noise at the offset frequency of $f_m = 10$ kHz. It is seen that a major reduction of the noise constant is due to a decreased contribution of the flicker noise from the tail current source M_b.

Figure 4.18 shows the noise information for the tail current source M_b and transistor M_1 for the initial and improved designs. It is seen that capacitor C_x significantly reduces the PPV v_{1cs} (Figure 4.18 (b)) which improves the oscillator's rejection of the noise from M_b. While the M_1 drain-source PPV difference (Figure 4.18 (a)) and the noise from M_1 (Figure 4.18 (c), (e)) are reshaped by

Table 4.3: Parameters and performance of the infeasible LC VCO design without C_x, initial design without and with C_x from the PSS-DEC analysis, and the improved design with C_x and optimum values of circuit parameters.

	Units	Infeasible	Initial	Initial with C_x	Improved with C_x
f_0	[GHz]	4.07	4.00	4.00	4.00
P_c	[mW]	1.55	1.50	1.50	1.50
$\mathcal{L}$(10 kHz)	[dBc/Hz]	−67.01	−67.04	−73.69	−78.60
C_x	[pF]	0.00	0.00	1.00	1.00
W_b	[μm]	50.00	50.00	50.00	50.02
$W_{1,2}$	[μm]	50.00	50.00	50.00	33.67
L_b	[μm]	0.15	0.15	0.15	0.23
$L_{1,2}$	[μm]	0.15	0.15	0.15	0.44
V_{bn}	[mV]	500.00	497.43	496.65	548.58
$W_{c1,c2}$	[μm]	300.00	313.87	316.56	302.01

adding C_x, the contributions of M_1 to the phase noise (Figure 4.17) is nearly unchanged.

While the capacitor C_x improves the phase noise by improving the oscillator's noise rejection, the optimization of circuit parameters helps to reduce the noise intensities of the transistors M_b, M_1, and M_2. It is seen from Figure 4.18 that after optimization the flicker noise intensities of M_1 (Figure 4.18 (e)) and M_b (Figure 4.18 (f)) are significantly decreased.

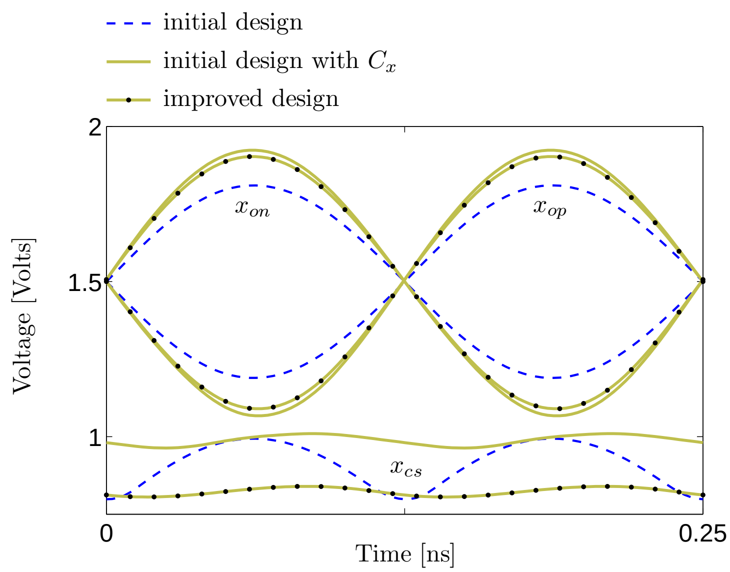

Figure 4.15: The PSS solution of the initial and improved *LC* VCO designs.

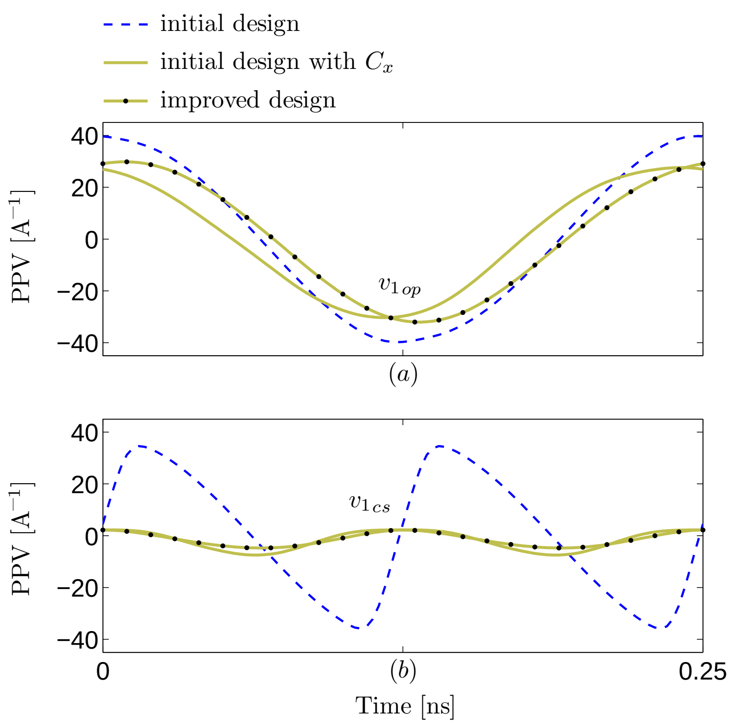

Figure 4.16: The PPV of the initial and improved *LC* VCO designs.

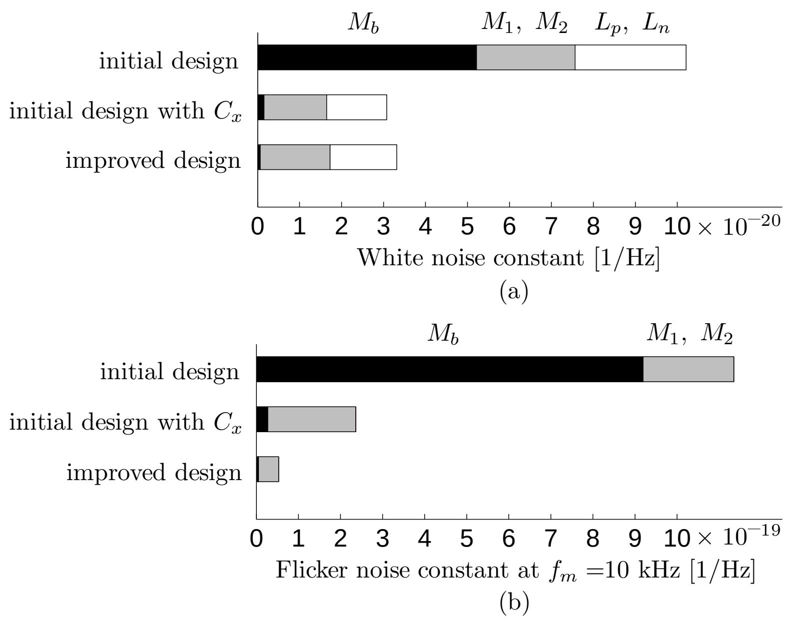

Figure 4.17: (a) Contributions of white noise from the tail current source M_b, transistors M_1, M_2, and the tank inductors L_p, L_n to the noise constant, and (b) contributions of flicker noise from M_b, M_1, and M_2 to the noise constant at 10 kHz offset frequency for the initial and improved LC VCO designs.

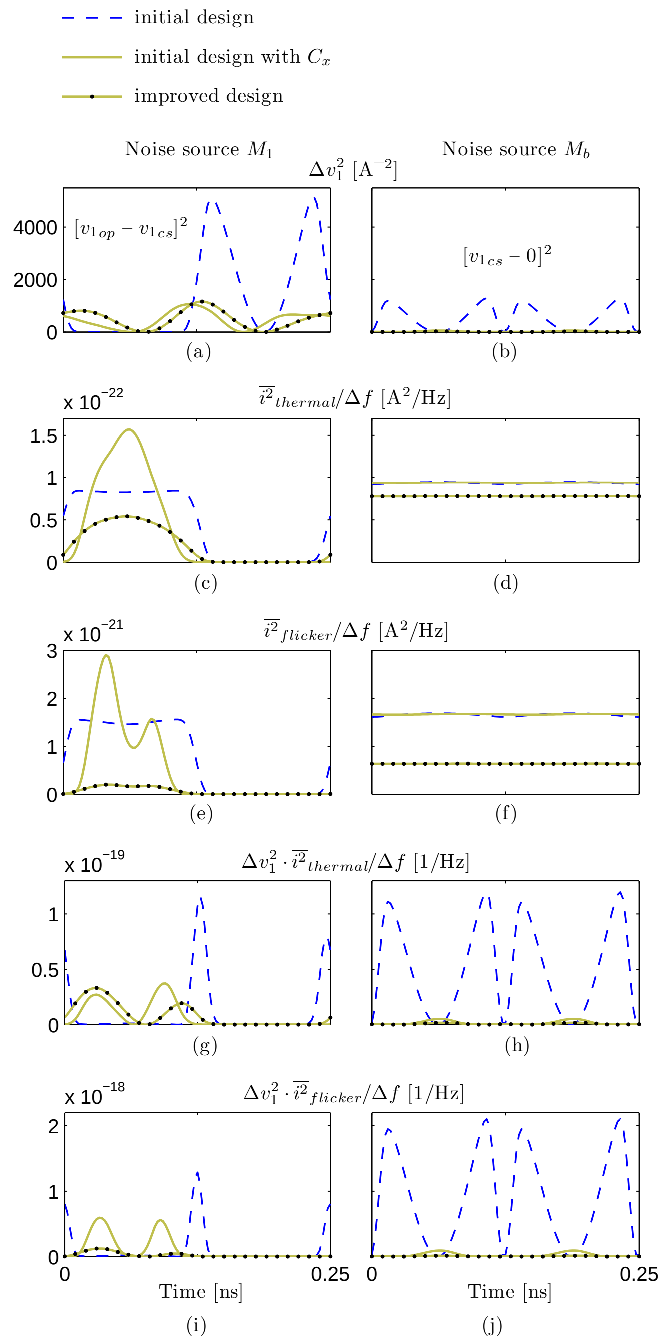

Figure 4.18: The squared difference between the source and drain PPV for (a) M_1, and (b) M_b, thermal noise for (c) M_1, and (d) M_b, flicker noise at 10 kHz for (e) M_1, and (f) M_b, thermal noise projected into the phase noise for (g) M_1, and (h) M_b, and flicker noise projected into the phase noise for (i) M_1, and (j) M_b, along one period, for the initial and improved LC VCO designs.

Chapter 5 – Conclusions

In this dissertation several key aspects of automated low noise oscillator design have been addressed. First, a continuous-time formulation and numerical methods for oscillator sensitivity analysis have been presented. The new sensitivity formulation enables the calculation of the sensitivities of an oscillator's PSS and PPV with respect to design, process, or environmental parameters. It is shown that the proposed analysis is more efficient than brute force finite difference based approaches to sensitivity computation. The new analysis is a useful tool for design optimization, macromodeling, and predicting the impact of process variations.

Then, a general theoretical formulation for a new design-oriented approach to circuit analysis has been presented. The new analysis efficiently finds the values of circuit parameters that result in a desired circuit performance, defined by equality constraints. In contrast to a conventional design approach, there is no need for performing a sequence of conventional circuit analyses. As an example, it was shown how the design specifications can be handled in the periodic steady-state analysis, PSS-DEC analysis. Existing numerical techniques, such as finite difference, shooting, and harmonic balance methods for the conventional PSS analysis are also applicable to the new PSS-DEC analysis. Examples demonstrate usage scenarios for the PSS-DEC analysis in nominal circuit design and in analysis of marginally acceptable parameter variations. While having adequate convergence properties, the new design-oriented analysis is 2 to 4 times faster than a carefully implemented Newton-based search method.

Finally, a novel gradient-based optimization technique for oscillators has been presented that employs design oriented periodic steady-state and sensitivity analyses. The PSS-DEC analysis encapsulates the design specifications and reduces the dimensionality of the design space that needs to be explored. The new sensitivity analysis for oscillators provides the feasible directions for design improvement, such that the design specifications are satisfied at each optimization step. The optimization technique presented in this dissertation is general and applicable to all types of oscillators, independent of the circuit topology.

Several extensions can be explored in future work. Inclusion of multiple objective functions for optimization is useful for several applications. One possibility is to combine each objective into a single objective function by weighting the objectives based on their importance. Alternatively, a set of Pareto-optimal designs in terms of, e.g., phase noise, power supply noise rejection, and power consumption can be made available to a designer.

For voltage controlled oscillator optimization, the transfer curve linearity specification can also be satisfied during optimization. In this case a set of PSS formulations for various control voltages can be combined in a single system of equations, augmented with the VCO specifications for linearity.

The sensitivity analysis for oscillators presented in this dissertation can be applied to oscillator macromodeling. Existing PPV-based VCO phase macromodels can be used to extend the range of control voltages and frequencies of operation.

Also, the effect of VCO parameter variations can be incorporated in the macromodel. This eliminates the need for costly PPV re-extractions for different values of control voltages and parameter variations.

In the design-oriented analysis, design specifications can be used as variables in a sensitivity analysis. Then the resulting sensitivities provide information on how the design parameters should be changed to satisfy a tighter design specification, such as power consumption, while the remaining design equality constraints are satisfied.

The work presented in this dissertation provides a solid foundation for these future enhancements.

Bibliography

[1] T. J. Aprille, Jr. and T. N. Trick, "A computer algorithm to determine the steady-state response of nonlinear oscillators," *IEEE Trans. Circuit Theory,* vol. CT19, pp. 354-360, July 1972.

[2] K. S. Kundert, J. K. White, and A. L. Sangiovanni-Vincentelli, *Steady-State Methods for Simulating Analog and Microwave Circuits*, Kluwer Academic Publishers, 1990.

[3] A. Demir, A. Mehrotra, and J. Roychowdhury, "Phase noise in oscillators: A unifying theory and numerical methods for characterization," *IEEE Trans. Circuits and Systems I*, vol. 47, pp. 655-674, May 2000.

[4] A. Hajimiri and T. H. Lee, *The Design of Low Noise Oscillators*, Kluwer Academic Publishers, 2000.

[5] I. Vytyaz, D. C. Lee, P. Hanumolu, U. Moon, and K. Mayaram "Sensitivity analysis for oscillators," *ICCAD 2007*, pp. 458-463, Nov 2007.

[6] P. Maffezzoni, "Unified computation of parameter sensitivity in nonlinear oscillators," *IEEE Trans. Computer-Aided Design of Integrated Circuits and Systems*, vol 27, pp. 781-790, May 2008.

[7] A. Demir, "Floquet theory and non-linear perturbation analysis for oscillators with differential-algebraic equations," *International Journal of Circuit Theory and Applications*, vol. 28, pp. 163-185, Mar-Apr. 2000.

[8] A. Demir, D. Long, and J. Roychowdhury, "Computing phase noise eigenfunctions directly from steady-state Jacobian matrices," *DAC 2000*, pp. 283-288, Nov. 2000.

[9] T. Mei, and J. Roychowdhury, "Oscillator-AC: restoring rigour to linearized small-signal analysis of oscillators," *ICCAD 2005*, pp. 604-609, Nov. 2005.

[10] T. Mei and J. Roychowdhury. "Efficient AC Analysis of oscillators using least-squares methods," *DATE 2006*, pp. 263-268, March 2006.

[11] J. W. Bandler, Q. J. Zhang, and R. M. Biernacki, "A unified theory for frequency-domain simulation and sensitivity analysis of linear and nonlinear circuits," *IEEE Trans. Microwave Theory and Techniques*, vol. 36, pp. 1661-1669, Dec. 1988.

[12] J. Roychowdhury, "Theory and algorithms for RF sensitivity computation," *ISCAS 2002*, vol. 5, pp. 225-228, May 2002.

[13] P. Maffezzoni, "Efficient multiparameter sensitivity computation of amplifier harmonic distortion," *IEEE Trans. Circuits and Systems II*, vol 54, pp. 257-261, March 2007.

[14] K. Mayaram, D. C. Lee, S. Moinian, D. Rich, and J. Roychowdhury, "Computer-aided circuit analysis tools for RFIC simulation: algorithms, fea-

tures, and limitations," *IEEE Trans. Circuits and Systems II*, pp. 274-286, April 2000.

[15] U. M. Ascher, R. M. M. Mattheij, and R. D. Russell, *Numerical Solution of Boundary Value Problems for Ordinary Differential Equations*, SIAM, 1995.

[16] J. Maneatis, and M. Horowitz, "Precise delay generation using coupled oscillators," *IEEE J. Solid-State Circuits*, vol. 28, pp. 1273-1282, Dec. 1993.

[17] Y. Saad, *Iterative Methods for Sparse Linear Systems*, Second Edition, SIAM, 2003.

[18] F. M. Gardner, "Charge pump phase locked loops," *IEEE Trans. Communications*, vol. COM-28, pp. 1849-1858, Nov. 1980.

[19] X. Lai and J. Roychowdhury, "Capturing oscillator injection locking via nonlinear phase-domain macromodels," *IEEE Trans. Microwave Theory and Techniques*, vol. 52, pp. 2251-2261, Sep. 2004.

[20] A. Mehrotra, S. Lu, D. C. Lee and A. Narayan, "Steady-state analysis of voltage and current controlled oscillators," *ICCAD 2005*, pp. 618-623, Nov 2005.

[21] I. Vytyaz, D. C. Lee, S. Lu, A. Mehrotra, U. Moon, and K. Mayaram, "Parameter finding methods for oscillators with a specified oscillation frequency," *DAC 2007*, pp. 424-429, June 2007.

[22] I. Vytyaz, P. Hanumolu, U. Moon, and K. Mayaram, “Periodic steady-state analysis augmented with design equality constraints,” *DATE 2008*, pp. 312-317, March 2008.

[23] P. C. Maulik, L. Carley and D. J. Allstot, “Sizing of cell-level analog circuits using constrained optimization techniques”, *IEEE J. Solid-State Circuits*, vol. 28, pp. 233-241, March 1993.

[24] P. Wambacq and W. Sansen, *Distortion Analysis of Analog Integrated Circuits*, Kluwer Academic Publishers, 1998.

[25] P. R. Gray, P. J. Hurst, S. H. Lewis, and R. G. Meyer, *Analysis and Design of Analog Integrated Circuits*, 4th edition, Wiley, 2001.

[26] A. Hajimiri, S. Limotyrakis, and T. H. Lee, “Jitter and phase noise in ring oscillators,” *IEEE J. Solid-State Circuits*, vol. 34, pp. 790-804, June 1999.

[27] J. Lee and B. Kim, “A low-noise fast-lock phase-locked loop with adaptive bandwidth control,” *IEEE J. Solid-State Circuits*, vol. 35, pp. 1137-1145, Aug 2000.

[28] A. Hajimiri and T. H. Lee, “A general theory of phase noise in electrical oscillators,” *IEEE J. Solid-State Circuits*, vol. 33, pp. 179-194, Feb. 1998.

[29] M. Hershenson, A. Hajimiri, S. S. Mohan, S. P. Boyd, T. H. Lee, “Design and optimization of *LC* oscillators,” *ICCAD 1999*, pp. 65-69, Nov. 1999.

[30] C. R. C. D. Ranter, G. V. D. Plas, M. S. J. Steyaert, G. G. E. Gielen, and W. M. C. Sansen, "CYCLONE: Automated design and layout of RF *LC*-oscillators," *IEEE Trans. Computer-Aided Design*, vol. 21, pp. 1161-1170, Oct. 2002.

[31] M. Kamon, M. J. Tsuk, J. K. White, "FASTHENRY: a multipole-accelerated 3-D inductance extraction program," *IEEE Trans. Microwave Theory Tech.*, vol. 42, p. 1750-1758, Sep. 1994.

[32] Nye, B., D. Riley, and A. Sangiovanni-Vincentelli *DELIGHT.SPICE User's Guide*, Dept. EECS, University of California, Berkeley, 1984.

[33] W. Nye, D. C. Riley, A. Sangiovanni-Vincentelli, and A. L. Tits, "DELIGHT.SPICE: An optimization-based system for the design of integrated circuits," *IEEE Trans. Computer-Aided Design.*, vol. 7, pp. 501-519, Apr. 1988.

[34] J.-M. Shyu and A. Sangiovanni-Vincentelli, "ECSTASY: A new environment for IC design optimization," *ICCAD 1988*, pp. 484-487. Nov. 1988.

[35] I. Vytyaz, D. C. Lee, U. Moon, and K. Mayaram, "Parameter variation analysis for voltage controlled oscillators in phase-locked loops," *ISCAS 2008*, pp. 716-719, May 2008.

[36] A. Demir, "Phase noise and timing jitter in oscillators with colored-noise sources," *IEEE Trans. Circuits and Systems I*, vol. 49, pp. 1782-1791, Dec 2002.

[37] A. Demir, E. Liu, and A. Sangiovanni-Vincentelli, "Time-domain non Monte-Carlo noise simulation for nonlinear dynamic circuits with arbitrary excitations," *IEEE Trans. Computer-Aided Design*, vol. 15, pp. 493-505, May 1996.

[38] J. Nocedal, S. J. Wright, *Numerical Optimization*, Springer, 1999.

[39] R. Jonnalagedda and K. Mayaram, "Design of very low noise 4.2 GHz Clapp VCOs," *ISCAS 2007*, pp. 2862-2865, May 2007.

[40] E. Hegazi, H. Sjoland, A. A. Abidi, "A filtering technique to lower *LC* oscillator phase noise," *IEEE J. Solid-State Circuits*, vol. 36, pp. 1921-1930, Dec. 2001.

[41] B. Soltanian and P. Kinget, "A tail current-shaping technique to reduce phase noise in *LC* VCOs," *CICC 2005*, pp. 579-582, Sep. 2005.